AD_____

Award Number: DAMD17-98-1-8251

TITLE: Understanding the Role of Replication Protein A and RAD52 in Breast Cancer

PRINCIPAL INVESTIGATOR: Gloria E. Borgstahl, Ph.D.

CONTRACTING ORGANIZATION: University of Nebraska Medical Center
Omaha, NE 68198-7835

REPORT DATE: April 2004

TYPE OF REPORT: Final

PREPARED FOR: U.S. Army Medical Research and Materiel Command
Fort Detrick, Maryland 21702-5012

DISTRIBUTION STATEMENT: Approved for Public Release;
Distribution Unlimited

The views, opinions and/or findings contained in this report are those of the author(s) and should not be construed as an official Department of the Army position, policy or decision unless so designated by other documentation.

20040907 005

REPORT DOCUMENTATION PAGE

1. AGENCY USE ONLY (Leave blank)	2. REPORT DATE April 2004	3. REPORT TYPE AND DATES COVERED Final (25 Sep 1998 – 24 Mar 2004)

4. TITLE AND SUBTITLE

Understanding the Role of Replication Protein A and RAD52 in Breast Cancer

5. FUNDING NUMBERS

DAMD17-98-1-8251

6. AUTHOR(S)

Gloria E. Borgstahl, Ph.D.

7. PERFORMING ORGANIZATION NAME(S) AND ADDRESS(ES)

University of Nebraska Medical Center
Omaha, NE 68198-7835

E-Mail: gborgstahl@unmc.edu

8. PERFORMING ORGANIZATION REPORT NUMBER

9. SPONSORING / MONITORING AGENCY NAME(S) AND ADDRESS(ES)

U.S. Army Medical Research and Materiel Command
Fort Detrick, Maryland 21702-5012

10. SPONSORING / MONITORING AGENCY REPORT NUMBER

11. SUPPLEMENTARY NOTES

Original contains color plates: All DTIC reproductions will be in black and white

12a. DISTRIBUTION / AVAILABILITY STATEMENT

Approved for Public Release; Distribution Unlimited

12b. DISTRIBUTION CODE

13. ABSTRACT (Maximum 200 Words)

This research focuses on structural studies of human replication protein A (RPA) and RAD52 in recombination-based repair of double-stranded DNA breaks. This DNA repair pathway has been directly linked to breast cancer through BRCA1 and BRCA2 protein-protein interactions. Also, mutations in the ataxia telangiectasia (AT) gene are implicated in breast cancer and recently AT kinase was shown to phosphorylate the N-terminus of the 32 kDa subunit of RPA. The goals of the Borgstahl Laboratory are to understand the role of RPA phosphorylation and RPA/RAD52 protein-protein interactions in DNA repair. The ultimate goal of this research is to provide an understanding of this process at the atomic level.

14. SUBJECT TERMS

Breast Cancer

15. NUMBER OF PAGES

116

16. PRICE CODE

17. SECURITY CLASSIFICATION OF REPORT Unclassified	18. SECURITY CLASSIFICATION OF THIS PAGE Unclassified	19. SECURITY CLASSIFICATION OF ABSTRACT Unclassified	20. LIMITATION OF ABSTRACT Unlimited

Table of Contents

1. Abstract & seminar announcement: Jeffrey F. Ohren M.S. thesis May 5, 1999

2. Abstract & seminar announcement: Cathy M. Schellert M.S. thesis April 12, 1999

3. Abstract & seminar announcement: Krishnamurthy Rajeswari M.S. thesis July 12, 1999

4. Abstract & seminar announcement: Wasantha Ranatunga Ph.D. thesis July 24, 2002

5. Abstract & seminar announcement: Doba Jackson Ph.D. thesis July 31, 2002.

6. Abstract American Crystallographic Association National Meeting Buffalo, NY, May 1999.

7. Program Sigma Xi Scientific Research Society, Toledo, OH April 21, 1999.

8. Abstract for poster presentation: J. E. Habel and G. E. O. Borgstahl. "Dynamic Light Scattering Analysis of Full-Length, Human RPA14/32 Dimer: Purification, Crystallization and Self- Association." ACA National Meeting, St. Paul, MN , July 2000.

9. Abstract for poster presentation: G. Borgstahl, W. Ranatunga, D. Jackson, J. Habel, "Biochemical and Structural Studies on Replication Protein A and RAD52" Era of Hope Department of Defense Breast Cancer Research Program Meeting, Atlanta, GA, June 8-11, 2000.

10. Abstract for poster presentation: V. Kabaleeswaran and G. E. O. Borgstahl "Structural studies on full-length human replication protein A heterodimer", ACA National Meeting (V) Los Angeles, CA, July 2001.

11. Abstract for Talk: Doba Jackson and G. Borgstahl, "Characterization of the Human RAD52wt and RPA Protein protein Interaction", Sigma Xi Scientific Research Society (V), Toledo, OH April 20, 2001.

12. Abstract for Talk: Wasantha Ranatunga and G. Borgstahl, "Human Rad52 Protein has Extreme Thermal Stability", Sigma Xi Scientific Research Society (V), Toledo, OH April 20, 2001.

13. Abstract for poster presentation: W. Ranatunga, D. Jackson, Robert A Flowers III and G. E. O. Borgstahl "Human Rad52 Protein Has Extreme Thermal Stability", The Protein Society Meeting Philadelphia, 2001.

14. Abstract for poster presentation: D. Jackson, W. Ranatunga, and G. E. O. Borgstahl "Self-association of the C-terminal half of human Rad52 and its interaction with human replication protein A", The Protein Society Meeting Philadelphia, 2001.

15. Abstract for poster presentation: W. Ranatunga, D. Jackson and G. E. O. Borgstahl "Temperature Modulates the Higher-ordered Self-association of Rad52", Era of Hope Meeting, Orlando, Florida, September, 2002.

16. Abstract for poster presentation: D. Jackson, K. Dhar, M. Wold and G. E. O. Borgstahl "Analysis of the Rad52/RPA Complex: Evidence for Crosstalk Between RPA32, RPA70, Rad52 and ssDNA", Era of Hope Meeting, Orlando, Florida, September, 2002.

17. Reprint of publication: Habel, J. E., Ohren, J. F. and Borgstahl, G. E. O.[*] "Dynamic light scattering analysis of full-length, human RPA14/32 dimer: purification crystallization and self-association" *Acta Cryst.* **D57**, 254-259 (2001).

18. Reprint of publication: Ranatunga, W., Jackson, D., Lloyd, J. A., Forget, A. L., Knight, K. L. and Borgstahl, G. E. O.[*] "Human Rad52 Exhibits Two Modes of Self-association" *J. Biol. Chem.* **276**, 15876-15880 (2001).

19. Reprint of publication: Ranatunga, W., Jackson, D., Flowers II, R. A. and Borgstahl, G. E. O.[*] "Human Rad52 Protein Has Extreme Thermal Stability" *Biochemistry* **40**, 8557-8562 (2001)

20. Reprint of publication: D. Jackson, K. Dhar, J. K. Wahl, M. S. Wold and G. E. O. Borgstahl, G. E. O. "Analysis of the Rad52/RPA Complex: Evidence for Crosstalk Between RPA32, RPA70, Rad52 and ssDNA" *J. Mol. Biol.* **321**, 133-148 (2002).

21. Preprint of publication: Borgstahl, G. E. O. "The Use of Dynamic Light Scattering to Improve Your Chances of Growing Crystals of a Macromolecule" Invited Chapter in *Methods in Molecular Biology.* Accepted.

Introduction

This is the final report for Career Development Award (CDA) and IDEA award. These two awards have been combined under one award number (DAMD17-98-1-8251) and this report describes the progress made for both awards. A no-cost extension was issued October 2002 extending the project period until March 24, 2004.

Career Development

I am grateful to the BCRP and the CDA award which has made a tremendous difference in my career. Upon the award of the CDA the chair of the Chemistry department at the University of Toledo relieved me of my formal teaching responsibilities (which constituted 40% of my effort) in order to permit me to focus my efforts on breast cancer research and to develop a breast cancer focus in my research laboratory. I continued, during the course of the year, to train graduate students. This training includes an informal special topics course in protein crystallography. Six graduate students were involved in getting this program off the ground. Three of the students (Jeff Ohren, Krishnamurthy Rajeswari and Cathy Schellert) received M.S. degrees for their efforts in the summer of 1999. Summer 2002, two doctoral students (Doba Jackson and Wasantha Ranatunga) completed their dissertations and went on to postdoctoral fellowships (at Penn State and Lawrence Berkeley National Laboratory). One other Ph.D. student (Jennifer Garlitz) is in the process of writing her dissertation and is anticipated to graduate in 2004. All students worked on various aspects of this project for their dissertation research.

Tremendous progress was made in the development of my career in breast cancer research. I have received two prestigious awards for this research. On April 12, 2002 I was awarded the Sigma Xi, Dion D. Raftopoulos Award for Outstanding Research and on April 26, 2002 I was awarded the University of Toledo Outstanding Research Award. I have served on several study sections for the Army Breast Cancer NIH, NSF, NASA and most recently AHA. I was awarded an American Cancer Society Research Scholars Grant for Beginning Investigators for four years. Last year I was able to secure an exciting research intensive position in an excellent research environment to further my career in Breast Cancer research. I accepted a tenured Associate Professor position at the Eppley Cancer Research Institute and moved my laboratory to the University Of Nebraska Medical Center in Omaha, NE. I resigned from the University of Toledo September 13, 2002 and this grant was successfully transferred to the Eppley Cancer Research Institute. My new contact information is as follows:

Dr. Gloria Borgstahl
Eppley Institute for Cancer Research
987696 Nebraska Medical Center
10732A Lied Transplant Center
Omaha, NE 68198-7696
Office (402) 559-8578
FAX (402) 559-8577

Introduction to the project

This research focuses on structural studies of human replication protein A (RPA) and RAD52. RPA is a central molecule of the molecular machinery of DNA metabolism and is essential for DNA replication, recombination and repair [15]. RPA interacts specifically with RAD52 [10] and is involved in the early stages of recombination-based repair of double-stranded DNA breaks [12]. This DNA repair pathway has been directly linked to breast cancer through BRCA1 and BRCA2 protein-protein interactions [1]. Mutations in the ataxia telangiectasia (AT) gene are also implicated in breast cancer [8] and recently AT kinase was shown to phosphorylate threonine and serine residues of the 32 kDa subunit of RPA [6]. The goals of the Borgstahl laboratory are to understand the role of RPA phosphorylation and RPA/RAD52 protein-protein interactions in DNA repair. The ultimate goal of this research is to provide an understanding of this process at the atomic level. Towards this aim constructs of RPA, RAD52 and the RPA/RAD52 complex that are suitable for crystallization will be found and then crystallized for structure determination by X-ray crystallography.

Body

Changes to the original statement of work objectives from the original proposal were explained in the progress report for the period 25-Sep-98 – 24-Sep-99 and are repeated here, as appropriate. These changes to the statement of work were approved. In summary, objective 1 was abandoned, objectives 2 and 3 were completed and objective 4 is in progress. The text of the objective has been copied and below each objective the tasks which have been completed are described. When appropriate any changes that have occurred are explained and how the project will proceed in the next year of this award is explained.

Objective 1: Characterize the *in vitro* phosphorylation of RPA by immuneprecipitated preparations of ATM kinase.

Purified samples of RPA dimer and trimer were sent by the Borgstahl lab to Dr. Mira Jung at Georgetown University multiple times. This collaboration was confirmed in a letter from Dr. Jung in the original CDA and IDEA proposals. Initial results from the Jung lab (data not shown) were very encouraging and indicated that RPA was phosphorylated by ATM kinase. Unfortunately, then the postdoc in Dr. Jung's lab quit and Dr. Jung did not want to continue the collaboration. Since that time results demonstrating the phosphorylation of RPA by ATM kinase have been published by another group [6]. Therefore, this objective has been abandoned.

Objective 2: Characterize the effect RPA phosphorylation has on RPA interactions with RAD52.

Unpublished results communicated by Dr. Marc Wold at the University of Iowa indicated that a mutant form of RPA (with Asp replacing eight Ser and Thr phosphorylation sites on the N-terminus of RPA32) mimicked the changes in protein-protein interaction seen with *in vitro* phosphorylated RPA. By studying this eight-Asp mutant RPA we have been able to make critical decisions in the early stages of this award. ELISA assays with eight-Asp mutant RPA were performed to see if the interaction between RPA and RAD52 was modulated in any fashion. Results show that the wild-type RPA trimer and the eight-Asp mutant RPA trimer have similar interactions. This indicates that N-terminal phosphorylation of RPA32 probably does not effect RAD52 binding. In fact

6

ELISA data on other RPA mutants demonstrate that the N-terminus of RPA32 is not involved in the RPA-RAD52 interaction and we decided to not pursue the *in vitro* phosphorylation of RPA in the next year of the award, but to continue structural studies using the mutant RPAs as described below. Therefore, this objective was completed and was published. The reprint is included in the appendix: D. Jackson, K. Dhar, J. K. Wahl, M. S. Wold and G. E. O. Borgstahl, G. E. O. "Analysis of the Rad52/RPA Complex: Evidence for Crosstalk Between RPA32, RPA70, Rad52 and ssDNA" *J. Mol. Biol.* **321**, 133-148 (2002).

Objective 3: *Identify regions of RPA that interact with RAD52.*

Regions on the C-terminal domain of RPA32 and midsection of RPA70 have been identified as interacting with RAD52 in the previous reports. Recently we have found that Rad52 binding to RPA increases the ssDNA affinity of RPA. We have also found that binding by RPA disrupts the higher order self-association of Rad52. Of particular interest was the crosstalk between RPA70 and RPA32 binding to Rad52 that increase the affinity of RPA32 for ssDNA. These results have mechanistic implications in double strand break repair and together with our previously reported ELISA protein-protein interaction results were published this year. The reprint is included in the appendix: D. Jackson, K. Dhar, J. K. Wahl, M. S. Wold and G. E. O. Borgstahl, G. E. O. "Analysis of the Rad52/RPA Complex: Evidence for Crosstalk Between RPA32, RPA70, Rad52 and ssDNA" *J. Mol. Biol.* **321**, 133-148 (2002).

We also found that the RPA32 and RPA70 sites on Rad52 were separate but competitive. We determined that the RPA70 and the RPA32 sites lie within residues 218-313 of Rad52. These data are presented in the figures below. Several abstracts for presentations on this research are included in the appendix.

RPA70 and RPA32 binding sites on Rad52
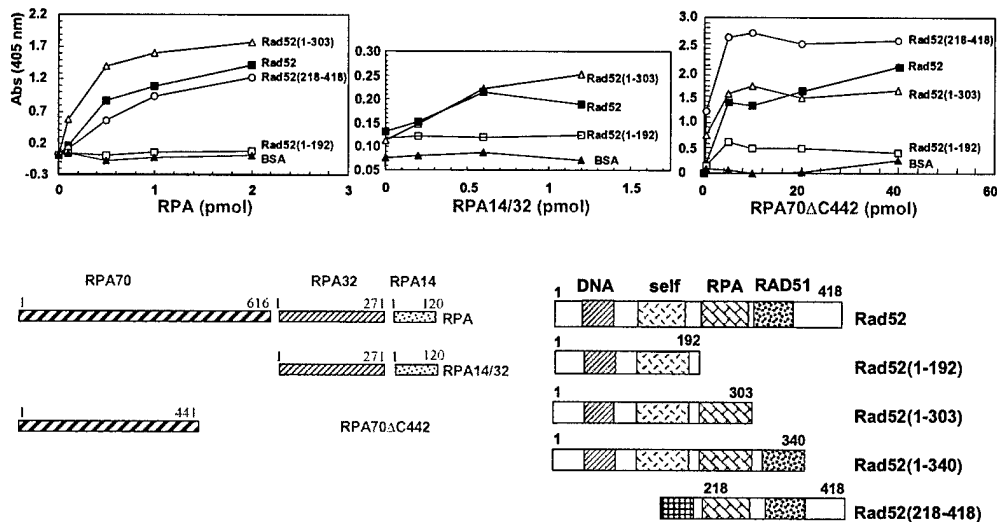
RPA70 and RPA32 both interact with amino acids 218-303 of Rad52.

Does RPA32 have a separate site on Rad52 or compete with RPA70?
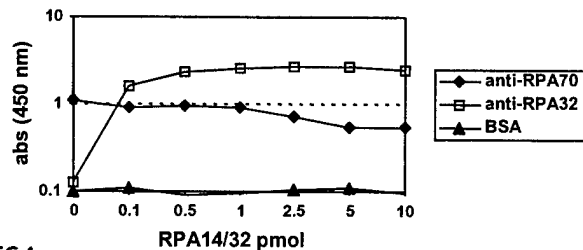
Competitive ELISA
• Coated plate with 10 pmol of Rad52 and washed.
• Knew 5 pmol RPA70ΔC442 saturated the complex with Rad52.
• 5 pmol of RPA70ΔC442 was mixed with a varying amount of RPA14/32 and added to the plate.
• anti-RPA1 detects RPA70ΔC442 and anti-RPA2 detects RPA14/32
• Detection with anti-RPA1 and anti-RPA2 was performed in separate wells.

Binding site determinants for RPA70 and RPA32 are separate on each subunit of Rad52. At high amounts of RPA14/32 there is competition with RPA70.

We reported results on differential scanning calorimetry data on wild-type and mutant human Rad52. Wild-type and mutant hRad52 data showed that the wild-type

protein has extreme thermal stability (T_M 115 °C). The N-terminal half is responsible for ring formation and the C-terminal half participates in the higher order self-association of rings. This work was written up and published in Biochemistry last year. The reprint is included in the appendix: Ranatunga, W., Jackson, D., Flowers II, R. A. and Borgstahl, G. E. O. "Human Rad52 Protein Has Extreme Thermal Stability" *Biochemistry* **40**, 8557-8562 (2001).

The study of the protein-protein interactions and thermal stability of Rad52 was extended to the homologous Rad52 from *S. cerevisia*. We developed purification protocols for wild-type and mutant scRAD52. By calorimetry, we found that the scRad52 was less stable than human and that the quaternary structure of the N-terminal mutant of scRad52 was less stable than in humans. Figures of these data are presented below. Several abstracts for presentations on this research are included in the appendix.

scRAD52 proteins expressed and purified
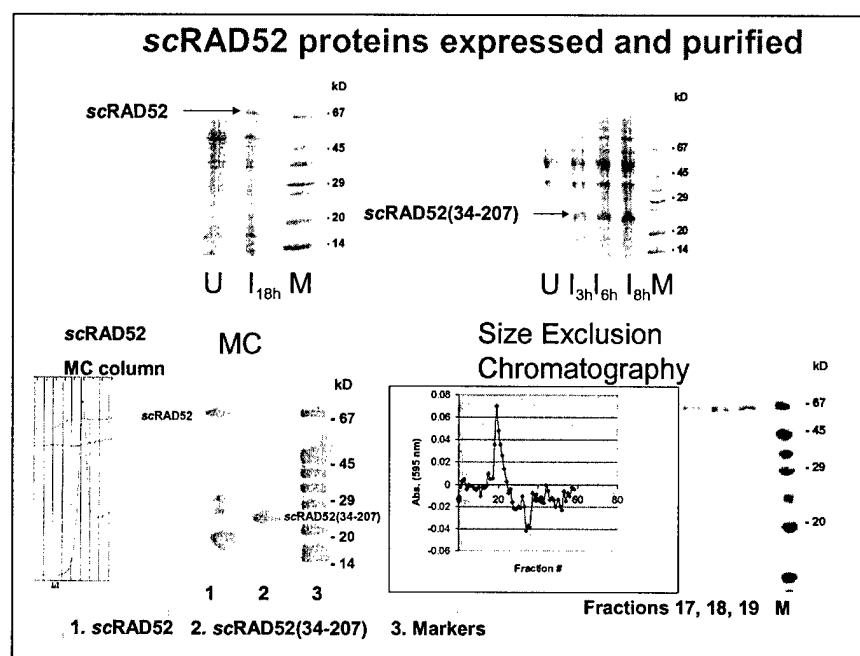
scRAD52 is not stable as scRAD52(34-207)

(DSC profiles)

scRAD52 — 0.58 mg/mL, 1.28 mg/mL, 2.50 mg/mL

scRAD52(34-207) — 0.69 mg/mL, 1.64 mg/mL, 1.90 mg/mL
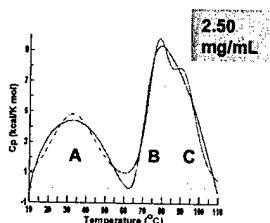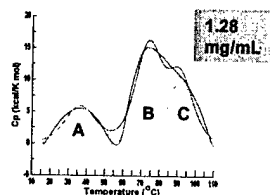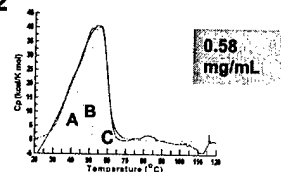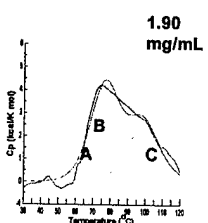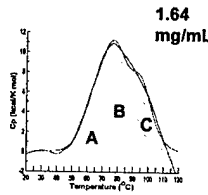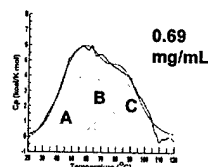
DSC melting temperatures for hRAD52 and scRAD52 proteins in nano-DSC

Line #	Protein	Comp.	Conc.	T_M (°C)	Conc.	T_M (°C)	Conc.	T_M (°C)	Conc.	T_M (°C)
1	scRAD52	A B C	0.58	41.4 51.8 57.5	0.66	34.3 48.1 88.2	1.3	37.0 74.1 91.7	2.5	33.7 77.9 91.5
2	scRAD52 (34-207)	A B C	0.69	47.6 62.0 85.6	0.76	59.8 74.7 84.4	1.6	62.5 77.5 96.0	1.9	60.2 77.1 99.3
3	hRAD52	A B C	0.50	38.7 80.5 89.9	0.52	38.5 74.2 90.1	1.2	36.3 75.5 90.8	2.5	35.2 78.8 96.1
4	hRAD52 (1-192)	B C' C	0.45	40.4 78.1	0.69	41.1 80.9	1.2	43.0 85.8	2.3	56.0 78.4 93.9

These results will be published this year.

<u>Objective 4:</u> *Test the feasibility of crystallizing the phosphorylated proteins obtained in objectives 1 and 2 and perform crystallization trials on the proteins obtained in objective 3.*

Several soluble active fragments (SAF) of RAD52 have been obtained for crystallization. Crystallization efforts have been continuously underway this year with no reportable outcomes. Of brighter note, several crystal forms of RPA heterodimer have been grown in four different space groups and excellent diffraction data collected at the synchrotron. A manuscript reporting the use of dynamic light scattering to promote crystallization and to study the self association of RPA14/32 was published and is included in the appendix: Habel, J. E., Ohren, J. F. and Borgstahl, G. E. O. "Dynamic light scattering analysis of full-length, human RPA14/32 dimer: purification crystallization and self-association" *Acta Cryst.* D57, 254-259 (2001). Also a review article for Methods in Molecular Biology was submitted and accepted on the same subject and a preprint is included in the appendix: Borgstahl, G. E. O. "The Use of Dynamic Light Scattering to Improve Your Chances of Growing Crystals of a Macromolecule" Invited Chapter in *Methods in Molecular Biology* accepted. Several abstracts for presentations on this research are included in the appendix.

The solution of this structure by MAD phasing continued this year and the structure is still in progress.

<u>Significance – first RPA14/32 structure.</u> The crystal structure of human RPA14/32 will reveal for the first time the structure of the intact RPA32 subunit, including the N-terminus, which is hyperphosphorylated during apoptosis and in response to DNA damage, and the C-terminal domain, which interacts with several DNA metabolic proteins, including Rad52. Comparison of this structure with that of the already determined proteolytic core of RPA14/32 (protein data bank entry 1QUQ) will reveal why the core binds ssDNA weakly while the intact protein does not bind ssDNA [2].

A combination of two phasing methods, molecular replacement and multi-wavelength anomalous dispersion (MAD), are being used to solve the phase problem for the first structure of RPA14/32 [7]. As soon as the first native diffraction data on RPA14/32 were collected, extensive attempts to solve the structure by molecular replacement using the coordinates of RPA14(3-116)/RPA32(45-170) from the protein data bank (entry 1QUQ) were made. Solutions were found and in some cases, weak density for the missing domains could be seen. However, phasing was never sufficient to produce clean maps that could be reliably interpreted for the missing domains. All attempts on all crystal forms failed. There are three possible reasons for this. Entry 1QUQ provides only 56% of the structure in the crystals. RPA14(3-116) and RPA32(45-170) are structurally very similar (see Fig. 4 and Fig. 2 in Bochkarev et al. (1999)) and molecular replacement may put 14 where 32 belongs and vice versa. Finally, perhaps the structure of the full-length RPA14/32 differs from the protease resistant core. Ambiguity between the hexagonal space groups and number of molecules in the asymmetric unit has also been a problem.

Unfortunately, the two MAD datasets reported in last years report were insufficient to completely phase the RPA14/32 crystal [5]. This is most likely due to problems in data quality and some personnel problems. A new student has been recruited to work on this project, he has learned the techniques and he has been very successful this year in growing fresh crystals of RPA14/32 for more data collection.

This data collection on heavy atom derivatives will be performed in the last year of the grant.

Purification of several RPA and Rad52 constructs were performed. Unfortunately no crystals grew. Neither protein will crystallize by itself. Light scattering data indicates that the complex of RPA/Rad52 is more condensed and stable than the holoproteins alone. Crystallization screening will continue into the last year of this award. In particular, as a result of our protein-protein results we will pursue crystals of the full length Rad52 in complex with a peptide of RPA, as well as, the full length RPA in complex with a peptide of Rad52.

Key Research Accomplishments

- Developed many mouse monoclonal antibodies against RAD52.
- Determined phosphorylation of RPA is unlikely to alter the interaction of RPA with RAD52.
- Determined that the RAD52 interaction surface on RPA is composed of the C-terminal domain of RPA32 and a central section of RPA70.
- Identified several constructs of RAD52 suitable for crystallization trials.
- Crystallized human RPA14/32 dimer in several space groups
- Collected cryocooled synchrotron X-ray diffraction data on native and heavy atom derivatives of RPA14/32 crystals.
- Grew selenylmethionine RPA14/32 crystals and collected several MAD diffraction data sets for solution of the phase problem.
- Constructs of phosphorylation mutant of RPA14/32 and yeast RFA14/32 were made and proteins purified for crystallization.
- Purified several mutant RPA and RAD52 mutants for examination of the role of RPA./RAD52 interaction in activity.
- Electron micrograph data in combination with dynamic light scattering data indicate that the N-terminal half of RAD52 is involved in ring formation and the C-terminal half is responsible for super ring aggregation.
- Differential scanning calorimetry data indicates RAD52 has extreme thermal stability.
- Solved of the crystallographic phase problem for crystals of full length human RPA14/32.
- Constructs of phosphorylation mutant of heterotrimeric and dimeric human RPA and yeast RFA were purified and screened for crystallization.
- Purified several mutant RPA and RAD52 mutants for examination of the role of RPA/RAD52 interaction in activity.
- Determined the location of the binding site for Rad52 on RPA70 and discovered that the formation of Rad52/RPA complex increases the ssDNA affinity of RPA through DNA binding domain D on RPA32.
- Found that the RPA32 and RPA70 sites on Rad52 were separate but competitive.
- Determined that the RPA70 and the RPA32 binding sites lie within residues 218-313 of Rad52.
- Partially solved of the crystallographic phase problem for crystals of full length human RPA14/32.

- Purified wild-type and mutant scRAD52, tested for aggregation, screened for crystals and calorimetry data was collected.

Reportable Outcomes

- The following personnel received pay from this grant
    1. Dr. Gloria Borgstahl
    2. Cathy Schellert
    3. Jeffrey Ohren
    4. Krishnamurthy Rajeswari
    5. Doba Jackson
    6. Wasantha Ranatunga
    7. Jennifer Garlitz
- Degrees obtained that were supported by this award (attached in appendix):
    1. Cathy Schellert, M.S. "Purification and Crystallization of Pyruvate Dehydrogenase Kinase and Purification and Characterization of RAD52 Domains" April 12, 1999.
    2. Jeffrey F. Ohren, M.S. "The Purification, Crystallization and Initial Crystallographic Analysis of the Dimer of the 14 and 32 KDa Subunits of Human Replication Protein A" May 5, 1999.
    3. Krishnamurthy Rajeswari, M. S. "The Cloning, Expression, Purification and Characterization of Soluble, Active Fragment (SAF) Constructs of Human RAD52 Suitable for Crystallization" July 12, 1999.
    4. Wasantha Ranatunga, "Expression, purification, biophysical characterization and preliminary crystallization of human and yeast RAD52 proteins", July 24, 2002.
    5. Doba Jackson, "Analysis of the human Rad52/RPA complex: characterization of the interacting regions, DNA binding activity, and higher-order complexes", July 31, 2002.
- Development of cell lines, tissue or serum repositories:

    Several mouse monoclonal antibodies to human RAD52 were developed and are available upon request.
- Employment received on experience supported by this award.
    1. Cathy Schellert was accepted to Medical School at the University of Cincinnati, OH. This admission into medical school was based in part on her masters thesis research.
    2. Based on the research experience she gained from her masters thesis Krishnamurthy Rajeswari has taken a research position at Genentech in San Francisco, CA.
    3. Matthew Pokross, a research technician in the Borgstahl laboratory, has taken a research position at Proctor and Gamble in Cincinnati, OH. This position was offered to him based on the protein purification and crystallization experience he gained in the Borgstahl laboratory.
    4. Upon his graduation Dr. Wasantha Ranatunga obtained a postdoctoral position at the University of California, Berkeley.

5. Upon his graduation Dr. Doba Jackson obtained a postdoctoral position at Penn State.

6. Promotion and tenure of the Principal Investigator

    May 2002   Associate Professor with tenure; The University of Toledo, Department of Chemistry, Toledo, OH.

    Aug 2002   Associate Professor with tenure; Eppley Cancer Research Institute, Omaha, NE.

Manuscripts, abstracts, presentation (attached in appendix):

1. Jeff E. Habel, Jeff Ohren, and Gloria Borgstahl, "Enhanced Crystallization of Human Replication Protein A", American Crystallographic Association National Meeting (V) Buffalo, NY, May 22-27, 1999.

2. Krishnamurthy Rajeswari and Gloria Borgstahl, "Cloning, Expression, Purification and Characterization of Soluble Active Fragments (SAF) of RAD52 Suitable for Crystallization", Sigma Xi Scientific Research Society (V), Toledo, OH April 21, 1999. *Award winning Masters Thesis presentation.*

3. poster presentation: J. E. Habel and G. E. O. Borgstahl. "Dynamic Light Scattering Analysis of Full-Length, Human RPA14/32 Dimer: Purification, Crystallization and Self- Association." ACA National Meeting, St. Paul, MN , July 2000.

4. poster presentation: G. Borgstahl, W. Ranatunga, D. Jackson, J. Habel, "Biochemical and Structural Studies on Replication Protein A and RAD52" Era of Hope Department of Defense Breast Cancer Research Program Meeting, Atlanta, GA, June 8-11, 2000.

5. manuscript accepted into Acta Crystallographica D "Dynamic light scattering analysis of full-length, human RPA14/32 dimer: purification, crystallization and self-association"

6. Poster presentation: V. Kabaleeswaran and G. E. O. Borgstahl "Structural studies on full-length human replication protein A heterodimer", ACA National Meeting (V) Los Angeles, CA, July 2001.

7. Talk: Doba Jackson and G. Borgstahl, "Characterization of the Human RAD52wt and RPA Protein protein Interaction", Sigma Xi Scientific Research Society (V), Toledo, OH April 20, 2001.

8. Talk: Wasantha Ranatunga and G. Borgstahl, "Human Rad52 Protein has Extreme Thermal Stability", Sigma Xi Scientific Research Society (V), Toledo, OH April 20, 2001.

9. Publication: Habel, J. E., Ohren, J. F. and Borgstahl, G. E. O. "Dynamic light scattering analysis of full-length, human RPA14/32 dimer: purification crystallization and self-association" *Acta Cryst.* **D57**, 254-259 (2001).

10. Publication: Ranatunga, W., Jackson, D., Lloyd, J. A., Forget, A. L., Knight, K. L. and Borgstahl, G. E. O. "Human Rad52 Exhibits Two Modes of Self-association" *J. Biol. Chem.* **276**, 15876-15880 (2001). *Accepted without revision.*

14

11. Publication: Ranatunga, W., Jackson, D., Flowers II, R. A. and Borgstahl, G. E. O. "Human Rad52 Protein Has Extreme Thermal Stability" *Biochemistry* **40**, 8557-8562 (2001).

12. Abstract for poster presentation: W. Ranatunga, D. Jackson and G. E. O. Borgstahl "Temperature Modulates the Higher-ordered Self-association of Rad52", Era of Hope Meeting, Orlando, Florida, September, 2002.

13. Abstract for poster presentation: D. Jackson, K. Dhar, M. Wold and G. E. O. Borgstahl "Analysis of the Rad52/RPA Complex: Evidence for Crosstalk Between RPA32, RPA70, Rad52 and ssDNA", Era of Hope Meeting, Orlando, Florida, September, 2002.

14. Abstract for poster presentation: W. Ranatunga, D. Jackson and G. E. O. Borgstahl "Temperature Modulates the Higher-ordered Self-association of Rad52", The Protein Society Meeting Pittsburg, 2002.

15. Abstract for poster presentation: D. Jackson, K. Dhar, M. Wold and G. E. O. Borgstahl "Analysis of the Rad52/RPA Complex: Evidence for Crosstalk Between RPA32, RPA70, Rad52 and ssDNA", The Protein Society Meeting Pittsburg, 2002.

16. Reprint of publication: D. Jackson, K. Dhar, J. K. Wahl, M. S. Wold and G. E. O. Borgstahl, G. E. O. "Analysis of the Rad52/RPA Complex: Evidence for Crosstalk Between RPA32, RPA70, Rad52 and ssDNA" *J. Mol. Biol.* **321**, 133-148 (2002).

Research Proposal activity

1. "Structural Studies on Replication Protein A" Borgstahl PI, American Cancer Society Research Scholars Grant for Beginning Investigators, Funded, Total budget $720,000 for 4 years. *This proposal was ranked 1/57 by the Genetic Mechanisms in Cancer Committee and rated as "Outstanding".*

Conclusions

Protein-protein interactions between RPA and RAD52 are important in the first step of the double-strand break repair pathway. RPA is phosphorylated in a cell-cycle dependent manner and by several enzymes *in vitro* including AT kinase. The role of RPA phosphorylation is not well understood, but it does not appear to modulate the interaction of RPA with RAD52. Interestingly, RPA phosphorylation has recently been shown to promote the dissociation of RPA14/32 dimer from the RPA70 subunit. In the final year of this award we will continue to investigate the structural consequences of phosphorylation on RPA structure in the context of the RPA heterotrimer and the dimer. Mutation of Thr and Ser to Asp will be used to mimic phosphorylation. To date, only proteolytically stable core fragments of RPA have been crystallized and their structures solved. During year 1, of this award the full-length RPA14/32 dimer was crystallized in two crystal forms, many sets of X-ray diffraction data were collected and the structure will be solved in the second year of this award. RAD52 was been found to aggregate in solution and electron micrograph studies show that it forms ring structures in solution. These aggregates are polydisperse with 8-10 monomers per ring and multiple rings can associate to form higher molecular weight aggregates. Such aggregation has been problematic for crystallization. Fortunately, we have found several suitable constructs that are soluble and retain single-stranded DNA binding and/or RPA binding activities.

During year 2, the crystallization of RPA14/32 was further extended and more data was collected and a manuscript concerning this work was published. Constructs for expression of yeast RFA14/32 and a phosphorylation mimic of human RPA14/32 were created. Dynamic light scattering data and electron micrographs and have delineated the roles of the N- and C-terminal halves of RAD52 in ring formation and super ring aggregation. Differential scanning calorimetry data demonstrated the extreme thermal stability of RAD52 and stimulated new ideas on how to crystallize and purify RAD52. Crystallization trials for all constructs discussed are continuing. Structural determination of these proteins by X-ray crystallography will reveal a wealth of information on how they function in double-strand break repair. In year 3, several manuscripts were prepared and published. Key information on the effect of Rad52 binding to RPA on ssDNA affinity and Rad52 self-association were made. The crystallographic phase problem for human RPA14/32 was partially solved. In year 4, the details of the contact regions of the RPA/Rad52 complex and the effect of the RPA/Rad52 complex on the ssDNA affinity was published. Wild-type and mutant scRad52 was purified and screened for crystals. Interesting calorimetric data for scRad52 was obtained. New crystals of RPA14/32 were obtained for solution of the phase problem. The laboratory moved to the Eppley Cancer Research Institute.

References

1. Bertwistle, D. and A. Ashworth, *Functions of the BRCA1 and BRCA2 genes.* Curr. Opin. Genet. Dev., (1998). **8**, 14-20.

2. Bochkareva, E., L. Frappier, A.M. Edwards and A. Bochkarev, *The RPA32 Subunit of Human Replication Protein A Contains a Single-stranded DNA-binding Domain.* J. Biol. Chem., (1998). **273**, 3932-3936.

3. Bourgeois, D., *New processing tools for weak and/or spatially overlapped macromolecular diffraction patterns.* Acta Cryst., (1999). **D55**, 1733-1741.

4. Dauter, Z., M. Dauter and K.R. Rajashankar, *Novel approach to phasing proteins: derivatization by short cryo-soaking with halides.* Acta Cryst., (2000). **D56**, 232-237.

5. Doublie, S., *Preparation of selenomethionyl proteins for phase determination.* Methods Enzymol., (1997). **276**, 523-530.

6. Gately, D.P., J.C. Hittle, G.K.T. Chan and T.J. Yen, *Characterization of ATM Expression, Localization and Associated DNA-dependent Protein Kinase Activity.* Mol. Biol. Cell, (1998). **9**, 2361-2374.

7. Hendrickson, W.A. and C.M. Ogata, *Phase Determination from Multiwavelength Anomalous Diffraction Measurements.* Methods Enzymol., (1997). **276**, 494-523.

8. Lavin, M., *Role of the ataxis-telangiectasia gene (ATM) in breast cancer.* BMJ, (1998). **317**, 486-487.

9. McRee, D.E., *Practical Protein Crystallography.* 1993, San Diego, CA: Academic Press, Inc.

10. Park, M.S., D.L. Ludwig, E. Stigger and S.H. Lee, *Physical interaction between Human RAD52 and RPA is Required for Homologous Recombination in Mammalian Cells.* J. Biol. Chem., (1996). **271**, 18996-19000.

11. Read, R.J., *Model phases: Probabilities and bias.* Methods Enzymol., (1997). **277**, 110-128.

12. Shinohara, A. and T. Ogawa, *Homologous recombination and the roles of double-strand breaks.* Trends Biochem Sci, (1995). **20**, 387-391.

13. Terwilliger, T.C., *Maximum-likelihood density modification.* Acta Cryst., (2000). **D56**, 965-972.

14. Terwilliger, T.C. and J. Berendzen, *Automated structure solution for MIR and MAD.* Acta Cryst., (1999). **D55**, 849-861.

15. Wold, M.S., *RPA: A Heterotrimeric, Single-Stranded DNA-Binding Protein Required for Eukaryotic DNA Metabolism.* Ann. Rev. Biochem., (1997). **66**, 61-91.

SEMINAR

The University of Toledo
Department of Chemistry

❖❖❖

Jeffrey F. Ohren
M.S. Presentation

"The Purification, Crystallization and Initial Crystallographic Analysis of the dimer of the 14- and 32-Kilodalton Subunits of Human Replication Protein A"

Wednesday, May 5, 1999 at 4:00 p.m.

BO 1053

Inquiries can be made of Dr. Gloria Borgstahl, 530-1501

Refreshments courtesy of Takayo Inoue and Doba Jackson

a

An Abstract of

The Purification, Crystallization and Initial Crystallographic
Analysis of the Dimer of the 14- and 32- Kilodalton
Subunits of Human Replication Protein A

Jeffrey F. Ohren

As Partial Fulfillment of the Requirements of
the Master of Science Degree in Chemistry

The University of Toledo
May 1999

Replication protein A (RPA) is a single-stranded DNA-binding protein that has been found in all eukaryotic cells examined to date. The importance of RPA in DNA replication was first identified in the *in vitro* SV40 replication assay. Subsequently, RPA has been shown to be absolutely required for DNA replication, DNA recombination and DNA damage repair. Human RPA is a heterotrimeric protein and consists of three subunits of approximately 14-, 32- and 70- kDa. While the heterotrimer is required for enzymatic function, the 14- and 32- kDa subunits (RPA14/32) form a soluble, stable complex both *in vivo* and *in vitro*.

The dimer of RPA14/32 has been recombinantly expressed in *E. coli*, purified, characterized and crystallized as part of this research. Crystals of RPA14/32 have been grown in hanging-drop vapor-diffusion trials using ammonium sulfate (A/S) as a precipitating reagent. Results from dynamic light scattering experiments confirmed the importance of the addition of organic modifiers in the crystallization of the dimer. Large hexagonal single crystals of RPA14/32 have been grown from 20% saturated A/S, 10% methanol or 10% acetonitrile and 0.1 M Hepes pH 7. A small cryo-preserved crystal of RPA14/32 was grown from 2.4 M A/S, 30% MPD and 0.1 M Hepes pH 7.0 and was analyzed by X-ray diffraction at the Stanford Synchrotron Radiation Laboratory beamline

1-5 area detector. The crystal has initially been classified in the trigonal crystal system with lattice constants a = b = 62.5, c = 273.0 Å; $\alpha = \beta = 90°$, $\chi = 120°$. The crystal diffracted to a lattice spacing of approximately 3.2 Å.

SEMINAR

THE UNIVERSITY OF TOLEDO
DEPARTMENT OF CHEMISTRY

Cathy M. Schellert
M.S. Presentation

"Purification and Crystallization of
Pyruvate Dehydrogenase Kinase and
Purification and Characterization of Rad52
Domains"

Monday, April 12 at 4:00 p.m.

BO 1053

Inquiries can be made of Dr. Gloria Borgstahl, 530-1501

Refreshments courtesy of Jennifer Tesar and Patrick Wheeler

An abstract of

**Purification and Crystallization of Pyruvate Dehydrogenase Kinase
and Purification and Characterization of Rad52 Domains**

Cathy M. Schellert

**Submitted as partial fulfillment
of the requirements for the
Master of Science Degree in Chemistry**
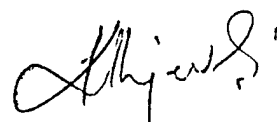
The University of Toledo
May, 1999

The three dimensional structure of high molecular weight proteins can be visualized via crystallography. Good crystals are required in order to get useful information from X-ray diffraction. For crystallization to be effective, proteins need to be pure in terms of lack of contaminants as well as conformationally pure, or monodisperse. The protein pyruvate dehydrogenase kinase from *Ascaris suum* has been purified using metal chelate and anion exchange chromatography. Through dynamic light scattering, the kinase has been shown to be conformationally pure, or monodisperse. Crystallization conditions have been identified in ammonium sulfate/HEPES, sodium cacodylate/sodium acetate trihydrate, potassium sodium tartrate tetrahydrate, imidazole/sodium acetate trihydrate, and Tris-HCl/PEG 4000 conditions. Crystallization was optimized using seeding techniques and additives. Small rectangular crystal rods of 200 μm x 20 μm size were grown in ammonium sulfate/HEPES that did not result in diffraction in the X-ray beam. Polycrystalline thin plates were obtained upon the addition of NAD^+.

The protein human Rad52 domain constructs have been purified using metal chelate chromatography. Dynamic light scattering analysis of the domain constructs shows severe aggregation of the domains 1+2+3, 1+2+3+4, and full length Rad52 alone and when incubated with detergents and additives. However, the domain 1+2 is present in a monodisperse solution upon the addition of 5% ethanol and is thereby most likely to crystallize.

SEMINAR

THE UNIVERSITY OF TOLEDO
DEPARTMENT OF CHEMISTRY

Krishnamurthy Rajeswari
M.S. Presentation

"The Cloning, Expression, Purification and Characterization of Soluble, Active Fragment (SAF) Constructs of Human RAD52 Suitable for Crystallization"

Monday, July 12 at 4:00 p.m.

BO 1059

Inquiries can be made of Dr. Gloria Borgstahl, 530-1501

An Abstract of
The Cloning, Expression, Purification and Characterization of Soluble, Active Fragment
(SAF) Constructs of Human RAD52 Suitable for Crystallization

Krishnamurthy Rajeswari

DNA can be damaged by various factors like chemicals, sunlight and ionizing radiation. This damage can lead to cell cycle arrest and eventually cell death, or if propagated, can result in degenerative diseases like cancer. Cells are equipped with mechanisms for repairing such damages to the DNA. Recombination-based DNA repair is one such process. In eukaryotes, the proteins encoded by the *Rad52* epistasis group (*Rad50-52, 54, 55, 57, 59, MRE11 and XRS2*) along with replication protein A (*RPA*) are mainly involved in the recombination-based repair of double-strand breaks (DSB) in DNA.[1,2] The primary focus of this study is on human RAD52 protein.

Human RAD52 is implicated as an essential player in DSB repair in eukaryotes, and the repair is mainly thought to be achieved by homologous recombination.[3] Despite the crucial role played by RAD52 in recombination and DSB repair, very little is known about the biochemistry of the protein. The human *Rad52* gene codes for a protein of 418 amino acids with a predicted molecular weight of 46.1 kDa. Homologues of *Rad52* gene have been found in several other eukaryotic organisms. The versatility of the RAD52 protein is highlighted by the fact that various domains within the protein take part in diverse biochemical roles like DNA binding, self-association, interaction with RPA and interaction with RAD51.[4,5,6,7] It would be interesting to understand the interactions between RAD52 and other proteins at the molecular level.

Protein crystallography can help us understand the structure-function relationship of proteins. To use this technique, one must attempt to have high quality crystals that diffract X-rays to high resolution. However, in order to attempt to crystallize a protein, the protein sample must be highly pure, monodisperse, homogeneous and soluble at a concentration of at least 4-10 mg/mL. In our lab, we have found that RAD52 cloned and expressed in pET28b vector is a highly aggregated molecule in solution. Recently, it has been shown by electron microscopic studies, that RAD52 aggregates in solution to form ring structures. The size of the ring increases with increasing concentration of RAD52.[8] The aggregation of RAD52 is a major stumbling block for structural studies on this protein. In order to circumvent this problem, soluble active fragment (SAF) constructs of human RAD52 that are suitable for crystallization and X-ray crystallographic studies have been designed and synthesized. Design, synthesis and characterization of the SAF constructs of human Rad52 will be presented.

References:

1. Shinohara. A. & Ogawa. T. (1995). Homologous recombination and the roles of double-strand breaks. *Trends Biochem. Sci.* 20, 587-591.

2. Dyke, E.V., Stasiak, A.Z., Stasiak, A. & West, S.C. (1999). Binding of double-strand breaks in DNA by human RAD52 protein. *Nature* **398**, 728-731.

3. Park, M.S., Ludwig, D.L., Stigger, E. & Lee. S.H. (1996). Physical interaction between human Rad52 and RPA is required for homologous recombination in mammalian cells. *J. Biol. Chem.* **271**, 18996-19000.

4. Reddy, G., Golub, E.I. & Radding. C.M. (1997). Human Rad52 promotes single-strand annealing followed by branch migration. *Mutat. Res.* **377**, 53-59.

5. Shen, Z., Peterson, S.R., Comeaux, J.C., Zastrow, D., Moyzis, R.K. & Bradbury, E.M. (1996). Self-association of human Rad52 protein. *Mutat. Res.* **364**, 81-89.

6. Shen, Z., Cloud, K.G., Chen, D.J. & Park, M.S. (1996). Specific interaction between human Rad51 and rad52 proteins. *J. Biol. Chem.* **271**, 148-152.

7. Benson, F.E., Baumann, P. & West, S.C. (1998). Synergistic actions of Rad51 and Rad52 in recombination and DNA repair. *Nature* **391**, 401-406.

8. Dyke, E.V., Hajibhageri, M.A., Stasiak, A. & West, S.C. (1998). Visualization of human Rad52 protein and its complexes with human Rad51 and DNA. *J. Mol. Biol.* **284**, 1027-1038.

THE UNIVERSITY OF
TOLEDO

DEPARTMENT OF CHEMISTRY
SEMINAR SERIES

Wasantha K.W. Ranatunga
Ph.D. Presentation

"Expression, purification, biophysical characterization and prelinary crystallization of human and yeast RAD52 proteins"

Wednesday, July 24, 2002

4:00 p.m.

BO 1053

Inquiries can be made of:
Dr. Gloria Borgstahl, 419-530-1501

An Abstract of

Expression, purification, biophysical characterization and

preliminary crystallization of

human and yeast RAD52 proteins

by

Wasantha K. W. Ranatunga

Submitted as partial fulfillment of the requirements for

the Doctor of Philosophy in Chemistry

The University of Toledo
August 2002

Defects in recombination-based DNA repair lead to human breast cancer and familial degenerative diseases.[1,2] The RAD52 epistasis group gene products, especially the human RAD52 (hRAD52) protein, play important roles in double strand break (DSB) repair.[3,4] The focus of this work is to further characterize hRAD52 protein in order to contribute to our understanding of DSB repair and to contribute to the future solution of the three-dimensional structure. Subunits of hRAD52 interact with each other to form rings.[3] hRAD52 rings cluster with each other to form higher-order aggregates. This nature of hRAD52 makes it hard to crystallize. The main task of this research was to disrupt the aggregation and make hRAD52 suitable for crystallization. Due to the biological interest of hRAD52 and

the apparent biochemical importance of RAD52 self-association in DNA-repair, its multiple levels of self-association[5] and stability[6] were studied using biophysical methods such as dynamic light scattering (DLS) and differential scanning calorimetry (DSC). The stability of hRAD52 was studied by using DSC. To investigate the basis for the extreme stability of hRAD52 that was discovered, two mutants were also studied, hRAD52(1-192) and hRAD52(218-418).[6] The effects of temperature and protein concentration on the hydrodynamic radius (R_H) of hRAD52 were studied by DLS. Results showed that the aggregation was due to two levels of self-association of hRAD52, ring formation and association of rings with rings. DSC profiles and DLS data indicated that hRAD52 protein was extremely stable and multiple levels of self-association of hRAD52 could be disrupted by heating up to 50 °C.[6] Furthermore, the samples of hRAD52 at 50 °C and hRAD52(1-192) at 20 °C were monomodal and suitable for crystallization. A hypothetical model of the effects of protein aggregation state on thermal stability was developed. Based on these findings, a novel approach for purification of hRAD52 and for crystallization was established. Similar studies were performed for *Saccharomyces cerevisiae* RAD52 (*sc*RAD52) and mutant *sc*RAD52(34-207). DSC and DLS data indicated that the *sc*RAD52 was less stable than hRAD52 and *sc*RAD52(34-207). Crystallization trials were set-up at 50 °C for hRAD52 and preliminary microcrystalline aggregates of hRAD52, *sc*RAD52 and hRAD52(1-192) were obtained.

[1] Sharan, S. K., Morimatsu, M., Albrecht, U., Lim, D. -S., Regal, E., Dinh, C., Sands, A., Eichele, G., Hasty, P., and Bradley, A., Embryonic lethality and radiation hypersensitivity mediated by RAD51 in mice lacking BRAC2. *Nature*, **386**, 804-810 (1997).

[2] Venkitaraman, A. R., Functions of BRCA1 and BRCA2 in the biological response to DNA damage. *J. Cell Sci.*, **114**, 3591-3598 (2001).

[3] Park, M.S., Ludwig, D. L., Stigger, E., and Lee, S. -H., Physical interaction between human RAD52 and RPA is required for homologous recombination in mammalian cells. *J. Biol. Chem.*, **271**, 18996-19000 (1996).

[4] Shen, Z., Cloud, K. G., Chen, D. J. and Park, M. S., Specific interaction between the human RAD51 and RAD52 protein. *J. Biol. Chem.*, **271**, 148-152 (1996).

[5] Ranatunga, W., Jackson, D., Lloyd, J., Forget, A. L., Knight, K. L., and Borgstahl, G. E. O., Human RAD52 exhibits two modes of self-association. *J. Biol. Chem.*, **276**, 15876-15880 (2001).

[6] Ranatunga, W., Jackson, D., Flowers II, R. A., and Borgstahl, G. E. O., Human RAD52 protein has extreme thermal stability. *Biochemistry*, **40**, 8557-8562 (2001).

THE UNIVERSITY OF
TOLEDO

DEPARTMENT OF CHEMISTRY
SEMINAR SERIES

Doba Jackson
Ph.D. Presentation

"Analysis of the human Rad52/RPA Complex: Characterization of the interacting regions, DNA binding activity, and higher-order complexes"

Wednesday, July 31, 2002

4:00 p.m.

BO 1053

Inquiries can be made of:
Dr. Gloria Borgstahl, 419-530-1501

An Abstract of

Analysis of the human Rad52/RPA complex: characterization of the interacting regions, DNA binding activity, and higher-order complexes

by

Doba Jackson

Submitted as partial fulfillment of the requirements for the Doctor of Philosophy degree

in Chemistry

The University of Toledo

Aug 2002

Rad52 and replication protein A (RPA) are two proteins involved in the repair of double-stranded breaks in DNA. Knowing how these two proteins interact is necessary to understand how cells repair double-stranded breaks.

In this thesis, the interaction of Rad52 and RPA, as well as the functional aspects of the complex, was examined. A series of deletion mutants for RPA and Rad52 were

iii

used to map out the binding sites on each protein. Two sites were found on RPA (RPA70 residues 168-327; RPA32 residues 240-271) and one site on Rad52 (residues 218-303). The binding sites on RPA for Rad52 were similar to the binding sites mapped for other DNA repair proteins such as xeroderma pigmentosa group A (XPA), uracil DNA glycosylase (UNG) and Rad51. The binding regions of RPA and Rad52 contain an abundance of charged surface residues. The complex was modulated by the ionic strength of the medium. A putative RPA70 binding site with sequence homology of 32% identity (79% similar) to the RPA32 binding site was found. The complex also had enhanced ssDNA binding affinity relative to RPA. The enhanced ssDNA binding affinity was due to the activation of the fourth ssDNA binding domain (DBD-D) in RPA. Rad52 self-association of monomers to form rings was found to be governed by an N-terminal domain. The C-terminal interactions were found to be responsible for higher-order interactions between Rad52 rings. Rad52 self interactions and Rad52/RPA binding interactions were studied by dynamic and static light scattering. RPA binding to Rad52 competes with the formation of higher-order aggregates of Rad52 ring in solution. Future implications of Rad52 self-association and RPA interactions was discussed. The work here further extends the current level of knowledge for the Rad52/RPA complex.

American Crystallographic Association

1999 Annual Meeting
in conjunction with the
an Association for Crystal Gr

Buffalo, New York
May 22-27, 1999

E0111

Enhanced Crystallization of Human Replication Protein A. Jeff E. Habel, Jeff Ohren, and Gloria Borgstahl.

Human replication protein A (hRPA) is an essential protein in DNA metabolism including processes such as DNA replication, repair, recombination and transcription. In addition to binding both double and single stranded DNA, hRPA also interacts with other DNA metabolic proteins including RAD51, RAD52, P53, T antigen, polymerase (, etc. A fundamental problem in the crystallization of DNA metabolizing proteins is the inherent "stickiness" of the purified protein. This stickiness can, in part, be attributed to all of the protein-protein interaction surfaces on the protein molecule which results in a solution where the conformation of the protein can vary widely, also known as a polydisperse solution. Protein crystallization occurs more readily in solutions where the conformation of the protein molecules are identical and monodisperse. Dynamic light scattering (DLS) is one method used for determining the dispersity of a solution and was utilized in the crystallization of hRPA to elucidate certain organic modifiers that, when added to a solution of concentrated hRPA, caused the resulting protein solution to become monodisperse. As a result, the amount of time necessary for the crystallization of hRPA was reduced from several months to several days in addition to the discovery of new crystallization conditions and possibly new crystal habits.

ΣΞ

Sigma Xi Scientific Research Society of The University of Toledo

presents

The Twentieth Annual Graduate Research Symposium

The Student Union
rooms 2591 and 2592
Friday April 23, 1999
1:00-5:00 p.m.

Judges
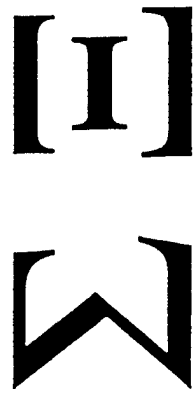
Dr. Andrew Layden
Bowling Green State University

Dr. Lakshmidevi Pulakat
Bowling Green State University

Dr. Felix Castellano
Bowling Green State University

Dr. James Byers
The University of Toledo

Evaluation Criteria

*Originality of the research (25 pts)

*Application of scientific method (25 pts)

*Quality of visual aids (25 pts)

*Quality of oral technical presentation (25 pts)

Session A: Student Union 2591

1:00 Arnette, Robin, "Characterization of a Novel Dihydrolipoyl Dehydrogenase-binding Protein from the Pyruvate Dehydrogenase Complex of the Parasitic Nematode, *Ascaris suum*" Ph.D. Project, Biology, Richard W. Komuniecki advisor

1:12 Harnych, Sally E., "The Role of the Dihydrolipoamide Dehydrogenase Subunit of the Pyruvate Dehydrogenase Complex from the Parasitic Nematode, *Ascaris suum*, in the Reduced Sensitivity of the Complex to NADH Inhibition" Ph.D. Project, Biology Richard Komuniecki advisor

1:24 Chen, Wei, "Nematode Pyruvate Dehydrogenase Kinases: Identification, Characterization and Role of the C-terminus in binding to the dihydrolipol transacetylase Core of the Pyruvate Dehydrogenase Complex" Ph.D. Project, Biology Department, Richard Komuniecki and Patricia R. Komuniecki advisors

1:36 Zhou, Xiao-feng "RAR Inhibits AP1 Transactivation by Disrupting cJun/cFos Dimerization" Doctoral Project, Biology, Lirim Shemshedini advisor

1:48 Nieman, Marvin "N-cadherin Expression Promotes Invasive Phenotype in Breast Carcinoma Cell Lines" Ph.D. Project, Biology, Margaret Wheelock and Keith Johnson advisors

2:00 Brickley, Deanna, "Production of a Monoclonal Antibody to the Extracellular Region of the Mouse Insulin Receptor", M.S. Project, Medicinal & Biological Chemistry, Marcia McInerney advisor

2:12 Krishna, Vyjayanthi, "Gαi Peptide Analogs and HM2 Receptor Coupling" Ph.D. Project, Medicinal & Biological Chemistry, Steven Pesecxis advisor

2:24 Suleman, Ali Shabbir "Structure Based Design, Synthesis and Evaluation of HIV-RT Strand Transfer Inhibitors", Ph.D. Project, Chemistry, Richard A. Hudson advisor

2:36 Kholzaoui, Moussa "Irreversible Inhibitors of Carbonic Anhydrase" M.S. Project, Chemistry, Richard A. Hudson advisor

2:48 Rajeswari Krishnamurthy "Cloning, Expression, Purification and Characterization of Soluble, Active Fragments (SAf) of RADS2 Suitable for Crystallization" M.S. Project, Chemistry, Gloria Borgstahl advisor

3:00 Summers, Catherine A. "Investigation into Protein Stability and Refolding in Ethylammonium Nitrate", Ph. D. Project, Chemistry, Robert A. Flowers advisor

Session A: Student Union 2591
BREAK

3:18 Brault, Pierre-Alexandre "Action of Hydroperoxides on Lipoxygenase Activity" M.S. Project, Chemistry, Max O. Funk advisor

3:30 Inoue, Takayo "Electrochemical Detection of Thiols at a PQQ/Pyrrole-Modified Electrode", Ph.D. Project, Chemistry, Jon R. Kirchhoff advisor.

3:42 Plesescu, Mihaela, "Molten Salt Solutions as Media for the Analysis of Pyrroloquinoline Quinone", M.S. Project, Chemistry, Jon R. Kirchhoff advisor

3:54 Bozon, Jerome P. "Silica-coated Tungsten Wire as a Platform to Develop Modified Electrode Systems", M.S. Project, Chemistry, Dean M. Giolando and Jon R. Kirchhoff advisors

4:06 Casper, Jamie "Examination of the Binding of iron(III)-based Magnetic Resonance Imaging Contrast Agents to Human Serum Albumin" Ph.D. Project, Chemistry Julian A. Davies advisor

4:18 Citeau, Helene "Synthesis of Alk-1-Ynyl Alkyl Tellurides and Characteristic Features of Their 125 TE NMR Spectra", Ph.D. Project, Chemistry, Dean M. Giolando advisor

4:18 Rosen, Thomas "The Preparation and Characterization of Homoleptic Phenolate Complexes of Zirconium (IV)" M.S. Project, Chemistry, Dean M. Giolando advisor

4:42 Plynale, Christopher "Evaluation of the Ground-Water Pollution Potential of Fulton County, Ohio, Using the Drastic Maping System" M.S. Project, Geology, James Harrell advisor

4:54 Fulkerson, Anne L. "The Influence of Language on Categorization: Does Labeling Objects Affects Infants' Acquisition of Novel Categories?" M.S. Project, Psychology, Robert A. Haaf advisor

5:06 Lewin, Linda, "Mothers of Child Abuse Victims" Ph.D. Project, Psychology, Christi Bergin advisor

W0089

Dynamic Light Scattering Analysis of Full-Length, Human RPA14/32 Dimer: Purification, Crystallization and Self-Association. Jeff Habel, Gloria Borgstahl, Dept. of Chemistry, Univ. of Toledo, 2801 W. Bancroft St., Toledo, OH 43606

Replication protein A (RPA) is the eukaryotic single stranded DNA binding protein. Due to the multi dimensional role RPA plays in DNA metabolism, it is of great interest to understand the structure in atomic detail. A NMR solution structure of the N-terminal RPA70 domain (Jacobs et al. (1999) *J Biomol* NMR **14**: 321) and crystal structures at moderate resolution of proteolytic core fragments of RPA70 (Bochkarev et al (1997) *Nature* **385**: 176) and RPA14/32 (Bochkarev et al. (1999) *EMBO J* **18**, 4498) have been reported. Unfortunately, the intact, full-length holoenzyme is very difficult to purify and structural data remains elusive. A soluble dimeric form of RPA is composed of 14 and 32 kDa subunits (RPA14/32). Dynamic light scattering (DLS) analysis was used to improve the purification, stabilization and crystallization of RPA14/32. Increasing concentration of reducing agent in the last stage of purification diminished the size of a secondary peak in the anion exchange chromatograph and promoted a single species in solution. This resulted in decreased polydispersity in the purified protein and enhanced crystallization time. With this homogeneous preparation the reversible association of RPA14/32 into a dimer-of-dimers was demonstrated. Four, different, diffraction-quality, crystal-forms of RPA14/32 were obtained for structure determination. Complete data sets have been collected on hexagonal, spacegroup $P6_5$ at 2.1Å resolution, and orthorhombic, spacegroup $P2_12_12_1$ at 1.9Å resolution, crystal forms of the protein. Progress on the structure determination of full-length RPA14/32 will be reported.

BIOCHEMICAL AND STRUCTURAL STUDIES ON REPLICATION PROTEIN A AND RAD52

Gloria E. O. Borgstahl, Wasantha Ranatunga, Doba Jackson and Jeff Habel

Department of Chemistry, The University of Toledo,
Toledo, OH 43606

E-mail: gborgst@uoft02.utoledo.edu

Replication Protein A (RPA) and RAD52 are both involved in the metabolism of DNA. RPA is composed of 70, 32 and 14 kDa subunits and has two forms, heterotrimeric and heterodimeric (RPA14/32). RPA heterotrimer is essential for the replication of DNA and is intrinsic to DNA transcription, recombination and repair. RPA14/32 separates from the heterotrimer during apotosis. RAD52 is a 50 kDa protein that forms ring structures composed of 8-10 subunits. RAD52 is fundamental to the recombination-based repair of double-strand DNA breaks. RPA, RAD52 together with RAD51 are responsible for the first steps of double-strand DNA break repair. Most interestingly, the breast cancer genes BRCA1 and BRCA2 have been associated with the double-strand DNA break repair pathway. Biochemical studies on the protein-protein interactions between RPA, RAD52 and RAD51 as well as the self-association of RAD52 will be presented. Protein crystallographic studies on RPA will be presented. We have crystallized the RPA14/32 dimer in three crystal forms. X-ray diffraction data to 2.0 Å resolution has been collected and the phase problem solved through molecular replacement. Up-to-date structural results will be presented. It is anticipated that the three-dimensional structure of the RPA32 C-terminal protein-protein interaction domain will be revealed in these studies.

P098 Structural Studies on Full-length Human Replication Protein A Heterodimer.

Venkataraman Kabaleeswaran, Gloria Borgstahl, Dept. of Chemistry, Univ. of Toledo, Toledo, OH 43606.

Human replication protein A (RPA) is a single stranded DNA binding protein, which plays a major role in DNA replication, DNA-repair and recombination. It exists in two forms as heterotrimer with three subunits of 70, 32 and 14 kDa and heterodimer of two subunits 32 and 14 kDa. The heterodimer is known to separate from the heterotrimer upon apoptotic phosphorylation. The heterodimer contains a protein-protein interaction, DNA binding and phosphorylation domain. The structure of a protease resistant core of RPA heterodimer has been solved. The DNA binding properties and the mode and role of phosphorlyation has not been established clearly. The function of human RPA heterodimer is still not well understood due to the lack of a complete structure. In order to contribute to the functional understanding of the heterodimer, we have focused on solving the complete structure of RPA heterodimer. Native data were collected at SSRL beam line 7-1. Initial efforts to solve this structure by molecular replacement failed. Therefore, four wavelength MAD data were collected at APS on a selenomethionyl derivative at 3.0 Å and initial phases were obtained from 12 selenium sites using SOLVE. In order to improve the phases further, two wavelength MAD data at 2.5 Å resolution were collected on a NaBr derivative at SSRL beam line 9-2. Bromide sites were obtained using SOLVE and attempts are being made to combine both phase sets to solve the structure. Up to date results on the structure solution will be presented.

Characterization of the human Rad52wt and RPA protein-protein interaction

Doba Jackson

Advisor- Gloria Borgstahl

Department of Chemistry, ext. 1581, djackso2@uoft02.utoledo.edu

Double-strand breaks (DSB's) in DNA are a direct result of ionizing radiation. The human Rad52 and RPA proteins play an important role in the earliest stages of chromosomal double-stranded break repair via the homologous recombination pathway. The protein-protein interactions between Rad52 and RPA are well established with both yeast and human proteins (1,2). Rad52 and RPA both have been found to stimulate homologous recombination *in vitro*. The stimulation by RPA has been found to have two components. The first is to remove secondary structure from ssDNA. The second component is to interact specifically with other proteins relieving of secondary structure of ssDNA. The second component involves making specific protein-protein contacts with Rad52 and Rad51 (3).

The presented work will describe the molecular characterization of Rad52 and RPA interaction using a modified enzyme-linked immunosorbant assay (ELISA), immunoprecipitation, dynamic light scattering (DLS) and static light scattering (SLS). The Rad52 binding site for RPA32 was previously established to reside between residues 221-280 on Rad52, which has been, established as a RPA 32 kDa subunit (RPA32) binding domain (1). The RPA 70 kDa subunit (RPA70) binding site on Rad52 was not established in the previous study. Here I describe a c-terminal deletion mutant of Rad52 (amino acids 218-418) that carries both binding sites of RPA70 subunit and RPA32 subunit. Activity of the mutant Rad52 is similar to wild-type in binding RPA. Also, the solution properties of mutant Rad52 exhibits the high-order aggregation properties of the wild-type Rad52 without forming a heptameric ring-structure (5). The Rad52 binding site on RPA was investigated and found to reside on amino-acid residues 224 to 271 on RPA32 subunit and residues 168-326 on RPA70 kDa subunit. The RPA32 interaction appears to be mediated by electrostatic interactions similar to other protein interactions with RPA32 such as XPA and UNG1 (4). The RPA70 interaction resides in the domain, which is known to bind ssDNA . Interestingly, a 20-fold increase in RPA binding to DNA was found when in complexed to mutant Rad52. The mutant Rad52 has no DNA binding capability which suggest that the Rad52 interaction with RPA is involved in regulating RPA single-strand DNA binding.

References

1) M. S. Park, Ludwig D. L., Stigger E., Lee S., *J. Biol. Chem., 271(31), 18996 (1996)*

2) S. Hays, Firminich A., Massay P., Banerjee R., Berg P., *Mol. Cell. Biol.*, 18(7),4400 (1998)

3) New J., Tomohiko S., Zaitseva E., Kowalczykowski S., *Nature,* 391, 407 (1998)

4) Mer g., A bocharev, R. Gupta, A. Edwards, W. Chazin, *Cell,* 103, 449 (2000)

5) Ranatunga W., D. Jackson, Lloyd J., Forget A., Knight K., Borgstahl G., *J. Biol. Chem.,* (published on Feb. 13, 2001)

Human RAD52 Protein Has Extreme Thermal Stability[†]

Wasantha Ranatunga, Doba Jackson, Robert A. Flowers II, and Gloria E. O. Borgstahl*

Department of Chemistry, The University of Toledo, Toledo, Ohio 43606-3390

Received February 2, 2001; Revised Manuscript Received April 27, 2001

ABSTRACT: The human RAD52 protein plays an important role in the earliest stages of chromosomal double-strand break repair via the homologous recombination pathway. Individual subunits of RAD52 associate into seven-membered rings. These rings can form higher order complexes. RAD52 binds to DNA breaks, and recent studies suggest that the higher order self-association of the rings promotes DNA end joining. Monomers of the RAD52(1–192) deletion mutant also associate into ring structures but do not form higher order complexes. The thermal stability of wild-type and mutant RAD52 was studied by differential scanning calorimetry. Three thermal transitions (labeled A, B, and C) were observed with melting temperatures of 38.8, 73.1, and 115.2 °C. The RAD52(1–192) mutant had only two thermal transitions at 47.6 and 100.9 °C (labeled B and C). Transitions were labeled such that transition C corresponds to complete unfolding of the protein. The effect of temperature and protein concentration on RAD52 self-association was analyzed by dynamic light scattering. From these data a four-state hypothetical model was developed to explain the thermal denaturation profile of wild-type RAD52. The three thermal transitions in this model were assigned as follows. Transition A was attributed to the disruption of higher order assemblies of RAD52 rings, transition B to the disruption of rings to individual subunits, and transition C to complete unfolding. The ring-shaped quaternary structure of RAD52 and the formation of higher ordered complexes of rings appear to contribute to the extreme stability of RAD52. Higher ordered complexes of rings are stable at physiological temperatures in vitro.

RAD52[1] protein plays a critical role in mitotic and meiotic recombination as well as double-strand break repair (*1, 2*). On the basis of a series of protein–protein interaction assays and DNA binding studies (*3–5*), a domain map of human RAD52 (RAD52) was proposed by Park et al. (Figure 1). Electron microscopy (EM) studies of *Saccharomyces cerevisiae* and human RAD52 have revealed formation of ring-shaped structures (9–13 nm in diameter), as well as higher order aggregates (*6–8*). The RAD52 rings appear to be composed of seven subunits (*9*). EM studies also showed t' t RAD52 recognizes and binds to double-stranded DNA ends as an aggregated complex that ranges in size from approximately 15 to 60 nm in diameter (*8*). This binding promoted end-to-end association between DNA molecules and stimulated the ligation of both cohesive and blunt DNA ends (*8*). Recently, by studying wild type and two deletion mutants of RAD52 (Figure 1), we demonstrated that the self-association domain in the N-terminal half of RAD52 is responsible for ring formation and that elements in the C-terminal half of the molecule participate in the formation of higher order complexes of rings (*10*).

Due to the biological interest of human RAD52 and the apparent biochemical importance of RAD52 self-association in DNA repair, we studied its multiple levels of self-association and stability using biophysical methods. The stability of wild-type RAD52 was studied by differential scanning calorimetry (DSC). To investigate the basis for the extreme stability of RAD52 that was discovered, two mutants were also studied, RAD52(1–192) and RAD52(218–418) (Figure 1). The effects of temperature and protein concentration on the hydrodynamic radius (R_H) of RAD52 were studied by dynamic light scattering (DLS). Finally, a hypothetical model of the effects of protein aggregation state on thermal stability was developed.

MATERIALS AND METHODS

Protein Purification. The domain structures for wild-type RAD52, RAD52(1–192), and RAD52(218–418) are described in Figure 1. Proteins were expressed, purified under reducing conditions, and concentrated as described (*10*). Unfortunately, enterokinase cleavage was nonspecific, and the histidine-patch thioredoxin (Invitrogen) could not be separated from the 218–418 peptide (Jackson, unpublished results). After the extreme thermal stability of wild-type RAD52 was observed, subsequent purifications included a heat treatment step. The lysate was heated to 55 °C for 30 min prior to the chromatography steps. Samples were concentrated using an Ultrafree-15 centrifugal filter device. After each step of concentration, the samples were analyzed by DLS. Protein concentrations were determined using the Bradford assay (Bio-Rad) with bovine serum albumin as a standard.

---

* To whom correspondence should be addressed. Telephone: 419-530-1501. Fax: 419-530-4033. E-mail: gborgst@uoft02.utoledo.edu.

[1] Abbreviations: RAD52, human RAD52; DLS, dynamic light scattering; DSC, differential scanning calorimetry; EM, electron microscopy; MnSOD, manganese superoxide dismutase; SOS, sum of squares; R_H, hydrodynamic radius; T_M, melting temperature.
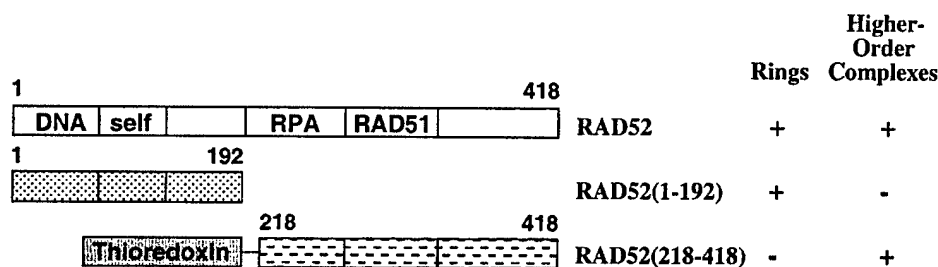
FIGURE 1: Wild-type RAD52 and deletion mutants. Beginning and ending residue numbers of each mutant are indicated along with domain structure. The following domains and residue numbers were defined by Park et al. (*16*): DNA binding (39−80), self-association (85−159), RPA binding (221−280), and RAD51 binding (290−330). The structural characterization of wild-type and mutant RAD52 by Ranatunga et al. is summarized on the right (*10*). Wild-type RAD52 and RAD51(1−192) have six histidines fused to the C-terminus. For the RAD52-(218−418) mutant, a thrombin-cleavable six-histidine tag is fused to the N-terminus of the histidine-patch thioredoxin, and an enterokinase cleavage site separates histidine-patch thioredoxin from RAD52(218−418).

Differential Scanning Calorimetry. Protein and reference solutions were degassed under a vacuum for 15 min before data acquisition. The concentration of wild-type RAD52 was 2.0 and 3.5 mg/mL, RAD52(1−192) was 7.2 mg/mL, and RAD52(218−418) was 3.1 mg/mL. The wild-type RAD52 sample was concentrated to 11.5 mg/mL before dilution to either 2.0 or 3.5 mg/mL. The concentrations of wild-type RAD52 and RAD52(218−418) were limited by the quantity of protein available. The protein samples and reference solutions were loaded into their respective cells in the MicroCal MC-2 differential scanning calorimeter. An external pressure of 30 psi was applied with nitrogen gas to both sample and reference cells. The sample was scanned relative to the reference solution over a temperature range of 5−120 °C at a rate of 45 °C/h. DSC measurements on buffer alone had no transitions for the temperature range 5−120 °C. The baseline and change in specific heat (ΔC_p) upon denaturation were corrected according to standard techniques (*11*). DSC data were fit to a two- or three-state model using the Origin DSC software provided by Microcal Inc.

Dynamic Light Scattering Analysis. DLS was carried out using a DynaPro-801 molecular sizing instrument equipped with a temperature-controlled microsampler (Protein Solutions). A 50 μL sample was passed through a filtering assembly equipped with a 100 nm filter into a 12 μL chamber quartz cuvette. For each experiment, 35−60 measurements were taken. The data were first analyzed using Dynamics 4.0 software and then with DynaLS software. The refractive index and viscosity of the buffer at each temperature were measured and the proper corrections applied to the data. Baseline and sum of squares (SOS) error values were reported by Dynamics 4.0. The baseline is the measured value of the last coefficient in the correlation curve. Baselines within the range from 0.977 to 1.002 were interpreted as monomodal, and those greater than 1.002 were bi- or multimodal. The SOS error is the sum of squares difference between the measured correlation curve and the best-fit curve. SOS errors less than 5.000 were considered negligible. Errors between 5.000 and 20.000 were considered as low and probably due to low protein concentration or a small amount of polydispersity. Errors greater than 20.000 were considered as high and are probably due to high polydispersity in size distribution (aggregation) or irregular solvent. Mean R_H, standard deviation, and percent of peak area are reported from DynaLS using the optimized resolution. Due to the irregular solvent, the SOS errors increased for diluted samples, and it was necessary to use DynaLS to separate the solvent peak from the protein peak.

RESULTS AND DISCUSSION

Differential Scanning Calorimetry. Thermal stability profiles of wild-type RAD52, RAD52(1−192), and RAD52-(218−418) were obtained by DSC (Figure 2 and Table 1). For wild-type RAD52 and RAD52(1−192) the DSC transitions were labeled A, B, or C such that total unfolding was always labeled C. For wild-type RAD52, at 2.0 mg/mL, the DSC profile was composed of two transitions (labeled B and C) with melting temperatures (T_M) of 78.3 and 101.6 °C (Table 1). At 3.5 mg/mL, the wild-type RAD52 DSC profile was composed of three distinct transitions (labeled A, B, and C in Figure 2A) with T_M's of 38.8, 73.1, and 115.2 °C (Table 1). When the concentration of wild-type RAD52 was increased, transition C was shifted to a higher temperature by 13 °C. Transition A could be measured only if the sample was first concentrated to 11.5 mg/mL and then diluted to 3.5 mg/mL. For RAD52(1−192) two transitions were observed at 47.6 and 100.9 °C (labeled B and C in Figure 2B). The deletion of the C-terminal half of RAD52 decreased the T_M of transitions B and C by 25 and 14 °C, respectively.

Our earlier analysis demonstrated that wild-type RAD52 forms ring structures as well as higher order complexes of rings but RAD52(1−192) forms rings but not the aggregates of rings (*10*). The size of the wild-type RAD52 higher order complexes, as well as the proportion of the rings in a higher order complex, is dependent on concentration. RAD52(1−192) rings do not form higher ordered complexes, at any concentration. DSC transition A was dependent on the concentration of wild-type RAD52 and was not observed for RAD52(1−192). Therefore, it appeared that transition A corresponded to the thermal disruption of aggregates to form single rings in solution, transition B to the break up of rings to monomers, and transition C to the total unfolding of monomers.

The DSC profile of RAD52(218−418) is also consistent with this interpretation (Figure 2C). RAD52(218−418) forms a complex of two to four monomers depending on the concentration but does not form ring structures in solution (*10*). It has a relatively low T_M of 53−59 °C, and it appears that the C-terminal half of RAD52, which cannot form rings, is not as thermally stable as the ring-structured N-terminal half.

Wild-type *Escherichia coli* thioredoxin is a very stable protein with a T_M of ~85 °C for the oxidized form and ~73
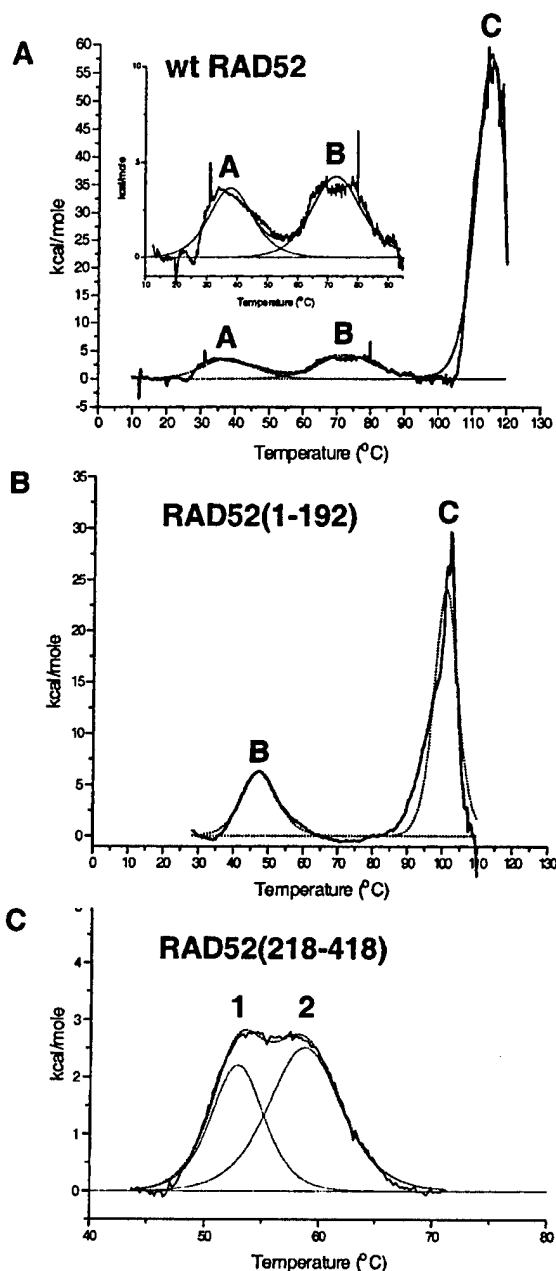
FIGURE 2: Thermal stability of wild-type RAD52 and deletion mutants. DSC profiles for (A) wild-type RAD52 were analyzed at 0.038 mM (3.5 mg/mL), (B) RAD52(1–192) at 0.325 mM (7.2 mg/mL), and (C) RAD52(218–418) at 0.082 mM (3.1 mg/mL). For RAD52(218–418) there were no transitions above 70 °C.

Table 1: Thermodynamic Parameters from DSC Measurement of RAD52 Proteins

protein	concn (mg/mL)	component	T_M (°C)
RAD52[a]	2.0	B	78.3
		C	101.6
RAD52[b]	3.5	A	38.8
		B	73.1
		C	115.2
RAD52(1–192)[c]	7.2	B	47.6
		C	100.9
RAD52(218–418)[d]	3.1	1	53.4
		2	59.1

[a] This sample was concentrated to 11.5 mg/mL and then diluted to 2.0 mg/mL (similar to Table 2, line 12) and does not contain higher ordered assemblies of rings. [b] This sample was concentrated to 11.5 mg/mL and then diluted to 3.5 mg/mL for DSC measurements (similar to Table 2, line 7, and Figure 3E) and contains higher ordered complexes of rings. [c] RAD52(1–192) forms rings but does not form higher ordered assemblies of rings (10). [d] RAD52(218–418) does not form rings but does self-associate (10).

ably have a T_M lower than that measured for the fusion protein.

The reversibility of transitions A, B, and C for wild-type RAD52 was studied by DSC, using an 11.5 mg/mL sample diluted to 3.5 mg/mL. Three experiments were performed, and the presence of precipitation was noted after each (data not shown). First, the sample was heated to 55 °C and then slowly returned to 20 °C overnight. Transition A was observed, and the protein remained in solution. Then the same sample was heated to 95 °C and slowly returned to 20 °C overnight. During this second experiment, transition A did not return, possibly due to the protein concentration used (see discussion of DLS data, Table 2, lines 7–9), and transition B was lowered to 65 °C. After the second experiment there was a slight amount of precipitate, but the majority of the protein was still in solution. For the third experiment, the sample was heated to 120 °C, and there was only one significant peak at 94 °C and the protein completely precipitated. The T_M for complete unfolding was lower than that measured from fresh sample (115 °C for peak C, Figure 2A), indicating that the protein did not properly reassemble after the second experiment and that the process of unfolding is irreversible under this set of experimental conditions.

The irreversibility of transition B was also noted in experiments performed during the addition of a heat step to the purification protocol for wild-type RAD52. Lysates were heated in 5 deg increments between 55 and 80 °C, centrifuged, and analyzed by SDS–PAGE. RAD52 began to precipitate after 65 °C (data not shown). This supports the conclusion that transition B in the thermal denaturation of RAD52 is irreversible.

Dynamic Light Scattering. The response of RAD52 rings and higher ordered complexes to concentration and temperature was studied by DLS. The upper temperature limit of the DLS microsampler was 50 °C so theoretically data on transition A of wild-type RAD52 and transition B of RAD52-(1–192) could be measured.

The procedure followed for sample preparation affected the detection of DSC transition A and the T_M value of transition C for wild-type RAD52, so the effects of protein concentration and temperature on the R_H of wild-type RAD52 were studied using DLS. In a series of experiments, the protein concentration was increased from 3.5 to 11.5 mg/

°C for the reduced form (12, 13). When thioredoxin is fused to other proteins, it can improve their solubility and, especially when in the oxidized form, improve their thermal stability, allowing a heat step during purification. Histidine-patch thioredoxin in the reduced state was expected to have a T_M of ~67 °C (12–14). We were unable to specifically cleave thioredoxin from RAD52(218–418) with enterokinase, so the exact contributions of thioredoxin and RAD52-(218–418) to the DSC profile of the fusion protein could not be determined. It is apparent that fusing thioredoxin to RAD52(218–418) has reduced the T_M of thioredoxin significantly and that RAD52(218–418) by itself would prob-

Table 2: Effect of Temperature and Concentration on R_H of Wild-Type RAD52

DLS expt	concn (mg/mL)	base-line	SOS error^a	R_H^b (nm)	peak area^c (%)	interpre-tation^d
1. 20 °C	3.5	1.001	4.22	15.0 (2.5)	98.3	>2 rings
2. heat to 50 °C	3.5	1.000	2.78	14.2 (4.5)	99.2	~2 rings
3. concd; 20 °C	4.9	1.002	2.03	4.3 (0.5)	3.4	monomer
				18.7 (2.3)	95.8	>2 rings
4. concd; 20 °C	11.5	1.009	7.78	5.1 (0.6)	4.2	mono/dimer
				17.8 (3.1)	56.9	>2 rings
				36.1 (4.4)	36.6	≫2 rings
5. heat to 50 °C	11.5	1.000	5.96	19.2 (8.5)	99.2	>2 rings
6. cool to 20 °C	11.5	1.010	8.24	5.9 (0.4)	9.7	mono/dimer
				11.2 (0.7)	6.6	1–2 rings
				20.6 (2.2)	81.6	>2 rings
7. sample from line 4 diluted; 20 °C	3.5	1.001	11.3	3.8 (0.2)	0.6	monomer
				23.2 (11.6)	98.1	>2 rings
8. heat to 50 °C	3.5	1.001	9.41	9.7 (1.2)	45.8	1 ring
				17.0 (1.0)	49.8	>2 rings
9. cool to 20 °C	3.5	1.001	16.1	3.9 (0.2)	1.1	monomer
				11.9 (1.9)	69.3	1–2 rings
				28.6 (3.5)	26.4	≫2 rings
10. sample from line 3 diluted; 20 °C	3.3	1.001	7.4	3.1 (0.2)	11.0	monomer
				16.8 (5.4)	84.0	>2 rings
				49.5 (8.7)	14.5	≫2 rings
11. heat to 37 °C	3.3	1.000	7.9	19.8 (10.9)	99.5	>2 rings
12. sample from line 4 diluted; 20 °C	2.3	1.001	50.9	8.75 (6.0)	79.7	1 ring
13. heat to 37 °C	2.3	1.000	24.5	8.0 (1.6)	71.9	1 ring
14. heat to 50 °C	2.3	1.000	15.9	8.7 (2.7)	87.4	1 ring

^{a} SOS = sum of squares. ^{b} Average R_H is given with the standard deviation given in parentheses. ^{c} DynaLS results; the percent peak area for the solvent peaks was not reported. DLS measurements at 20 and 50 °C on solvent alone indicate that very small and very large components in the RAD52 measurements were due to the solvent and not the protein. Therefore, only the peaks attributable to RAD52 protein are reported (R_H > 3.0 nm; see Figure 4). R_H and percent peak area of the primary species in solution (greater than 10%) are in bold. ^{d} Interpretation is based on estimated R_H in Figure 4. It is not possible to tell exactly how many rings of RAD52 are in the aggregates >14.1 nm since the structure of the higher order complexes of RAD52 rings is unknown.

mL and then diluted (see Table 2 and Figure 3). The microsampler cell was held at 20, 37, or 50 °C, and samples were equilibrated for 30 min at the target temperature before DLS measurements began. The smallest R_H measured for RAD52 was 8.0–8.75 nm (Table 2, lines 12–14). This is close to the size expected for single rings measured from electron micrographs (Figure 4) (*6–8*). A monomer of RAD52 is expected to have an R_H value of 3.2 nm, and complexes containing two rings are expected to have an R_H of 12.8–14.1 nm. The R_H for aggregates of more than two rings would be greater than 14 nm.

Using these estimates of particle sizes as a guide, four trends in the DLS data were noted. First, heating the protein samples from 20 to 50 °C caused the R_H to decrease in general, and frequently the baseline decreased to within the monomodal range. For example, heating a sample similar to that used for DSC measurements (Table 2, line 7, and Figure 3E) caused the particles to shift from a single population with R_H of 23.2 nm to two populations with R_H of 9.7 and 17.0 nm (Table 2, line 8, and Figure 3F). Second, the size of the sample population was dependent on the protein concentration. For example, the R_H of the sample

FIGURE 3: Effect of protein concentration and temperature on the R_H of wild-type RAD52. DLS data were analyzed using DynaLS software. The data correspond to the following lines in Table 2: (A) 3.5 mg/mL at 20 °C (line 1), (B) 11.5 mg/mL at 20 °C (line 4), (C) 11.5 mg/mL at 50 °C (line 5), (D) 11.5 mg/mL cooled to 20 °C (line 6), (E) diluted to 3.5 mg/mL at 20 °C (line 7), (F) diluted to 3.5 mg/mL at 50 °C (line 8), and (G) diluted to 3.5 mg/mL cooled to 20 °C (line 9). Panels E–G correspond to the sample used for DSC.

Model	R_H (nm)
Monomer	3.2
7-membered ring	8.5
Two edge on rings	14.1
Two stacked rings	12.8

13 nm

11 nm

FIGURE 4: Estimated R_H for RAD52 models. The R_H for a monomer was calculated from a molecular mass of 47.0 kDa with the molecular weight calculator included in the Dynamics 3.0 software. R_H for a seven-membered ring of RAD52 was estimated from the diagonal of the three-dimensional reconstruction on the basis of electron micrographs (9). Electron micrographs of RAD52 rings in the large, greater than 100 nm spherical aggregates appear to have an "edge-on" orientation (10). The three-dimensional reconstructions of RAD52 were adapted from Stasiak et al. (2000).

FIGURE 5: Hypothetical four- state model for the thermal denaturation of wild-type RAD52. Transitions A, B, and C correspond to those measured by DSC in Figure 2. There are three transitions in this model; transition A is attributed to the disruption of higher order assemblies of RAD52 rings, transition B to the disruption of rings to individual subunits, and transition C to complete unfolding. The individual subunits after transition B are probably partially unfolded as well as disassociated from the rings.

population increased from 15.0 to 18.7 to 36.1 nm, when the concentration was increased from 3.5 to 4.9 to 11.5 mg/mL (Table 2, lines 1, 3, and 4). Third, the modality of the sample population was dependent on the protein concentration. For example, the 11.5 mg/mL sample was multimodal at 20 °C (Table 2, line 4, and Figure 3B), and the 3.5 mg/mL sample was not (Table 2, line 1, and Figure 3A). Fourth, the reversibility of the assembly of RAD52 rings into higher ordered complexes was dependent on protein concentration. The majority of the particles in the samples at 11.5 mg/mL remained greater than 17 nm throughout the heat cycle (Table 2, lines 4–6, and Figure 3B–D). But, the superaggregation of rings was only partially reversible at 3.5 mg/mL with only 26% of the sample returning to greater than 17 nm after being heated (Table 2, lines 7–9, and Figure 3E–G). It is noteworthy that for the DSC measurements made on samples at 3.5 mg/mL the assembly of RAD52 rings into higher ordered complexes is not completely reversible at this concentration.

Finally, this DLS analysis facilitated the interpretation of DSC transition A. Transition A could not be detected for samples that were first concentrated to 11.5 mg/mL and then diluted to 2.0 mg/mL (prepared as in line 12, Table 2). The R_H value of 8.75 indicates that at 2.0 mg/mL there are primarily single rings in solution and little or no higher ordered complexes (Figure 4). Transition A was detectable for samples that were diluted to 3.5 mg/mL (prepared as in line 7, Table 2, and Figure 3E). The R_H value of 23.2 nm indicates that at 3.5 mg/mL there are primarily higher order complexes of many rings in solution. Heating this sample to 50 °C caused the R_H to decrease and form two populations of 9.7–17.0 nm (Table 2, line 8, and Figure 3F). Therefore, these DLS data indicate that DSC transition A can be attributed to the disassociation of rings from higher ordered complexes.

We were interested to know if the higher ordered complexes of RAD52 rings were stable at physiological temperatures. Protein samples diluted to 3.3 mg/mL did not form particles less than 9 nm upon heating to 37 °C (Table 2, lines 10 and 11) although the samples became monomodal. Therefore, the upper level aggregation of RAD52 rings is stable at physiological temperatures in vitro.

Transition B of the RAD52(1–192) mutant was 47.6 °C, and attempts were made to measure the effect of temperature on the structure of RAD52(1–192) with DLS. Higher ordered assemblies of rings are not formed by RAD52(1–
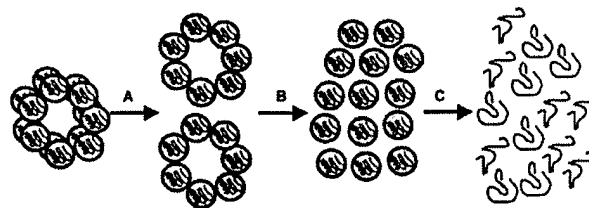
192), and single rings have an R_H of 5.7 nm (SD = 1.2) (10). As samples of RAD52(1–192) were heated, the R_H appeared to increase, perhaps indicating partial unfolding (data not shown). DLS measurements at elevated temperatures with RAD52(1–192) were very problematic, and at 50 °C no measurements could be obtained, perhaps due to large changes in structure.

CONCLUSIONS

Our data indicate that the RAD52 rings and higher ordered complexes of rings used in DNA repair and DNA recombination are extremely stable structures. The structure of wild-type RAD52 is very stable, and its multiple levels of self-association appear to contribute to this stabilization. The extreme stability of the wild-type RAD52 and RAD52(1–192) folds relative to RAD52(218–418) appears to be related to the assembly of multiple monomers into a ring. The enhanced stability of the wild-type RAD52 fold relative to RAD52(1–192) appears to be due in part to its ability to form higher order assemblies of rings.

A four-state hypothetical model has been developed to explain the thermal denaturation profile of wild-type RAD52 (Figure 5). There are three transitions in this model; transition A is attributed to the disruption of higher order assemblies of RAD52 rings, transition B to the disruption of rings to individual subunits, and transition C to complete unfolding. Individual rings of RAD52 appear to have an R_H on the order of 8.0–8.75 nm in solution (Table 2, lines 12–14). Higher order assemblies of rings are seen in the wild-type RAD52 DLS data as particles ranging from 15 to 50 nm. Note that the measured R_H values are not integral values of individual rings due to the presence of equilibrium mixtures of single rings and complexes of rings in solution as indicated by the high standard deviations in the R_H measurements (Table 2) and the width of the DLS peaks (Figure 3). This equilibrium is dependent upon concentration. At concentrations of 3.5 mg/mL or greater RAD52 appears to be primarily composed of assemblies of two or more rings with R_H values ranging from 15 to 36.1 nm. Raising the temperature from 20 to 50 °C disrupts the higher order particles, pushing the equilibrium toward the 9 nm particles (Table 2, lines 5 and 8, and Figure 3C and F). These data support our hypothetical model for transition A (Figure 5). Reliable DLS measurements varying temperature on RAD52(1–192) could not be made. Thermal expansion of the RAD52(1–192) rings was noted. The data indicate that a large structural transition occurs near transition

B, possibly the disassociation of individual subunits from the rings.

Only a handful of proteins have been measured with thermal stabilities on the order of RAD52. To our knowledge, the highest T_M for a protein reported in the literature to date is 125 °C for ferredoxin from the hyperthermophile *Thermotoga maritima* (*15*). Other proteins such as onconase and mitochondrial manganese superoxide dismutase (MnSOD) are extremely stable with T_M's approaching 90 °C (*16, 17*). Both ferredoxin and onconase are monomeric, and by studying their protein crystal structures, their stabilities were attributed to the compactness of their tertiary structures and to extensive hydrogen bonding involving charged amino acid side chains. Mitochondrial MnSOD is a homotetramer, and its enhanced stability was partially attributed to its quaternary structure. The DSC profile of MnSOD has three thermal transitions (labeled A, B, and C), similar to those seen with RAD52. Transition A was attributed to subunit disassociation, transition B to loss of the active site manganese, and transition C to complete unfolding. A cavity forming point mutation in the tetrameric interface of MnSOD resulted in the lowering of transition B by 13.6 °C and transition C by 16.5 °C (*17*). These results on MnSOD are somewhat similar to the results on RAD52. We conclude from our data that both components of RAD52 self-association, ring formation and higher order complex formation, contribute to its extreme thermal stability. A precise understanding of the structural determinants of RAD52 stability awaits the solution of its crystal structure.

ACKNOWLEDGMENT

REFERENCES

1. Game, J., and Mortimer, R. K. (1974) *Mutat. Res. 24*, 281−292.
2. Petes, T. D., Malone, R. E., and Symington, L. S. (1991) in *The Molecular and Cellular Biology of the Yeast, Saccharomyces* (Broach, J. R., Pringle, J. R., and Jones, E. W., Eds.) pp 407−522, Cold Spring Harbor Laboratory Press, Cold Spring Harbor, NY.
3. Shen, Z., Cloud, K. G., Chen, D. J., and Park, M. S. (1996) *J. Biol. Chem. 271*, 148−152.
4. Shen, Z., Peterson, S. R., Comeaux, J. C., Zastrow, D., Moyzis, R. K., Bradbury, E. M., and Chen, D. J. (1996) *Mutat. Res. 364*, 81−89.
5. Park, M. S., Ludwig, D. L., Stigger, E., and Lee, S. H. (1996) *J. Biol. Chem. 271*, 18996−19000.
6. Shinohara, A., Shinohara, M., Ohta, T., Matsuda, S., and Ogawa, T. (1998) *Genes Cells 3*, 145−156.
7. Van Dyck, E., Hajibagheri, N. M. A., Stasiak, A., and West, S. C. (1998) *J. Mol. Biol. 284*, 1027−1038.
8. Van Dyck, E., Stasiak, A. Z., Stasiak, A., and West, S. C. (1999) *Nature 398*, 728−731.
9. Stasiak, A. Z., Larquet, E., Stasiak, A., Muller, S., Engel, A., Dyck, E. V., West, S. C., and Egelman, E. H. (2000) *Curr. Biol. 10*, 337−340.
10. Ranatunga, W., Jackson, D., Lloyd, J. A., Forget, A. L., Knight, K. L., and Borgstahl, G. E. O. (2001) *J. Biol. Chem.* (in press).
11. Haynie, D. T., and Freire, E. (1994) *Anal. Biochem. 216*, 33−41.
12. Ladbury, J., Wynn, R., Hellinga, H., and Sturtevant, J. (1993) *Biochemistry 32*, 7526−7530.
13. Ladbury, J., Kishore, N., Hellinga, H., Wynn, R., and Sturtevant, J. (1994) *Biochemistry 33*, 3688−3692.
14. Lu, Z., DiBlasio-Smith, E., Grant, K., Warne, N., LaVallie, E., Collins-Racie, L., Follettie, M., Williamson, M., and McCoy, J. (1996) *J. Biol. Chem. 271*, 5059−5065.
15. Pfeil, W., Gesierich, U., Kleemann, G. R., and Sterner, R. (1997) *J. Mol. Biol. 272*, 591−596.
16. Notomista, E., Catanzano, F., Graziano, G., Piaz, F. D., Barone, G., D'Alessio, G., and Donato, A. D. (2000) *Biochemistry 39*, 8711−8718.
17. Borgstahl, G. E. O., Parge, H. E., Hickey, M. J., Johnson, M. J., Boissinot, M., Hallewell, R. A., Lepock, J. R., Cabelli, D. E., and Tainer, J. A. (1996) *Biochemistry 35*, 4287−4297.

Human Rad52 Protein Has Extreme Thermal Stability

Wasantha Kumara Ranatunga, Doba Donald Jackson, and Robert A Flowers II ; Gloria E.O Borgstahl
University of Toledo, 2801 W. Bancroft st., Toledo, OH 43606

<p> The human Rad52 (hRAD52) protein plays an important role in the earliest stages of chromosomal double-strand break repair via the homologous recombination pathway. Individual subunits of hRad52 self-associate into rings that can then form higher-order complexes. hRad52 binds to double- strand DNA ends and recent studies suggest that the higher order self-association of the rings promotes DNA end joining. The thermal stability of hRad52 was studied by differential scanning calorimetry. Three thermal transitions were observed with melting temperatures of 38.8, 73.1 and 115.2 °C. The hRad52 (1-192) mutant that does not form higher ordered complexes of rings had only two thermal transitions at 47.6 and 100.9 °C. The effect of temperature and protein concentration on hRad52 structures was analyzed by dynamic light scattering. From these data a four state hypothetical model was proposed to explain the thermal denaturation profile of wild-type hRad52. The three thermal transitions in this model were assigned as follows. Transition A was attributed to the disruption of higher order assemblies of hRad52 rings, transition B to the disruption of rings to individual subunits and transition C to complete unfolding. The extreme stability of hRad52 was attributed to is ring-shaped quaternary structure and to the formation of higher ordered complexes of rings. Higher ordered complexes of rings appear to be stable at physiological temperatures *in vitro*.

Fifteenth Symposium of the Protein Society

July 28 - August 1, 2001 • Philadelphia, PA

SELF-ASSOCIATION OF THE C-TERMINAL HALF OF HUMAN RAD52 AND ITS INTERACTION WITH HUMAN REPLICATION PROTEIN A

Doba Jackson, Wasantha, Ranatunga and Gloria Borgstahl
The University of Toledo, Toledo, OH

The human Rad52 and RPA proteins play an important role in the earliest stages of chromosomal double-strand break repair via the homologous recombination pathway. Individual subunits of RAD52 can self-associate into rings, which then form higher-order complexes. Rad52 is known to bind RPA and the two proteins are known to stimulate homologous recombination by promoting single-strand annealing and strand invasion pathways. Earlier studies defined the self-association domain of human RAD52 (hRAD52) to the N-terminal half of the protein. Here we show that there are, in fact, two experimentally separable self-association domains in hRAD52. The N-terminal self-association domain mediates the assembly of monomers into rings and the previously unidentified domain in the C-terminal half of the protein mediates higher-order self-association of the rings. We will also show that the C-terminal half binds two well conserved domains on hRPA and postulate how the protein-protein interaction with hRAD52 and hRPA is involved in promoting single-strand annealing and strand invasion pathways in the cell.

TEMPERATURE MODULATES THE HIGHER-ORDERED SELF-ASSOCIATION OF RAD52

**Wasantha Ranatunga, Doba Jackson,
and Gloria E. O. Borgstahl**

Department of Chemistry, The University of Toledo,
2801 West Bancroft Street, Toledo, OH 43606

wranatunga@hotmail.com

Defects in recombination-based DNA repair lead to human breast cancer and familial degenerative diseases. The RAD52 epistasis gene products, especially the human RAD52 protein plays important role in double-strand break (DSB) repair. hRAD52 has shown to be interacting with many proteins in recombination-based DSBs repair pathway. The focus of this work is to further understanding of the molecular basis of DSBs by solving the three-dimensional structure of hRAD52. The hRAD52 forms ring structure in solution and multiple level of aggregation of rings.

Due to the biological interest of hRAD52 and the apparent biochemical importance of RAD52 self-association in DNA-repair, we studied its multiple levels of self-association and stability using biophysical methods such as dynamic light scattering (DLS) and differential scanning calorimetry (DSC). The stability of wild-type RAD52 was studied by DSC. To investigate the basis for the extreme stability of RAD52 that was discovered, two mutants were also studied, RAD52 (1-192) and RAD52 (218-418). The effects of temperature and protein concentration on the hydrodynamic radius (RH) of RAD52 were studied by DLS.

We found that the aggregation is due to two levels of self-association of hRAD52, ring formation and association of rings with rings. DSC profiles and DLS data indicated that hRAD52 protein is extremely stable and multiple levels of self-association of hRAD52 can be disrupted by heating up to 50 °C.

A hypothetical model of the effects of protein aggregation state on thermal stability was developed. Based on these findings, a novel approach for purification of hRAD52 and for crystallization was established. This research will contribute a detailed understanding of the molecular mechanisms of breast cancer.

ANALYSIS OF THE RAD52/RPA COMPLEX: EVIDENCE FOR CROSSTALK BETWEEN RPA32, RPA70, RAD52, AND SSDNA

Doba Jackson, Kajari Dahr, Marc Wold, and Gloria Borgstahl

University of Toledo, Toledo, OH

djackso2@uoft02.utoledo.edu

The eukaryotic single-stranded DNA-binding protein, replication protein A (RPA), is essential for DNA replication, and plays important roles in DNA repair and DNA recombination. Rad52 and RPA, along with other members of the Rad52 epistasis group of genes, repair double-stranded DNA breaks (DSBs). Two repair pathways involve RPA and Rad52, homologous recombination and single-strand annealing. Two binding sites for Rad52 have been identified on RPA. They include the previously identified C-terminal domain (CTD) of RPA32 (residues 224 to 271) and the newly identified domain containing residues 169 to 326 of RPA70. A region on Rad52, that includes residues 218 to 303, binds RPA70 as well as RPA32. The N-terminal region of RPA32 does not appear to play a role in the formation of the RPA:Rad52 complex. It appears that the RPA32CTD can substitute for RPA70 in binding Rad52. Sequence homology between RPA32 and RPA70 was used to identify a putative Rad52 binding site on RPA70 that is located near DNA binding domains A and B. Rad52 binding to RPA increases ssDNA affinity significantly. Mutations in DBD-D on RPA32 show that this domain is primarily responsible for the ssDNA binding enhancement. RPA binding to Rad52 inhibits the higher-order self-association of Rad52 rings. Implications for these results for the "hand-off" mechanism between protein-protein partners, including Rad51, in homologous recombination and single-strand annealing are discussed..

electronic reprint

Dynamic light-scattering analysis of full-length human RPA14/32 dimer: purification, crystallization and self-association

Jeff E. Habel, Jeffrey F. Ohren and Gloria E. O. Borgstahl

research papers

Dynamic light-scattering analysis of full-length human RPA14/32 dimer: purification, crystallization and self-association

Jeff E. Habel, Jeffrey F. Ohren and Gloria E. O. Borgstahl*

University of Toledo, Department of Chemistry, 2801 West Bancroft Street, Toledo, OH 43606, USA

Correspondence e-mail:
gborgst@uoft02.utoledo.edu

Replication protein A (RPA) is a single-stranded DNA-binding protein involved in all aspects of eukaryotic DNA metabolism. A soluble heterodimeric form of RPA is composed of 14 and 32 kDa subunits (RPA14/32). Dynamic light-scattering (DLS) analysis was used to improve the purification, stabilization and crystallization of RPA14/32. Increasing the concentration of reducing agent in the last stage of purification diminished the size of a secondary peak in the anion-exchange chromatograph and promoted a single species in solution. This resulted in decreased polydispersity in the purified protein and enhanced the crystallization time from 9–12 months to 6 d. With this homogeneous preparation, the reversible association of RPA14/32 into a dimer of dimers was demonstrated by DLS. Four different crystal forms of RPA14/32 were obtained for structure determination and complete diffraction data were collected using synchrotron radiation for three of them. Data to 2.4 Å resolution was collected from hexagonal crystals ($P3_2$ or $P3_1$; $a = b = 63.0$, $c = 272.6$ Å) and to 2.2 and 1.9 Å resolution from two orthorhombic crystal forms (both $P2_12_12_1$; form I, $a = 61.4$, $b = 75.2$, $c = 131.6$ Å; form II, $a = 81.8$, $b = 140.4$, $c = 173.1$ Å).

1. Introduction

Replication protein A (RPA) is a single-stranded DNA-binding protein that has been implicated in all aspects of eukaryotic DNA metabolism, including replication, transcription, recombination and repair (for reviews, see Wold, 1997; Iftode *et al.*, 1999). The three subunits of RPA are designated RPA14, RPA32 and RPA70 according to their apparent molecular weights. RPA70 contains the primary ssDNA-binding site and interacts with several proteins, including P53 (Dutta *et al.*, 1993; He *et al.*, 1993; Li & Botchan, 1993) and XPA (Lee & Kim, 1995; Li *et al.*, 1995; Matsuda *et al.*, 1995). RPA32 is phosphorylated in a cell-cycle-dependent manner (Din *et al.*, 1990; Fang & Newport, 1993) during apoptosis (Treuner *et al.*, 1999) and in response to UV light (Carty *et al.*, 1994) and ionizing radiation (Liu & Weaver, 1993; Boubnov & Weaver, 1995; Fried *et al.*, 1996). *In vitro*, RPA32 is phosphorylated by ATM kinase (Gately *et al.*, 1998), cdc2 kinase (Dutta & Stillman, 1992) and DNA-dependent protein kinase (Brush *et al.*, 1994; Boubnov & Weaver, 1995). RPA32 contains a weak ssDNA-binding site (Bochkareva *et al.*, 1998) and its C-terminal domain interacts with several proteins, including RAD52 (Park *et al.*, 1996) and XPA. RPA14 plays a structural role in heterotrimer assembly and stability (Henricksen *et al.*, 1994). RPA is known to exist in two soluble forms: the heterotrimer and the RPA14/32 heterodimer

(Henricksen *et al.*, 1994). The RPA heterotrimer is extremely stable (Fairman & Stillman, 1988; Wold & Kelly, 1988; Brill & Stillman, 1991) and its roles in DNA metabolism are well known. Interestingly, the separation of the RPA14/32 dimer from RPA70 is promoted by hyperphosphorylation of RPA32 both *in vitro* (Treuner, Findeisen *et al.*, 1999) and in cells undergoing apoptosis (Treuner, Okuyama *et al.*, 1999). These studies suggest a physiological role for the RPA14/32 dimer.

Owing to the multidimensional role RPA plays in DNA metabolism, it is of great interest to understand the structure in atomic detail. An NMR solution structure of the N-terminal RPA70 domain (Jacobs *et al.*, 1999) and crystal structures at moderate resolution of proteolytic core fragments of RPA70 (Bochkarev *et al.*, 1997) and RPA14/32 (Bochkarev *et al.*, 1999) have been reported. Unfortunately, the intact full-length holoenzyme is very difficult to purify and structural data remain elusive. Here, we demonstrate the utility of using dynamic light-scattering (DLS) analysis in improving the purification, stabilization and crystallization of full-length recombinant human RPA14/32 dimer. Complete diffraction data from orthorhombic and hexagonal crystals are reported.

2. Experimental

2.1. Expression and purification

RPA14 and RPA32 subunits were co-expressed from a single pET16 plasmid (Novagen). A 6×His tag followed by a thrombin cleavage site was placed at the N-terminus of RPA14. BL21(DE3) cells (Novagen) were transformed and 8 l of Terrific Broth containing 100 µg ml^{-1} ampicillin was inoculated with an 8 ml starter culture and rested at room temperature overnight in a laboratory fermentor (Virtis). The next morning the culture was grown (300 rev min^{-1}, 310 K, 15 l O$_2$ min^{-1}) to an OD$_{600}$ of 4.0–5.0 (4.5–5 h), induced with 1 mM IPTG and grown for another 3.5–4 h. The cells were harvested by centrifugation (10 000 rev min^{-1}, 277 K, 10 min) and the cell pellet was resuspended in four volumes of lysis buffer (30 mM HEPES pH 7.8, 200 mM KCl) supplemented with 4–10 mM imidazole and 1 mM DTT.

For preparation *A*, the cells were lysed by sonication, centrifuged (15 000 rev min^{-1}, 277 K, 30 min) and the supernatant was passed through a 0.20 µm filter. The clarified lysate was loaded onto a 1.67 ml MC/M Ni^{2+} affinity column (PerSeptive Biosystems) equilibrated with lysis buffer with 4 mM imidazole. The column was washed with 15 column volumes (CV) of lysis buffer with 60 mM imidazole and the protein eluted with a 60–1000 mM, 20 CV imidazole gradient using the BioCAD Sprint. For preparations *B–G*, the cells were lysed by three passes through a French pressure cell (SLM-Aminco). The lysed cells were centrifuged and supernatant was passed through 5–10 ml of Cellular Debris Remover resin (Whatman) in a 60 ml syringe. The clarified lysate was loaded onto a 5 ml Ni-NTA Superflow column (Qiagen) equilibrated with lysis buffer with 10 mM imidazole. The column was washed with 10 CV of lysis buffer with 10 mM imidazole and the protein was eluted with a 10–500 mM 20 CV

Table 1
Interpretation and use of the statistical parameters calculated by *Dynamics* 4.0.

Parameter	Interpretation†
Baseline	
0.977–1.002	Monomodal distribution
1.003–1.005	Bimodal distribution, use *DynaLS*
>1.005	Bimodal/multimodal distribution, use *DynaLS*
Sum of squares (SOS)	
1.000–5.000	Low noise, negligible error
5.000–20.000	Background error owing to noise, low protein concentration or a small amount of polydispersity
>20.000	High noise/error owing to high polydispersity in size distribution (aggregation), irregular solvent
Polydispersity	Note: this parameter should be used for monomodal distributions only
$C_P/R_H < 15\%$	Monodisperse solution, very likely to crystallize
$C_P/R_H < 30\%$	A moderate amount of polydispersity, more likely to crystallize
$C_P/R_H > 30\%$	A significant amount of polydispersity, less likely to crystallize

† Adapted from the DynaPro-801 Operator Manual, Protein Solutions Inc.

imidazole gradient using a Bio-Logic LP system (Bio-Rad). For preparations *A–G*, the pooled fractions were diluted five times with 30 mM HEPES pH 7.8 and varying amounts of fresh DTT was added. The diluted protein was loaded onto a 1.67 ml POROS HQ/M strong anion-exchange column (PerSeptive Biosystems). The column was washed with 10 CV of 30 mM HEPES pH 7.8 containing DTT and 10 mM KCl. For preparation *A*, the protein was eluted with a 10–1000 mM KCl 10 CV gradient. For preparations *B–G*, a gradient from 10–700 mM KCl over 40 CV was used. All column fractions were analyzed by SDS–PAGE (Pharmacia LKB PhastSystem) and those HQ column fractions of sufficient concentration were also analyzed by DLS. Pooled fractions were concentrated with a Centriprep YM-10 (Amicon). Protein concentration was determined using the Bradford Protein Assay (BioRAD) with BSA as the standard.

2.2. Dynamic light-scattering analysis

DLS was carried out using a DynaPro-801 molecular-sizing instrument equipped with a microsampler (Protein Solutions). A 50 µl sample was passed through a filtering assembly containing a 0.02 µm filter into a 12 µl chamber quartz cuvette. The data were analyzed using the *Dynamics* 4.0 and *DynaLS* software as described by Moradian-Oldak *et al.* (1998). Interpretation of the statistical parameters generated by the *Dynamics* 4.0 software is summarized in Table 1.

2.3. Crystallization

All crystallization was performed at 293 K using vapor-diffusion methods with hanging or sitting drops. Drop volumes of 4 µl (by mixing equal volumes of protein and reservoir solutions) and reservoir volumes of 500 µl were used. Initial screening was performed with Hampton Research Crystal Screens 1 and 2 (Jancarik & Kim, 1991).

Table 2
Dynamic light-scattering data and resultant crystallization time.

Data with a monomodal distribution was analyzed using *Dynamics* 4.0 and multimodal data with *DynaLS*, with percentages of peak area given in parentheses. The concentration of DTT used in the HQ buffer system is given. Crystallization condition I was used for each preparation and monitored weekly.

| Preparation	Concentration (mg ml^{-1})	R_H (nm)	MW (kDa)	C_P (nm)	C_P/R_H (%)	Baseline	SOS error	DTT (mM)	Time (d)
A	5	3.1 (77) 1090 (23)	45.0	NA	NA	1.047	1.400	0	270–360
B	1–2	3.41	56.8	1.1	33.1	1.001	6.065	0	28
C	1–2	3.39	56.0	0.9	25.7	1.000	4.550	1	28
D	1–2	3.49	59.9	0.7	20.8	1.001	1.397	5	14
E	10	3.39	56.1	0.6	18.3	1.000	1.363	10	6
F	10	3.60	64.9	0.6	17.5	1.000	0.848	10	6
G	13	4.13	90.3	0.6	14.5	1.000	0.666	10	NA

2.4. Data collection

Single crystals were immersed in cryoprotectant (either the reservoir solution with 30% glycerol or paratone-N oil) for 3 s, mounted in a cryoloop and immediately placed in a 100 K nitrogen-gas stream. Diffraction data were collected on hexagonal (Fig. 1a) and orthorhombic crystal form II (Fig. 1d)

at Stanford Synchrotron Radiation Laboratory beamline 7-1 with a MAR345 detector at a wavelength of 1.08 Å. Low-resolution (LR) and high-resolution (HR) passes were designed using *MOSFLM/STRATEGY*. For hexagonal crystals, 28 HR images were collected at a crystal-to-detector distance (XTD) of 300 mm, $\Delta\varphi = 2°$ using the 345 mm plate (edge = 2.09 Å), 30 LR images were collected at an XTD of 350 mm and 58 LR images were collected at an XTD of 300 mm using the 180 mm plate (edge = 3.72–4.3 Å). For orthorhombic form II crystals, 365 HR images were collected at an XTD of 225 mm, $\Delta\varphi = 0.25°$ (0.5° for 20 images) using the 300 mm plate (edge = 1.86 Å) and 366 LR images were collected at an XTD of 240 mm, $\Delta\varphi = 0.5°$ (1.0° for 48 images) using the 180 mm plate (edge = 3.03 Å). Images were integrated with *MOSFLM* (Powell, 1999) and scaled using *SCALA* and the *CCP4i* graphical interface (Collaborative Computational Project, Number 4, 1994). The HR data from the orthorhombic crystals were difficult to integrate because all the data were recorded as partial reflections. A pre-release of a new version of *MOSFLM* was provided by Dr Harry Powell to integrate these images using the POSTREF MULTI keyword.

Diffraction data were collected from orthorhombic crystal form I (Fig. 1c) at beamline 17-ID in the facilities of the Industrial Macromolecular Crystallography Association Collaborative Access Team (IMCA-CAT) at the Advanced Photon Source (APS). 180 images were collected at a crystal-to-detector distance of 120 mm with $\Delta\varphi = 1°$, $\lambda = 1.2$ Å and using the MARCCD detector. Data were processed using the *HKL2000* program suite (Otwinowski & Minor, 1996).

3. Results and discussion

RPA14/32 was overexpressed in *Escherichia coli* and up to 15 mg of pure protein was obtained from a liter of culture. Since monodispersity is thought to be predictive of crystallizability (Zulauf & D'Arcy, 1992; Ferre-D'Amare & Burley, 1997), DLS was used to examine all preparations of RPA14/32. Initial
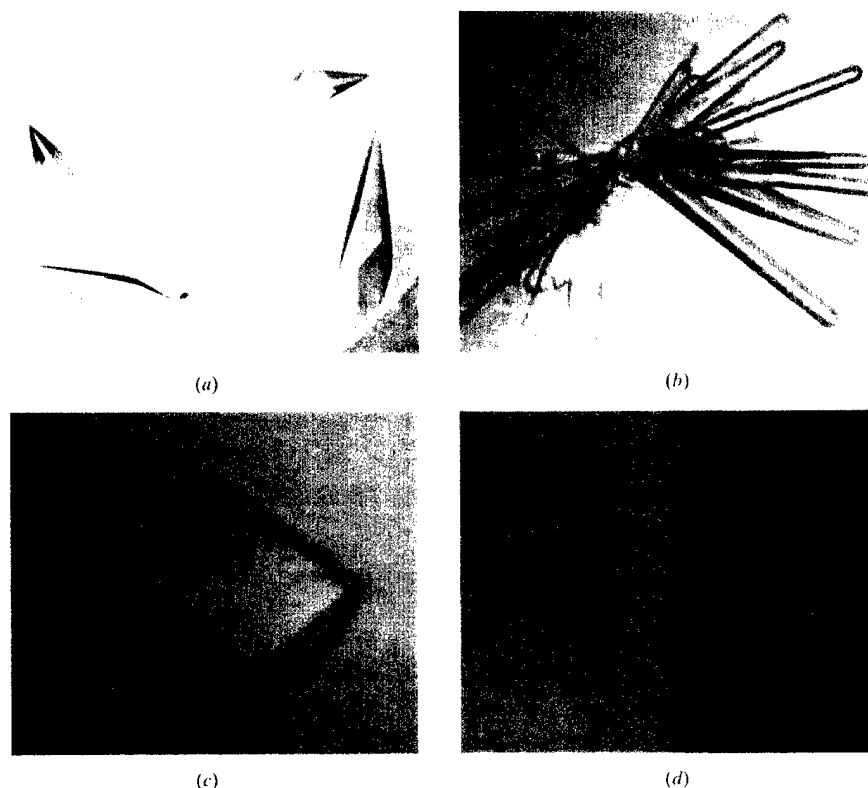
Figure 1
Crystals of RPA14/32. (a) Hexagonal crystals grown from preparation A with a precipitating solution of 0.1 M bicine pH 9.0, 10% acetonitrile and 20% saturated ammonium sulfate. The largest crystal was 90 × 150 μm. (b) Monoclinic crystals grown from preparation E with 10% dioxane, 0.1 M MES pH 6.5 and 37% saturated ammonium sulfate. The largest crystal was 44 × 440 μm. (c) Orthorhombic crystal form I grown from preparation P1 with 0.1 M MES pH 6.3, 5% saturated ammonium sulfate and 26% PEG MME 5000 (242 × 275 μm). (d) Orthorhombic crystal form II grown from preparation P1 with 10% dioxane, 0.1 M MES pH 6.5 and 39% saturated ammonium sulfate (132 × 220 μm).

purifications were multimodal (baseline 1.047) and poly-disperse (Table 2, preparation A) and did not crystallize unless organics were added to the crystallization setup. After 9–12 months, hexagonal crystals grew from solutions that contained 20–30% saturated ammonium sulfate, 0.1 M HEPES, Tris or bicine pH 7–9 and 6–10% organic solvent (acetonitrile, 2-propanol or methanol). Although of diffraction quality, these crystals were difficult to reproduce (Fig. 1a).

Preparation B was monomodal (baseline 1.001, Table 2) but was significantly polydisperse (C_P/R_H = 33.1). Initial crystallization screens produced microcrystals within a month. Grid-screen optimization resulted in the following crystallization condition that produced monoclinic diffraction-quality crystals (Fig. 1b): 10% dioxane, 0.1 M MES pH 5.7–6.5 and 34–41% saturated ammonium sulfate (condition I). Prepara-
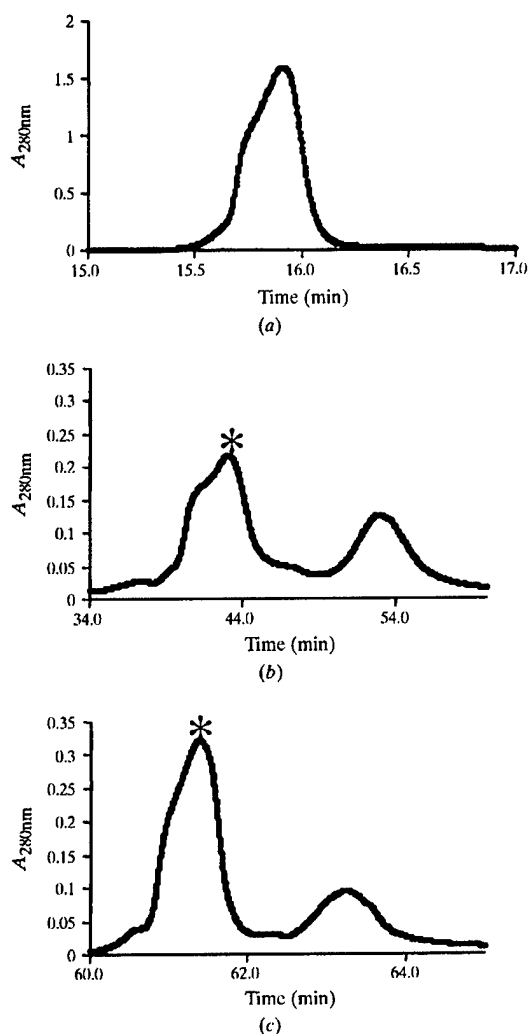
Table 3
Dynamic light-scattering data for chromatography peaks P and $P1$.

Preparation	Concentration (mg ml^{-1})	R_H (nm)	MW (kDa)	C_P (nm)	C_P/R_H (%)	Baseline error	SOS
P	8.2	4.12	89.7	0.9	22.8	1.001	1.201
$P1$	8.5	3.62	65.5	0.9	23.7	1.001	1.431
$P + P1$	8.35	3.9 (91) 1170 (6.6)	78.5	NA	NA	1.005	2.841

Figure 2
Representative chromatograms of RPA14/32 elution at ∼300 mM KCl from the HQ anion-exchange column. (a) Preparation A, (b) preparation B, (c) preparation C. SDS–PAGE analysis showed that all peaks are composed of hRPA14/32 dimer (data not shown). For preparations B–G, the fractions corresponding to the peak indicated with an asterisk (*) were collected.

tion B was significantly less polydisperse and crystallized in less time than preparation A. The differences between these preparations, the lysis method and the type of nickel affinity matrix used, do not account for the overall improvement in polydispersity. The elution profiles from the HQ anion-exchange column (Figs. 2a and 2b) show that in preparation B, where a shallower salt gradient was used, two peaks were separated, whereas in preparation A the protein eluted as one peak. In both preparations, analysis by SDS–PAGE indicated that all the peaks contained only RPA14/32. The lack of separation of these peaks in preparation A probably contributed greatly to the polydispersity of the early RPA14/32 samples (see below).

The primary sequence of RPA14/32 contains four cysteine residues (two in each subunit) and the structure of the proteolytic core of RPA14/32 had free cysteines (Bochkarev et al., 1999). These observations suggested the need for a reducing environment during protein purification. The effect of varying the concentration of dithiothreitol (DTT) in the HQ buffer system was monitored by DLS and crystallization time. In preparations B–G, as the DTT concentration was increased, polydispersity (C_P/R_H) and the time for crystal formation systematically decreased (Table 2). A DTT effect was also seen in the elution profiles. When fresh 1 mM DTT was added during the dilution of the protein sample and added to the HQ buffer system, the first peak increased and the second peak decreased (Figs. 2b and 2c). With 10 mM DTT, the second peak nearly disappears (data not shown). This suggests that the reduction of disulfide bond(s) is involved in converting the second peak into the first peak.

As frequently happens in science, an interesting observation on RPA14/32 came from careful analysis of a fortuitous mistake. Early in this work, the ionic strength of the protein sample was not reduced by dilution before loading onto the HQ column. The standard HQ protocol was run and a fraction of the protein sample was found to bind to the column (fraction P, Table 2). The flowthrough from this column was then diluted and reloaded onto the HQ column. The protein fraction $P1$ was eluted from the column. When analyzed by DLS (Table 3), fractions P and $P1$ were monomodal (baseline 1.001) with moderate polydispersity (C_P/R_H 23%). However, when the two fractions were mixed together, the solution became multimodal (baseline 1.005) with 7% high-molecular-weight aggregates. The molecular weight of fraction P (90 kDa) corresponded to that of a dimer of dimers, whereas fraction $P1$ was closer to that of a single dimer.

Table 4
Dynamic light-scattering data collected at various time points after the addition of acetonitrile to $P + P1$ mixture.

Time (h)	R_H (nm)	MW (kDa)	Baseline error	SOS
0	3.61 (77.5)	65.1	1.010	1.837
	1340 (8.7)			
1	3.84 (94.4)	75.6	1.003	1.539
	1310 (4.4)			
3	4.02 (96.4)	84.5	1.001	1.459
	1270 (1.9)			

Table 5
Dynamic light-scattering data on the dilution of preparation G.

Line No.	Concentration (mg ml^{-1})	R_H (nm)	MW (kDa)	C_P (nm)	C_P/R_H (%)	Baseline error	SOS
1	13	4.13	90.3	0.6	14.5	1.000	0.677
2	6.5	3.52 (77.7)	61.2	NA	NA	1.022	5.211
		30.1 (3.3)	11200				
		986 (18.3)					
3	6.5	3.52 (87.4)	61.2	NA	NA	1.005	0.881
		1330 (6.7)					
4	6.5	3.69	68.5	0.6	16.6	1.000	0.522

Crystallization conditions were screened and optimized for preparation $P1$. Large chunky crystals (Fig. 1c) were obtained from solutions containing 0–5% saturated ammonium sulfate, 0.1 M MES pH 5.9–6.5 and 16–36% PEG MME 5000 (condition II). These crystals were extremely sensitive and cracked easily when cryoprotected with glycerol. Diffraction data of reasonable quality was obtained using paratone-N oil as a cryoprotectant. Preparations B–G will not crystallize under condition II but preparation $P1$ will crystallize under condition I in an orthorhombic space group (Fig. 1d).

The different oligomerization state of the protein fractions P and $P1$ may explain the multimodality and polydispersity of preparation A. Since crystals were obtained when 6–10% organic solvent was added to preparation A, it was postulated that acetonitrile would reduce the polydispersity of the $P + P1$ mixture. Acetonitrile was added to the $P + P1$ mixture to a final concentration of 6%, incubated at 277 K for 3 h and monitored periodically by DLS (Table 4). Incubation with acetonitrile caused the amount of non-aggregated RPA14/32 to increase from 78 to 96% and the solution becomes monomodal. Interestingly, the molecular weight of the non-aggregated species continues to increase until it is roughly the size of a dimer of dimers.

It was noted that as the protein concentration increased, the molecular weight increased (Table 2) and at 13 mg ml^{-1} (preparation G) it was consistent with a dimer of dimers in solution. Therefore, this apparent self-association of the dimer was analyzed by dilution followed by DLS. Samples of preparation G (Table 5, row 1) were diluted with an equal volume of the following buffers: 30 mM HEPES pH 7.8 buffer (row 2), 30 mM HEPES pH 7.8 and 200 mM KCl (row 3) or 30 mM HEPES pH 7.8, 200 mM KCl and 10 mM DTT (row 4). Dilution with buffer alone produced a smaller molecular

Table 6
Data-collection statistics.

	Orthorhombic form I	Orthorhombic form II	Hexagonal
Beamline	APS 17-ID	SSRL 7-1	SSRL 7-1
Detector	MAR CCD	MAR345	MAR345
Temperature (K)	100	100	100
Wavelength (Å)	1.2	1.08	1.08
Space group	$P2_12_12_1$	$P2_12_12_1$	$P3_2$ (or $P3_1$)
Unit-cell parameters (Å)	$a = 61.4$,	$a = 81.8$,	$a = b = 63.0$,
	$b = 75.2$,	$b = 140.4$,	$c = 272.6$
	$c = 131.7$	$c = 173.1$	
Heterodimers in the asymmetric unit	1	3–5	2–3
V_M (Å^3 Da^{-1})	3.17	3.42–2.05	3.25–2.17
Solvent content (%)	61	64–40	62–43
Resolution (Å)	2.20	1.86	2.40
No. of measured reflections	181370	820454	141010
No. of unique reflections	31207	158549	43885
Completeness (%)	98.2 (97.9)	95.6 (81.4)	92.7 (91.9)
$I/\sigma(I)$	18.3 (2.5)	9.3 (1.0)	4.5 (1.0)
Multiplicity	5.8	5.2 (3.3)	3.2 (2.0)
R_{merge}† (%)	8.9	6.0	11.7

† $R_{merge} = \sum_{hkl} |\langle I_{hkl} \rangle - I_{hkl}| / \sum_{hkl} I_{hkl}$.

weight species in addition to large aggregates. Dilution with buffer and salt also produced large-molecular-weight aggregates, but more of the protein sample remains as the single dimer as indicated by an increase in the peak area (from 78 to 87%) associated with the 61 kDa species. Addition of DTT produced a monomodal solution and completely disrupted the large-molecular-weight aggregates. Therefore, the large aggregates of RPA14/32 are probably a consequence of inappropriate disulfide-bond formation and the dimer of dimers appears to be a reversible association. The physiological roles of the RPA14/32 dimer of dimers and the solvent-accessible cysteines on the surface of the molecule are unknown. The possibility of a RPA14/32 dimer of dimers was also suggested by Bochkarev et al. (1999).

Three complete sets of cryocooled synchrotron diffraction data have been collected for structure determination (Table 6). Space groups were assigned by autoindexing, comparing R_{merge} values for space groups within the indicated Laue group and by observed systematic absences. The hexagonal crystals (Fig. 1a) diffracted to 2.4 Å resolution, with space group $P3_2$ (or $P3_1$) and unit-cell parameters $a = b = 63.0$, $c = 272.6$ Å. The orthorhombic crystal form I (Fig. 1c) diffracted to 2.2 Å resolution, with space group $P2_12_12_1$ and unit-cell parameters $a = 61.4$, $b = 75.2$, $c = 131.7$ Å. The orthorhombic crystal form II (Fig. 1d) diffracted to 1.9 Å resolution with space group $P2_12_12_1$ and unit-cell parameters $a = 81.8$, $b = 140.4$, $c = 173.1$ Å. Interestingly, solvent-content analysis (Matthews, 1968) indicates several heterodimers in the asymmetric unit of the orthorhombic crystal form II and hexagonal unit cells. Solution of the phase problem using coordinates of a proteolytic fragment of RPA14/32 (containing intact RPA14 and 60% of RPA32; PDB code 1quq) is in progress.

References

Bochkarev, A., Bochkareva, E., Frappier, L. & Edwards, A. M. (1999). *EMBO J.* **18**, 4498–4504.

Bochkarev, A., Pfuetzner, R. A., Edwards, A. M. & Frappier, L. (1997). *Nature (London)*, **385**, 176–181.

Bochkareva, E., Frappier, L., Edwards, A. M. & Bochkarev, A. (1998). *J. Biol. Chem.* **273**, 3932–3936.

Boubnov, N. V. & Weaver, D. T. (1995). *Mol. Cell. Biol.* **15**, 5700–5706.

Brill, S. J. & Stillman, B. (1991). *Genes Dev.* **5**, 1589–1600.

Brush, G. S., Anderson, C. W. & Kelly, T. J. (1994). *Proc. Natl Acad. Sci. USA,* **91**, 12520–12524.

Carty, M. P., Zernik-Kobak, M., McGrath, S. & Dixon, K. (1994). *EMBO J.* **13**, 2114–2123.

Collaborative Computational Project, Number 4 (1994). *Acta Cryst.* D**50**, 760–763.

Din, S.-U., Brill, S. J., Fairman, M. P. & Stillman, B. (1990). *Genes Dev.* **4**, 968–977.

Dutta, A., Ruppert, J. M., Aster, J. C. & Winchester, E. (1993). *Nature (London)*, **365**, 79–82.

Dutta, A. & Stillman, B. (1992). *EMBO J.* **11**, 2189–2199.

Fairman, M. P. & Stillman, B. (1988). *EMBO J.* **7**, 1211–1218.

Fang, F. & Newport, J. W. (1993). *J. Cell Sci.* **106**, 983–994.

Ferre-D'Amare, A. R. & Burley, S. K. (1997). *Methods Enzymol.* **276**, 157–166.

Fried, L. M., Koumenis, C., Peterson, S. R., Green, S. L., Zijl, P. V., Turner, J. A., Chen, D. J., Fishel, R., Giaccia, A. J., Brown, J. M. & Kirchgessner, C. U. (1996). *Proc. Natl Acad. Sci. USA*, **93**, 13825–13830.

Gately, D. P., Hittle, J. C., Chan, G. K. T. & Yen, T. J. (1998). *Mol. Biol. Cell*, **9**, 2361–2374.

He, Z., Brinton, B. T., Greenblatt, J., Hassell, J. A. & Ingles, C. J. (1993). *Cell*, **73**, 1223–1232.

Henricksen, L. A., Umbricht, C. B. & Wold, M. S. (1994). *J. Biol. Chem.* **269**, 11121–11132.

Iftode, C., Daniely, Y. & Borowiec, J. A. (1999). *Crit. Rev. Biochem. Mol. Biol.* **34**, 141–180.

Jacobs, D. M., Lipton, A. S., Isern, N. G., Daughdrill, G. W., Lowry, D. F., Gomes, X. & Wold, M. S. (1999). *J. Biomol. NMR*, **14**, 321–331.

Jancarik, J. & Kim, S.-H. (1991). *J. Appl. Cryst.* **24**, 409–411.

Lee, S. H. & Kim, D. K. (1995). *J. Biol. Chem.* **270**, 12801–12807.

Li, L., Lu, X., Peterson, C. A. & Legerski, R. J. (1995). *Mol. Cell. Biol.* **15**, 5396–5402.

Li, R. & Botchan, M. R. (1993). *Cell*, **73**, 1207–1221.

Liu, V. F. & Weaver, D. T. (1993). *Mol. Cell. Biol.* **13**, 7222–7231.

Matsuda, T., Saijo, M., Kuraoka, I., Kobayashi, T., Nakatsu, Y., Nagai, A., Enjoji, T., Masutani, C., Sugasawa, K., Hanaoka, F., Yasui, A. & Tanaka, K. (1995). *J. Biol. Chem.* **270**, 4152–4157.

Matthews, B. W. (1968). *J. Mol. Biol.* **33**, 491–497.

Moradian-Oldak, J., Leung, W. & Fincham, A. G. (1998). *J. Struct. Biol.* **122**, 320–327.

Otwinowski, Z. & Minor, W. (1996). *Methods Enzymol.* **276**, 307–326.

Park, M. S., Ludwig, D. L., Stigger, E. & Lee, S. H. (1996). *J. Biol. Chem.* **271**, 18996–19000.

Powell, H. R. (1999). *Acta Cryst.* D**55**, 1690–1695.

Treuner, K., Findeisen, M., Strausfeld, U. & Knippers, R. (1999). *J. Biol. Chem.* **274**, 15556–15561.

Treuner, K., Okuyama, A., Knippers, R. & Fackelmayer, F. O. (1999). *Nucleic Acids Res.* **27**, 1499–1504.

Wold, M. S. (1997). *Annu. Rev. Biochem.* **66**, 61–91.

Wold, M. S. & Kelly, T. (1988). *Proc. Natl Acad. Sci. USA*, **85**, 2523–2527.

Zulauf, M. & D'Arcy, A. (1992). *J. Cryst. Growth*, **122**, 102–106.

Human RAD52 Exhibits Two Modes of Self-association*

Wasantha Ranatunga‡§, Doba Jackson‡§, Janice A. Lloyd§¶, Anthony L. Forget§¶, Kendall L. Knight¶, and Gloria E. O. Borgstahl‡‖

From the ‡Department of Chemistry, University of Toledo, Toledo, Ohio 43606-3390 and the ¶Department of Biochemistry and Molecular Pharmacology, University of Massachusetts Medical School, Worcester, Massachusetts 01655-0103

The human RAD52 protein plays an important role in the earliest stages of chromosomal double-strand break repair via the homologous recombination pathway. Individual subunits of RAD52 self-associate into rings that can then form higher order complexes. RAD52 binds to double-strand DNA ends, and recent studies suggest that the higher order self-association of the rings promotes DNA end-joining. Earlier studies defined the self-association domain of RAD52 to a unique region in the N-terminal half of the protein. Here we show that there are in fact two experimentally separable self-association domains in RAD52. The N-terminal self-association domain mediates the assembly of monomers into rings, and the previously unidentified domain in the C-terminal half of the protein mediates higher order self-association of the rings.

The repair of double-strand breaks in chromosomal DNA is of critical importance for the maintenance of genomic integrity. In *Saccharomyces cerevisiae*, genes of the *RAD52* epistasis group, *RAD50*, *RAD51*, *RAD52*, *RAD54*, *RAD55*, *RAD57*, *RAD59*, *MRE11*, and *XRS2*, were identified initially by the sensitivity of mutants to ionizing radiation (1, 2). These genes have been implicated in an array of recombination events including mitotic and meiotic recombination as well as double-strand break repair. *RAD52* mutants show the most severe pleiotropic defects suggesting a critical role for the protein in homologous recombination and double-strand break repair (2). The importance of specific protein-protein interactions in the catalysis of homologous recombination is suggested by studies demonstrating specific contacts and functional interactions between Rad52p and a number of proteins involved in recombination including Rad51p (3–8), which catalyzes homologous pairing and strand exchange, and replication factor A (RPA)[1] (8–10), a heterotrimeric single-stranded DNA binding protein (11).

Studies of the equivalent human proteins have identified similar interactions between the RAD52, RAD51, and replication protein A proteins (12–17). Based on a series of protein-protein interaction assays (15, 16, 18) and DNA binding studies[2] (16), a domain map of RAD52 was proposed by Park *et al.* (16) (see Fig. 1). The determinants of self-association were proposed to exist exclusively within a region defined by residues 65–165, a result supported by recent studies of several isoforms of RAD52 (19). Electron microscopy (EM) studies of Rad52p and RAD52 have revealed formation of ring-shaped structures (9–13 nm in diameter), as well as higher order aggregates (9, 12, 20). Stasiak *et al.* (21) performed image analyses of negatively stained electron micrographs and determined that the 10-nm RAD52 rings are composed of seven subunits. Scanning transmission electron microscopy (STEM) analysis indicated a mean mass of 330 ± 59 kDa supporting a heptameric ring-shaped RAD52 structure (21). Recent studies show that RAD52 binds to double-stranded DNA ends as an aggregated complex (20). These end-binding complexes were amorphous in shape and ranged in size from 15 to 60 nm. Within these complexes, RAD52 rings were observed occasionally. Binding of RAD52 to the DNA ends promoted end-to-end association between DNA molecules and stimulated ligation of both cohesive and blunt DNA ends (20).

Therefore, given that the formation of both ring-shaped oligomers and aggregates of these rings seem relevant to RAD52 function, we sought to investigate further the self-association properties of the RAD52 protein. We performed a series of analyses comparing full-length RAD52-(1–418) with two different mutant RAD52 proteins: (i) a 1–192 mutant that spans the N-terminal portion and includes the entire proposed DNA binding and self-association domains and (ii) a 218–418 mutant that spans the C-terminal portion of RAD52 that includes the proposed RPA- and RAD51-binding domains (Fig. 1). In contrast to previous studies, our results show that there are experimentally separable determinants for two different modes of self-association by RAD52, one in the N-terminal and one in the C-terminal portion of the protein.

EXPERIMENTAL PROCEDURES

RAD52 Constructs—Wild-type *RAD52* and *RAD52*-(1–192) pET28 expression plasmids were a gift from Dr. M. Park and have six histidines fused to the C terminus. A pET28 expression plasmid containing the thioredoxin-RAD52-(218–418) fusion protein was constructed using standard polymerase chain reaction techniques.

Protein Purification—Cultures of transformed BL21(DE3) Codon Plus *Escherichia coli* (Stratagene) were grown in a fermentor and induced with 0.5 mM isopropyl-1-thio-β-D-galactopyranoside. Wild-type *RAD52* and *RAD52*-(1–192) cells were resuspended in a buffer consisting of 20 mM HEPES, pH 6.0, 10% glycerol, 400 mM NaCl, 100 mM KCl, 5 mM β-mercaptoethanol, 1 mM dithiothreitol, 1 mM hexylglucopyranoside, and 1 mM EDTA. *RAD52*-(218–418) cells were resuspended in a

§ These authors contributed equally to this work.

‖ To whom correspondence should be addressed: Dept. of Chemistry, University of Toledo, 2801 W. Bancroft St., Toledo, OH 43606-3390. Tel.: 419-530-1501; Fax: 419-530-4033; E-mail: gborgst@uoft02.utoledo.edu.

[1] The abbreviations used are: RPA, replication protein A; MES, 4-morpholineethanesulfonic acid; EM, electron microscopy; STEM, scanning transmission electron microscopy; BSA, bovine serum albumin; DLS, dynamic light scattering.

[2] J. A. Lloyd, and K. L. Knight, unpublished data.

This paper is available on line at http://www.jbc.org

FIG. 4. **STEM histograms.** STEM mass analyses were performed as described under "Experimental Procedures." Histograms include pooled data from several separate analyses (eight for wild-type RAD52, six for RAD52-(1–192), and five for RAD52-(218–418)). Average mass values were as follows: *A*, wild-type RAD52 298 ± 69 kDa ($n = 309$); *B*, RAD52-(1–192) 227 ± 30 kDa ($n = 277$); *C*, RAD52-(218–418) 153 ± 40 kDa ($n = 119$).

wild-type hRad52
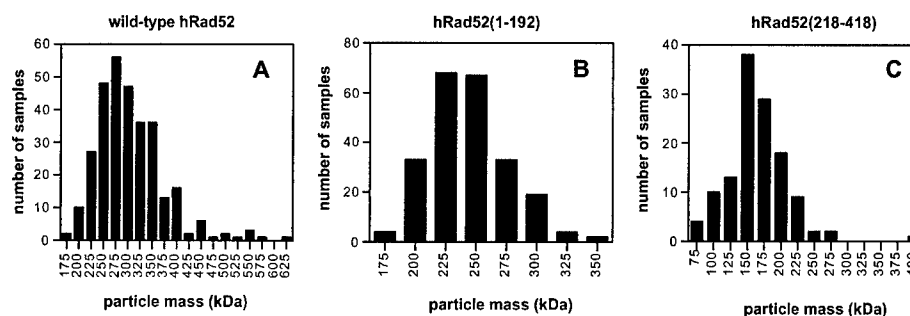
hRad52(1-192)

hRad52(218-418)

TABLE I

Dynamic light-scattering measurements of RAD52 proteins

Protein	Concentration	Base line	Modality	SOS[a]	R_H[b]	Molecular mass	Peak[c] area
	mg/ml			*error*	*nm*	*kDa*	*%*
RAD52	3.5	1.007	Multimodal	3.10	6.6 (0.7)	279	10.5
					27.6 (9.3)	9.05×10^3	85.8
					711.0 (245)	2.40×10^7	3.7
RAD52-(1–192)	15	1.001	Monomodal	1.95	5.7 (1.2)	200	
RAD52-(218–418)	2	1.001	Monomodal	0.64	4.6 (2.1)	118	
Thioredoxin	1	1.001	Monomodal	3.3	2.0 (0.8)	14.8	

[a] SOS, sum of squares.

[b] Average hydrodynamic radius (R_H) is reported with the polydispersity (width of the distribution in nm) given in parentheses.

[c] For DynaLS results the percent peak area for the solvent peak is not reported.

pressed structures. For RAD52-(1–192) the majority of protein forms ring-shaped oligomers, and no larger particles were seen (Fig. 3). Even at increased concentrations (6 and 10 μM) RAD52-(1–192) shows no larger aggregates (data not shown). Higher magnifications reveal "protrusions" extending from the 10-nm rings formed by wild-type RAD52 that are missing in the 1–192 protein (see *arrows* in Fig. 3, *B* and *D*). These protrusions likely correspond to those modeled by Stasiak *et al.* (21), and our data show that they are part of the C-terminal portion of RAD52.

STEM analyses of wild-type RAD52 (2 μM) showed particle sizes ranging from 175 to 625 kDa with a mass average of 298 ± 69 kDa ($n = 309$; Fig. 4*A*). Given a molecular mass of 48 kDa for the His-tagged RAD52 protein, this range corresponds to particles that contain from 4 to 13 subunits with an average of six subunits. Similar analyses of the 1–192 protein showed particle sizes ranging from 100 to 350 kDa with a mass average of 227 ± 30 kDa ($n = 277$; Fig. 4*B*). For a monomer molecular mass of 23 kDa, this range corresponds to particles that contain from 4 to 15 subunits with an average of 10 subunits. Resolution of the ring-shaped oligomers in the electron micrographs was not high enough to count individual subunits, but our STEM data are consistent with previous work in which oligomeric rings of wild-type RAD52 were determined to be heptameric (21).

The oligomeric distribution of these proteins in solution was investigated by DLS. Wild-type RAD52 shows a multimodal profile with three peaks corresponding to particles with an average hydrodynamic radius of 6.6, 27.6, and 711.0 nm, respectively (Table I). These likely correspond to ring-shaped oligomers, the 30-nm particles described previously as "super-rings" (12) and seen in our micrographs (Fig. 2), and larger aggregates also observed in our micrographs. We find that the percent distribution of these various sized particles is effected by protein concentration, *i.e.* with increasing concentration the larger aggregates account for a larger percentage of the population. In contrast to wild type, RAD52-(1–192) shows a monomodal light-scattering profile that corresponds to a particle with a hydrodynamic radius of 6.1 nm (Table I), which is in agreement with our EM analysis.

The above analyses indicate at least two modes of RAD52 self-association that are experimentally separable, (i) forma-

hRad52(218-418)
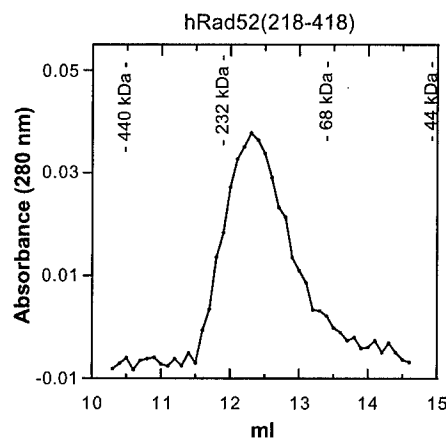
FIG. 5. **Gel filtration profile of the thioredoxin/218–418 fusion RAD52 protein.** The mutant protein (1.2 mg/ml, 35.8 μM) was loaded onto a Superdex 200 HR 10/30 gel filtration column, and elution of protein was followed at $A_{280\ nm}$. The indicated elution volumes of standards (ferritin, *440 kDa*; catalase, *232 kDa*; BSA, *68 kDa*; ovalbumin, *44 kDa*) were an average of four runs.

tion of ring-shaped oligomers and (ii) formation of larger aggregates. Because the latter seems to depend largely on the presence of residues C-terminal to position 192, we performed a number of assays to test for self-association on a mutant RAD52 containing only residues 218–418. Initial EM studies showed no distinct structural characteristics for this protein (data not shown), but STEM analysis revealed particle sizes ranging from 75 to 275 kDa (Fig. 4*C*) with a mass average of 153 ± 40 kDa ($n = 119$; Fig. 4*C*). Given a monomer molecular mass of 39 kDa, the particle composition ranges from two to seven subunits with an average of four subunits. Gel filtration shows a homogeneous peak corresponding to a molecular mass of 166 kDa (Fig. 5) and therefore to a particle containing approximately four subunits. Analysis by DLS shows a monomodal peak corresponding to a particle with an average R_H of 4.6 nm and a molecular mass of 118 kDa (therefore containing approximately three subunits). DLS measurements on thioredoxin alone show that it does not contribute to the oligomeric character of thioredoxin-RAD52-(218–418) (Table I). Together,

tein make important contributions to RAD52 self-association. Thus, the C-terminal region of RAD52 contains a novel self-association domain distinct from that previously identified within residues 65–165 (18).

Importantly, functional analyses of both the 1–192 and 218–418 mutant proteins show that each maintains an expected activity. Both wild-type RAD52 and the 1–192 proteins, which form ring-shaped oligomers, bound single-stranded DNA with similar affinities. This is consistent with previous studies that mapped the DNA binding domain of RAD52 to residues 39–80[2] (16). The elevated affinity of RAD52-(1–192) for single-stranded DNA was noted also for a similar Rad52p construct (24). Also as expected, RAD52-(218–418) showed a specific interaction with RPA. Again, this is consistent with previous studies that mapped the RPA interaction domain to residues 221–280 in RAD52 (16). The fact that both mutant proteins showed the expected functions demonstrates that they very likely maintain native structure, thereby supporting the relevance of differences observed in their oligomeric characteristics compared with wild-type RAD52.

In summary, our data support a model in which the self-association domain within the N-terminal region of RAD52 (residues 1–192) promotes the formation of ring-shaped oligomers that are functional for DNA binding, whereas the C-terminal domain (residues 218–418) mediates higher order self-association events. Additionally, the protrusions extending from the 10-nm ring structure of wild-type RAD52, originally modeled by Stasiak *et al.* (21) and seen clearly in our electron micrographs, correspond to the C-terminal region of the protein. Given the likely importance of higher order self-association to the ability of RAD52 to promote end-to-end joining of DNA breaks (20), these protrusions seem to mediate a critically important aspect of RAD52 function. Further studies of various mutant RAD52 proteins will clarify the contribution made by the different aspects of self-association toward the overall function of this important DNA repair protein.

REFERENCES

1. Game, J., and Mortimer, R. K. (1974) *Mutat. Res.* **24,** 281–292
2. Petes, T. D., Malone, R. E., and Symington, L. S. (1991) in *The Molecular and Cellular Biology of the Yeast, Saccharomyces* (Broach, J. R., Pringle, J. R., and Jones, E. W., eds) pp. 407–522, Cold Spring Harbor Laboratory Press, Cold Spring Harbor, NY
3. Shinohara, A., and Ogawa, T. (1998) *Nature* **391,** 404–407
4. Milne, G. T., and Weaver, D. T. (1993) *Genes Dev.* **7,** 1755–1765
5. Hays, S. L., Firmenich, A. A., and Berg, P. (1995) *Proc. Natl. Acad. Sci., U. S. A.* **92,** 6925–6929
6. Johnson, R. D., and Symington, L. S. (1995) *Mol. Cell. Biol.* **15,** 4843–4850
7. Sung, P. (1997) *J. Biol. Chem.* **272,** 28194–28197
8. New, J. H., Sugiyama, T., Zaitseva, E., and Kowalczykowski, S. C. (1998) *Nature* **391,** 407–410
9. Shinohara, A., Shinohara, M., Ohta, T., Matsuda, S., and Ogawa, T. (1998) *Genes Cells* **3,** 145–156
10. Sugiyama, T., New, J. H., and Kowalczykowski, S. C. (1998) *Proc. Natl. Acad. Sci. U. S. A.* **95,** 6049–6054
11. Wold, M. S. (1997) *Annu. Rev. Biochem.* **66,** 61–91
12. Van Dyck, E., Hajibagheri, N. M. A., Stasiak, A., and West, S. C. (1998) *J. Mol. Biol.* **284,** 1027–1038
13. Golub, E. I., Gupta, R. C., Haaf, T., Wold, M. S., and Radding, C. M. (1998) *Nucleic Acids Res.* **26,** 5388–5393
14. Baumann, P., and West, S. C. (1999) *J. Mol. Biol.* **291,** 363–374
15. Shen, Z., Cloud, K. G., Chen, D. J., and Park, M. S. (1996) *J. Biol. Chem.* **271,** 148–152
16. Park, M. S., Ludwig, D. L., Stigger, E., and Lee, S. H. (1996) *J. Biol. Chem.* **271,** 18996–19000
17. Benson, F. E., Baumann, P., and West, S. C. (1998) *Nature* **391,** 401–404
18. Shen, Z., Peterson, S. R., Comeaux, J. C., Zastrow, D., Moyzis, R. K., Bradbury, E. M., and Chen, D. J. (1996) *Mutat. Res.* **364,** 81–89
19. Kito, K., Wada, H., Yeh, E. T., and Kamitani, T. (1999) *Biochim. Biophys. Acta* **1489,** 303–314
20. Van Dyck, E., Stasiak, A. Z., Stasiak, A., and West, S. C. (1999) *Nature* **398,** 728–731
21. Stasiak, A. Z., Larquet, E., Stasiak, A., Muller, S., Engel, A., Dyck, E. V., West, S. C., and Egelman, E. H. (2000) *Curr. Biol.* **10,** 337–340
22. Henricksen, L. A., Umbricht, C. B., and Wold, M. S. (1994) *J. Biol. Chem.* **269,** 11121–11132
23. Wall, J. S., Hainfeld, J. F., and Simon, M. N. (1998) *Methods Cell Biol.* **53,** 139–164
24. Mortensen, U. H., Bendixen, C., Sunjevaric, I., and Rothstein, R. (1996) *Proc. Natl. Acad. Sci. U. S. A.* **93,** 10729–10734

Human RAD52 Protein Has Extreme Thermal Stability

Wasantha Ranatunga, Doba Jackson, Robert A. Flowers II, and Gloria E. O. Borgstahl

Department of Chemistry, The University of Toledo, Toledo, Ohio 43606-3390
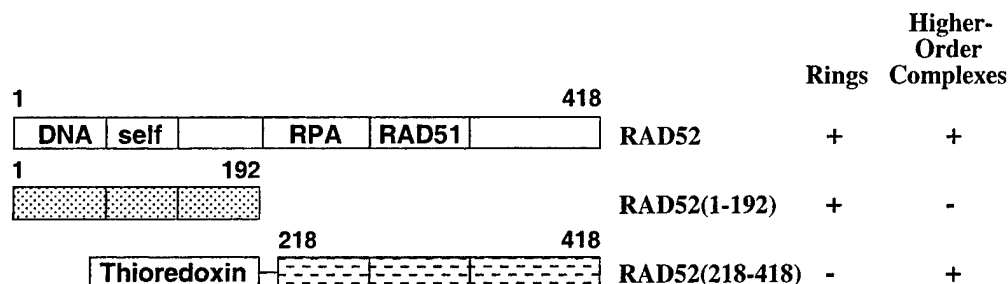
Biochemistry®

FIGURE 1: Wild-type RAD52 and deletion mutants. Beginning and ending residue numbers of each mutant are indicated along with domain structure. The following domains and residue numbers were defined by Park et al. (*16*): DNA binding (39−80), self-association (85−159), RPA binding (221−280), and RAD51 binding (290−330). The structural characterization of wild-type and mutant RAD52 by Ranatunga et al. is summarized on the right (*10*). Wild-type RAD52 and RAD51(1−192) have six histidines fused to the C-terminus. For the RAD52-(218−418) mutant, a thrombin-cleavable six-histidine tag is fused to the N-terminus of the histidine-patch thioredoxin, and an enterokinase cleavage site separates histidine-patch thioredoxin from RAD52(218−418).

Differential Scanning Calorimetry. Protein and reference solutions were degassed under a vacuum for 15 min before data acquisition. The concentration of wild-type RAD52 was 2.0 and 3.5 mg/mL, RAD52(1−192) was 7.2 mg/mL, and RAD52(218−418) was 3.1 mg/mL. The wild-type RAD52 sample was concentrated to 11.5 mg/mL before dilution to either 2.0 or 3.5 mg/mL. The concentrations of wild-type RAD52 and RAD52(218−418) were limited by the quantity of protein available. The protein samples and reference solutions were loaded into their respective cells in the MicroCal MC-2 differential scanning calorimeter. An external pressure of 30 psi was applied with nitrogen gas to both sample and reference cells. The sample was scanned relative to the reference solution over a temperature range of 5−120 °C at a rate of 45 °C/h. DSC measurements on buffer alone had no transitions for the temperature range 5−120 °C. The baseline and change in specific heat (ΔC_p) upon denaturation were corrected according to standard techniques (*11*). DSC data were fit to a two- or three-state model using the Origin DSC software provided by Microcal Inc.

Dynamic Light Scattering Analysis. DLS was carried out using a DynaPro-801 molecular sizing instrument equipped with a temperature-controlled microsampler (Protein Solutions). A 50 μL sample was passed through a filtering assembly equipped with a 100 nm filter into a 12 μL chamber quartz cuvette. For each experiment, 35−60 measurements were taken. The data were first analyzed using Dynamics 4.0 software and then with DynaLS software. The refractive index and viscosity of the buffer at each temperature were measured and the proper corrections applied to the data. Baseline and sum of squares (SOS) error values were reported by Dynamics 4.0. The baseline is the measured value of the last coefficient in the correlation curve. Baselines within the range from 0.977 to 1.002 were interpreted as monomodal, and those greater than 1.002 were bi- or multimodal. The SOS error is the sum of squares difference between the measured correlation curve and the best-fit curve. SOS errors less than 5.000 were considered negligible. Errors between 5.000 and 20.000 were considered as low and probably due to low protein concentration or a small amount of polydispersity. Errors greater than 20.000 were considered as high and are probably due to high polydispersity in size distribution (aggregation) or irregular solvent. Mean R_H, standard deviation, and percent of peak area are reported from DynaLS using the optimized resolution. Due to the irregular solvent, the SOS errors increased for diluted

samples, and it was necessary to use DynaLS to separate the solvent peak from the protein peak.

RESULTS AND DISCUSSION

Differential Scanning Calorimetry. Thermal stability profiles of wild-type RAD52, RAD52(1−192), and RAD52-(218−418) were obtained by DSC (Figure 2 and Table 1). For wild-type RAD52 and RAD52(1−192) the DSC transitions were labeled A, B, or C such that total unfolding was always labeled C. For wild-type RAD52, at 2.0 mg/mL, the DSC profile was composed of two transitions (labeled B and C) with melting temperatures (T_M) of 78.3 and 101.6 °C (Table 1). At 3.5 mg/mL, the wild-type RAD52 DSC profile was composed of three distinct transitions (labeled A, B, and C in Figure 2A) with T_M's of 38.8, 73.1, and 115.2 °C (Table 1). When the concentration of wild-type RAD52 was increased, transition C was shifted to a higher temperature by 13 °C. Transition A could be measured only if the sample was first concentrated to 11.5 mg/mL and then diluted to 3.5 mg/mL. For RAD52(1−192) two transitions were observed at 47.6 and 100.9 °C (labeled B and C in Figure 2B). The deletion of the C-terminal half of RAD52 decreased the T_M of transitions B and C by 25 and 14 °C, respectively.

Our earlier analysis demonstrated that wild-type RAD52 forms ring structures as well as higher order complexes of rings but RAD52(1−192) forms rings but not the aggregates of rings (*10*). The size of the wild-type RAD52 higher order complexes, as well as the proportion of the rings in a higher order complex, is dependent on concentration. RAD52(1−192) rings do not form higher ordered complexes, at any concentration. DSC transition A was dependent on the concentration of wild-type RAD52 and was not observed for RAD52(1−192). Therefore, it appeared that transition A corresponded to the thermal disruption of aggregates to form single rings in solution, transition B to the break up of rings to monomers, and transition C to the total unfolding of monomers.

The DSC profile of RAD52(218−418) is also consistent with this interpretation (Figure 2C). RAD52(218−418) forms a complex of two to four monomers depending on the concentration but does not form ring structures in solution (*10*). It has a relatively low T_M of 53−59 °C, and it appears that the C-terminal half of RAD52, which cannot form rings, is not as thermally stable as the ring-structured N-terminal half.

Wild-type *Escherichia coli* thioredoxin is a very stable protein with a T_M of ∼85 °C for the oxidized form and ∼73

Table 2: Effect of Temperature and Concentration on R_H of Wild-Type RAD52

DLS expt	concn (mg/mL)	base-line	SOS error[a]	R_H[b] (nm)	peak area[c] (%)	interpretation[d]
1. 20 °C	3.5	1.001	4.22	**15.0 (2.5)**	**98.3**	>2 rings
2. heat to 50 °C	3.5	1.000	2.78	**14.2 (4.5)**	**99.2**	~2 rings
3. concd; 20 °C	4.9	1.002	2.03	4.3 (0.5)	3.4	monomer
				18.7 (2.3)	**95.8**	>2 rings
4. concd; 20 °C	11.5	1.009	7.78	5.1 (0.6)	4.2	mono/dimer
				17.8 (3.1)	**56.9**	>2 rings
				36.1 (4.4)	**36.6**	≫2 rings
5. heat to 50 °C	11.5	1.000	5.96	**19.2 (8.5)**	**99.2**	>2 rings
6. cool to 20 °C	11.5	1.010	8.24	5.9 (0.4)	9.7	mono/dimer
				11.2 (0.7)	6.6	1–2 rings
				20.6 (2.2)	**81.6**	>2 rings
7. sample from line 4 diluted; 20 °C	3.5	1.001	11.3	3.8 (0.2)	0.6	monomer
				23.2 (11.6)	**98.1**	>2 rings
8. heat to 50 °C	3.5	1.001	9.41	**9.7 (1.2)**	**45.8**	1 ring
				17.0 (1.0)	**49.8**	>2 rings
9. cool to 20 °C	3.5	1.001	16.1	3.9 (0.2)	1.1	monomer
				11.9 (1.9)	**69.3**	1–2 rings
				28.6 (3.5)	**26.4**	≫2 rings
10. sample from line 3 diluted; 20 °C	3.3	1.001	7.4	**3.1 (0.2)**	**11.0**	monomer
				16.8 (5.4)	**84.0**	>2 rings
				49.5 (8.7)	**14.5**	≫2 rings
11. heat to 37 °C	3.3	1.000	7.9	**19.8 (10.9)**	**99.5**	>2 rings
12. sample from line 4 diluted; 20 °C	2.3	1.001	50.9	**8.75 (6.0)**	**79.7**	1 ring
13. heat to 37 °C	2.3	1.000	24.5	**8.0 (1.6)**	**71.9**	1 ring
14. heat to 50 °C	2.3	1.000	15.9	**8.7 (2.7)**	**87.4**	1 ring

[a] SOS = sum of squares. [b] Average R_H is given with the standard deviation given in parentheses. [c] DynaLS results; the percent peak area for the solvent peaks was not reported. DLS measurements at 20 and 50 °C on solvent alone indicate that very small and very large components in the RAD52 measurements were due to the solvent and not the protein. Therefore, only the peaks attributable to RAD52 protein are reported (R_H > 3.0 nm; see Figure 4). R_H and percent peak area of the primary species in solution (greater than 10%) are in bold. [d] Interpretation is based on estimated R_H in Figure 4. It is not possible to tell exactly how many rings of RAD52 are in the aggregates >14.1 nm since the structure of the higher order complexes of RAD52 rings is unknown.

mL and then diluted (see Table 2 and Figure 3). The microsampler cell was held at 20, 37, or 50 °C, and samples were equilibrated for 30 min at the target temperature before DLS measurements began. The smallest R_H measured for RAD52 was 8.0–8.75 nm (Table 2, lines 12–14). This is close to the size expected for single rings measured from electron micrographs (Figure 4) (6–8). A monomer of RAD52 is expected to have an R_H value of 3.2 nm, and complexes containing two rings are expected to have an R_H of 12.8–14.1 nm. The R_H for aggregates of more than two rings would be greater than 14 nm.

Using these estimates of particle sizes as a guide, four trends in the DLS data were noted. First, heating the protein samples from 20 to 50 °C caused the R_H to decrease in general, and frequently the baseline decreased to within the monomodal range. For example, heating a sample similar to that used for DSC measurements (Table 2, line 7, and Figure 3E) caused the particles to shift from a single population with R_H of 23.2 nm to two populations with R_H of 9.7 and 17.0 nm (Table 2, line 8, and Figure 3F). Second, the size of the sample population was dependent on the protein concentration. For example, the R_H of the sample

FIGURE 3: Effect of protein concentration and temperature on the R_H of wild-type RAD52. DLS data were analyzed using DynaLS software. The data correspond to the following lines in Table 2: (A) 3.5 mg/mL at 20 °C (line 1), (B) 11.5 mg/mL at 20 °C (line 4), (C) 11.5 mg/mL at 50 °C (line 5), (D) 11.5 mg/mL cooled to 20 °C (line 6), (E) diluted to 3.5 mg/mL at 20 °C (line 7), (F) diluted to 3.5 mg/mL at 50 °C (line 8), and (G) diluted to 3.5 mg/mL cooled to 20 °C (line 9). Panels E–G correspond to the sample used for DSC.

B, possibly the disassociation of individual subunits from the rings.

Only a handful of proteins have been measured with thermal stabilities on the order of RAD52. To our knowledge, the highest T_M for a protein reported in the literature to date is 125 °C for ferredoxin from the hyperthermophile *Thermotoga maritima* (*15*). Other proteins such as onconase and mitochondrial manganese superoxide dismutase (MnSOD) are extremely stable with T_M's approaching 90 °C (*16, 17*). Both ferredoxin and onconase are monomeric, and by studying their protein crystal structures, their stabilities were attributed to the compactness of their tertiary structures and to extensive hydrogen bonding involving charged amino acid side chains. Mitochondrial MnSOD is a homotetramer, and its enhanced stability was partially attributed to its quaternary structure. The DSC profile of MnSOD has three thermal transitions (labeled A, B, and C), similar to those seen with RAD52. Transition A was attributed to subunit disassociation, transition B to loss of the active site manganese, and transition C to complete unfolding. A cavity forming point mutation in the tetrameric interface of MnSOD resulted in the lowering of transition B by 13.6 °C and transition C by 16.5 °C (*17*). These results on MnSOD are somewhat similar to the results on RAD52. We conclude from our data that both components of RAD52 self-association, ring formation and higher order complex formation, contribute to its extreme thermal stability. A precise understanding of the structural determinants of RAD52 stability awaits the solution of its crystal structure.

ACKNOWLEDGMENT

REFERENCES

1. Game, J., and Mortimer, R. K. (1974) *Mutat. Res. 24*, 281−292.

2. Petes, T. D., Malone, R. E., and Symington, L. S. (1991) in *The Molecular and Cellular Biology of the Yeast, Saccharomyces* (Broach, J. R., Pringle, J. R., and Jones, E. W., Eds.) pp 407−522, Cold Spring Harbor Laboratory Press, Cold Spring Harbor, NY.

3. Shen, Z., Cloud, K. G., Chen, D. J., and Park, M. S. (1996) *J. Biol. Chem. 271*, 148−152.

4. Shen, Z., Peterson, S. R., Comeaux, J. C., Zastrow, D., Moyzis, R. K., Bradbury, E. M., and Chen, D. J. (1996) *Mutat. Res. 364*, 81−89.

5. Park, M. S., Ludwig, D. L., Stigger, E., and Lee, S. H. (1996) *J. Biol. Chem. 271*, 18996−19000.

6. Shinohara, A., Shinohara, M., Ohta, T., Matsuda, S., and Ogawa, T. (1998) *Genes Cells 3*, 145−156.

7. Van Dyck, E., Hajibagheri, N. M. A., Stasiak, A., and West, S. C. (1998) *J. Mol. Biol. 284*, 1027−1038.

8. Van Dyck, E., Stasiak, A. Z., Stasiak, A., and West, S. C. (1999) *Nature 398*, 728−731.

9. Stasiak, A. Z., Larquet, E., Stasiak, A., Muller, S., Engel, A., Dyck, E. V., West, S. C., and Egelman, E. H. (2000) *Curr. Biol. 10*, 337−340.

10. Ranatunga, W., Jackson, D., Lloyd, J. A., Forget, A. L., Knight, K. L., and Borgstahl, G. E. O. (2001) *J. Biol. Chem.* (in press).

11. Haynie, D. T., and Freire, E. (1994) *Anal. Biochem. 216*, 33−41.

12. Ladbury, J., Wynn, R., Hellinga, H., and Sturtevant, J. (1993) *Biochemistry 32*, 7526−7530.

13. Ladbury, J., Kishore, N., Hellinga, H., Wynn, R., and Sturtevant, J. (1994) *Biochemistry 33*, 3688−3692.

14. Lu, Z., DiBlasio-Smith, E., Grant, K., Warne, N., LaVallie, E., Collins-Racie, L., Follettie, M., Williamson, M., and McCoy, J. (1996) *J. Biol. Chem. 271*, 5059−5065.

15. Pfeil, W., Gesierich, U., Kleemann, G. R., and Sterner, R. (1997) *J. Mol. Biol. 272*, 591−596.

16. Notomista, E., Catanzano, F., Graziano, G., Piaz, F. D., Barone, G., D'Alessio, G., and Donato, A. D. (2000) *Biochemistry 39*, 8711−8718.

17. Borgstahl, G. E. O., Parge, H. E., Hickey, M. J., Johnson, M. J., Boissinot, M., Hallewell, R. A., Lepock, J. R., Cabelli, D. E., and Tainer, J. A. (1996) *Biochemistry 35*, 4287−4297.

JMB

Analysis of the Human Replication Protein A:Rad52 Complex: Evidence for Crosstalk Between RPA32, RPA70, Rad52 and DNA

Doba Jackson[1], Kajari Dhar[2], James K. Wahl[3], Marc S. Wold[2] and Gloria E. O. Borgstahl[1]*

[1]*Department of Chemistry University of Toledo 2801 West Bancroft Street Toledo, OH 43606-3390, USA*

[2]*Department of Biochemistry University of Iowa College of Medicine, 51 Newton Road Iowa City, IA 52242-1109 USA*

[3]*Department of Biology University of Toledo, Toledo OH 43606-3390, USA*

The eukaryotic single-stranded DNA-binding protein, replication protein A (RPA), is essential for DNA replication, and plays important roles in DNA repair and DNA recombination. Rad52 and RPA, along with other members of the Rad52 epistasis group of genes, repair double-stranded DNA breaks (DSBs). Two repair pathways involve RPA and Rad52, homologous recombination and single-strand annealing. Two binding sites for Rad52 have been identified on RPA. They include the previously identified C-terminal domain (CTD) of RPA32 (residues 224–271) and the newly identified domain containing residues 169–326 of RPA70. A region on Rad52, which includes residues 218–303, binds RPA70 as well as RPA32. The N-terminal region of RPA32 does not appear to play a role in the formation of the RPA:Rad52 complex. It appears that the RPA32CTD can substitute for RPA70 in binding Rad52. Sequence homology between RPA32 and RPA70 was used to identify a putative Rad52-binding site on RPA70 that is located near DNA-binding domains A and B. Rad52 binding to RPA increases ssDNA affinity significantly. Mutations in DBD-D on RPA32 show that this domain is primarily responsible for the ssDNA binding enhancement. RPA binding to Rad52 inhibits the higher-order self-association of Rad52 rings. Implications for these results for the "hand-off" mechanism between protein–protein partners, including Rad51, in homologous recombination and single-strand annealing are discussed.

© 2002 Elsevier Science Ltd. All rights reserved

Keywords: human Rad52; replication protein A; double-strand break repair; protein–protein interaction; single-stranded DNA binding

*Corresponding author

Introduction

The repair of double-strand breaks (DSBs) in chromosomal DNA is of critical importance for the maintenance of genomic integrity. In *Saccharomyces cerevisiae*, genes of the RAD52 epistasis group were identified initially by the sensitivity of mutants to ionizing radiation.[1] These genes have been implicated in an array of recombination events, including mitotic and meiotic recombination as well as DSB repair. The importance of specific protein–protein interactions in the catalysis of homologous recombination is suggested by studies that demonstrate specific contacts and functional interactions between scRad52, scRPA and scRad51.[2–6] Studies of the equivalent human proteins have identified similar interactions.[7–9]

Rad52 protein plays a critical role in mitotic and meiotic recombination as well as DSB repair.[1] On the basis of a series of protein–protein interaction assays and DNA-binding studies, a domain map of human Rad52 was proposed (shown in Figure 1).[10]

Abbreviations used: C_p, polydispersity; CTD, C-terminal domain; DBD, DNA-binding domain; DLS, dynamic light-scattering; DSB, double-strand break; EM, electron microscopy; GMSA, gel mobility-shift assay; mAb, mouse monoclonal antibody; OB-fold, oligonucleotide/oligosaccharide binding; Rad52, human Rad52 protein; R_H, hydrodynamic radius; RPA, human replication protein A; RPA14, 14 kDa subunit of RPA; RPA32, 32 kDa subunit of RPA; RPA70, 70 kDa subunit of RPA; scRad52, *Saccharomyces cerevisiae* Rad52; scRPA, *Saccharomyces cerevisiae* RPA; SLS, static light-scattering; SOS, sum of squares; SPR, surface plasmon resonance; ssDNA, single-stranded DNA.

E-mail address of the corresponding author: gborgst@uoft02.utoledo.edu

	Rings	Higher-order Complexes	Relative Binding Affinity to			mAb binding
			ssDNA	RPA	Rad51	
Rad52	+++	+++	+++	+++	+++	1,2,3,4,5,6
Rad52(1-192)	+++	-	+++	-	nd	1,2
Rad52(1-303)	+++	+++	+++	+++	nd	1,2,3
Rad52(1-340)	+++	+++	+++	+++	nd	1,2,3,4
Rad52(218-418)	-	+++	-	+++	nd	3,4,5,6
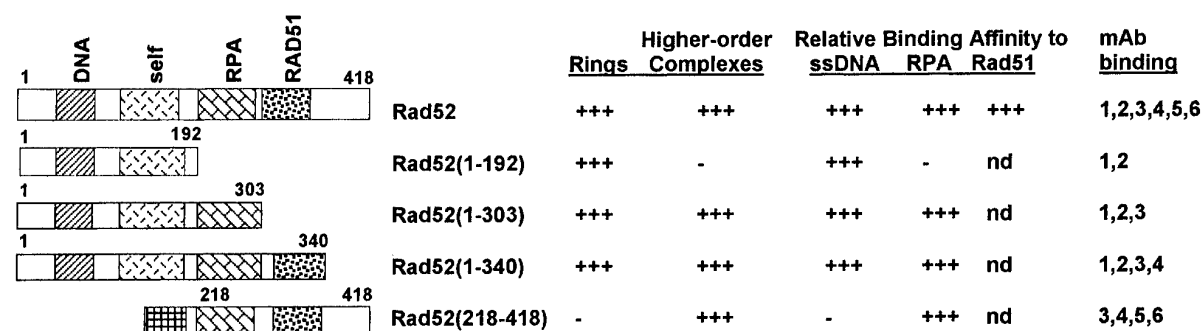
Figure 1. A diagram of the Rad52 domain structure, Rad52 mutants used and characterization of monoclonal antibodies developed against Rad52. Rad52 interaction domains with the residue numbers in parentheses were defined as follows: DNA-binding domain (residues 25–65), Rad52 heptameric ring binding (125–185), RPA32 binding (220–280), Rad51-binding domain (290–340).[10,14,53] Wild-type and mutant Rad52 are shown to the left with domains indicated and beginning and ending residue numbers included. Wild-type Rad52, Rad52(1–192), Rad52(1–303) and Rad52(1–340) pET28 expression plasmids were a gift from Dr Min Park and have six histidine residues fused to the C-terminus. For improved solubility, the Rad52(218–418) mutant has thioredoxin fused to the N terminus. This thioredoxin was modified with six histidine residues fused to its N terminus to improve purification. Characterization of each construct for ring structure, higher-order complexes, relative binding affinity for ssDNA, RPA and Rad51, as well as monoclonal antibody binding are summarized on the right.[14]
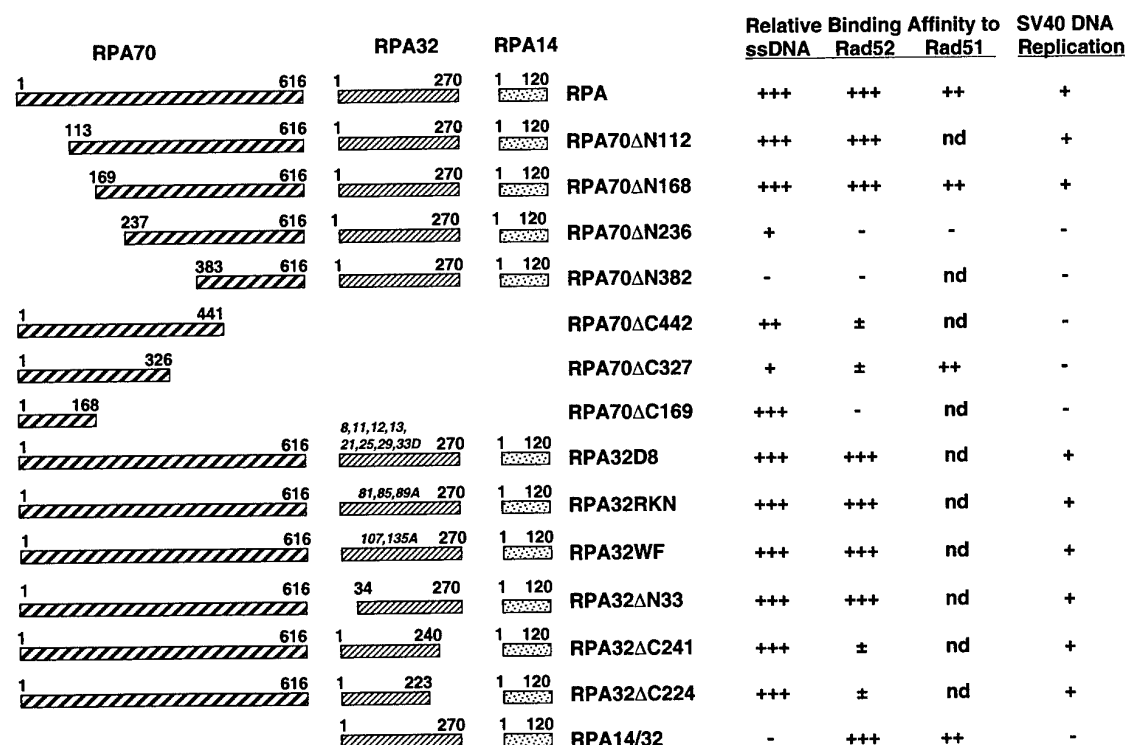
Rad52 has a homologous pairing activity thought to be important in Rad51-independent DSB repair, and this activity was localized to residues 1–237.[11] Electron microscopy (EM) studies of *S. cerevisiae* and human Rad52 have revealed formation of ring-shaped structures (9–13 nm in diameter), as well as higher-order aggregates.[4,9,12] The Rad52 rings appear to be composed of seven subunits.[13] EM studies showed that Rad52 binds to DNA ends as an aggregated complex that ranges in size from approximately 15–60 nm in diameter.[12] This binding has been found to promote end-to-end association between DNA molecules and to stimulate the ligation of both cohesive and blunt DNA ends. Recently, the studies with wild-type and two deletion mutants of Rad52 have demonstrated that the self-association domain in the N-terminal half of Rad52 is responsible for ring formation and that elements in the C-terminal half of the molecule participate in the formation of higher-order complexes of rings.[11,14] Such higher-ordered complexes of Rad52 rings have been shown by EM to mediate single-strand annealing.[15]

RPA is the single-stranded DNA (ssDNA) binding protein that has been found in all eukaryotes examined.[16,17] It is composed of three subunits that have been named for their molecular mass as RPA70, RPA32 and RPA14 (Figure 2). All three subunits of RPA are required for function. All RPA homologs bind ssDNA with high affinity and participate in specific protein–protein interactions. RPA binds tightly to ssDNA with apparent association constants of 10^9–10^{10} M^{-1} and prefers poly-pyrimidine sequences to polypurine sequences.[18–20] The major binding mode for RPA has an occluded binding site of 30 nucleotides per RPA heterotrimer.[21] The major ssDNA binding site is located in the middle of RPA70 and is composed of two structurally conserved oligonucleotide/oligosaccharide binding (OB) domains[19,22] called DBD-A (including residues 181–290) and DBD-B (residues 300–422). To date, four additional OB-folds have been identified in RPA. The N terminus (residues 1–110; called RPA70NTD), the C terminus of RPA70 (residues 432–616; called DBD-C), the central core of RPA32 and the core of RPA14 are all composed of OB-folds.[23–26] RPA is known to undergo a significant conformational change upon binding DNA.[19,27] This conformational shift has been suggested to alter the structure of RPA in a way that facilitates phosphorylation and interactions with other proteins.[27]

RPA is phosphorylated during the S phase of the cell-cycle, in response to DNA damage and during apoptosis.[27–29] The primary phosphorylation sites are located in the N-terminal 33 amino acid residues of RPA32. This DNA damage-induced phosphorylation is coincident with cell-cycle arrest and loss of the ability of cell extracts to support DNA replication[30,31] and in some studies leads to disassembly of the RPA heterotrimer complex.[32] The RPA complex appears to contain all three subunits at sites of ongoing DNA replication.[33,34] These observations suggest that phosphorylation of RPA serves as a mechanism for modulating RPA activity, quaternary structure and its interactions with other proteins. RPA mutants, designed to mimic biological phosphorylation by replacing Ser or Thr with Asp, have been shown to modify the activity of RPA (Braun & M.S.W., unpublished results).

RPA has specific interactions with many proteins; such as replication proteins T antigen, DNA polymerase, and DNA primase; the tumor suppressor p53; transcription factors Gal4 and VP16; and DNA repair factors, XPA, ERCC-1/XPF nuclease, XPG, uracil DNA glycosylase, Rad52 and Rad51.[10,16,17,35–38] Interactions between Rad51, Rad52, and RPA stimulate homologous recombination-based DSB repair.[5,7,8,39] An interaction region of RPA with Rad51 was located between residues

| RPA70	RPA32	RPA14		Relative Binding Affinity to			SV40 DNA Replication
				ssDNA	Rad52	Rad51	
1–616	1–270	1–120	RPA	+++	+++	++	+
113–616	1–270	1–120	RPA70ΔN112	+++	+++	nd	+
169–616	1–270	1–120	RPA70ΔN168	+++	+++	++	+
237–616	1–270	1–120	RPA70ΔN236	+	-	-	-
383–616	1–270	1–120	RPA70ΔN382	-	-	nd	-
1–441			RPA70ΔC442	++	±	nd	-
1–326			RPA70ΔC327	+	±	++	-
1–168			RPA70ΔC169	+++	-	nd	-
1–616	8,11,12,13, 21,25,29,33D 270	1–120	RPA32D8	+++	+++	nd	+
1–616	81,85,89A 270	1–120	RPA32RKN	+++	+++	nd	+
1–616	107,135A 270	1–120	RPA32WF	+++	+++	nd	+
1–616	34–270	1–120	RPA32ΔN33	+++	+++	nd	+
1–616	1–240	1–120	RPA32ΔC241	+++	±	nd	+
1–616	1–223	1–120	RPA32ΔC224	+++	±	nd	+
	1–270	1–120	RPA14/32	-	+++	++	-

Figure 2. Schematic of the RPA and RPA mutants used. The left portion shows diagrams of all RPA mutants used in this study. Beginning and ending amino acid residues of each mutant are indicated. The strength of the protein–protein interactions between RPA and Rad52 are indicated as follows (the data are summarized in Figure 1): (1) Strong complex forming (+++); (2) weak complex forming (±); (3) no complex forming (−). ELISA was used to determine protein–protein interactions with RPA mutants and Rad52 in this study. Only an interaction twofold above that of BSA was considered as a weak binding interaction, and the no complex forming proteins did not show a signal twofold above that of BSA even at higher concentrations (data not shown). Protein interactions with Rad51 by RPA and Rad52 mutants were determined in previous work.[37] ssDNA binding and SV40 DNA replication activities of the RPA mutants were determined in previous studies.[20,35,42] The nomenclature used for each RPA mutant is summarized below. Deletions from the N or C terminus are indicated by a RPA, (subunit of residues deleted—70,32), followed by Δ, then the terminus where the deletions occurred (N or C) and the amino acid residue number where the deletion started (for C-terminal deletions) or the last amino acid residue deleted (for N-terminal deletions). RPA32D8 has the following mutations S8D, S11D, S12D, S13D, T21D, S25D, S29D, and S33D, to mimic hyperphosphorylated RPA (Braun & M.S.W. unpublished results). RPA32RKN has the following mutations R81A, K85A, N89A in the putative ssDNA binding site of RPA32. RPA32WF has the following mutations W107A and F135A in the putative ssDNA binding site of RPA32.

168 and 236 of RPA70.[37] RPA14/32 also co-immunoprecipitated with Rad51 but the interaction with RPA32 was not explored further.[37] The interaction sites on RPA for Rad52 have not been mapped carefully. Human Rad52 was shown to interact strongly with RPA32 and weakly with RPA70.[10] Park and co-workers cited unpublished results that the acidic C terminus of RPA32 (including the last 33 amino acid residues) interacted with the basic patch of residues they had identified on Rad52.[10] Recently, a C-terminal fragment of RPA32 composed of residues 172–270 was studied by NMR, alone and in complex with peptides of UNG2, XPA and Rad52 (including residues 257–274).[40] Yet, the co-precipitation of RPA70 as well as RPA32 with Rad52 by Park indicated that the C terminus of RPA32 is only part of the Rad52 interaction surface. Two-hybrid and co-precipitation analysis of yeast proteins gave additional

evidence of the involvement of scRPA70 as well as scRPA32 in the interaction with scRad52.[38]

Since the interaction of Rad52 with RPA is important in DSB repair and the literature provides an incomplete description of the RPA surface that interacts with Rad52, the regions of RPA involved in binding Rad52 have been explored in detail. The protein–protein interactions of several mutants of RPA with Rad52 have been studied to define the role of the N or C terminus of RPA32, RPA phosphorylation and RPA70 in the RPA:Rad52 interaction. Our results reveal that the interaction of Rad52 with RPA involves two binding sites, one on RPA70 and one on RPA32. These results motivated a homology search that identified a putative Rad52-binding site near the major ssDNA-binding site of RPA70. A mixture of RPA:Rad52 has higher affinity for ssDNA than either RPA or Rad52 alone, and this increase
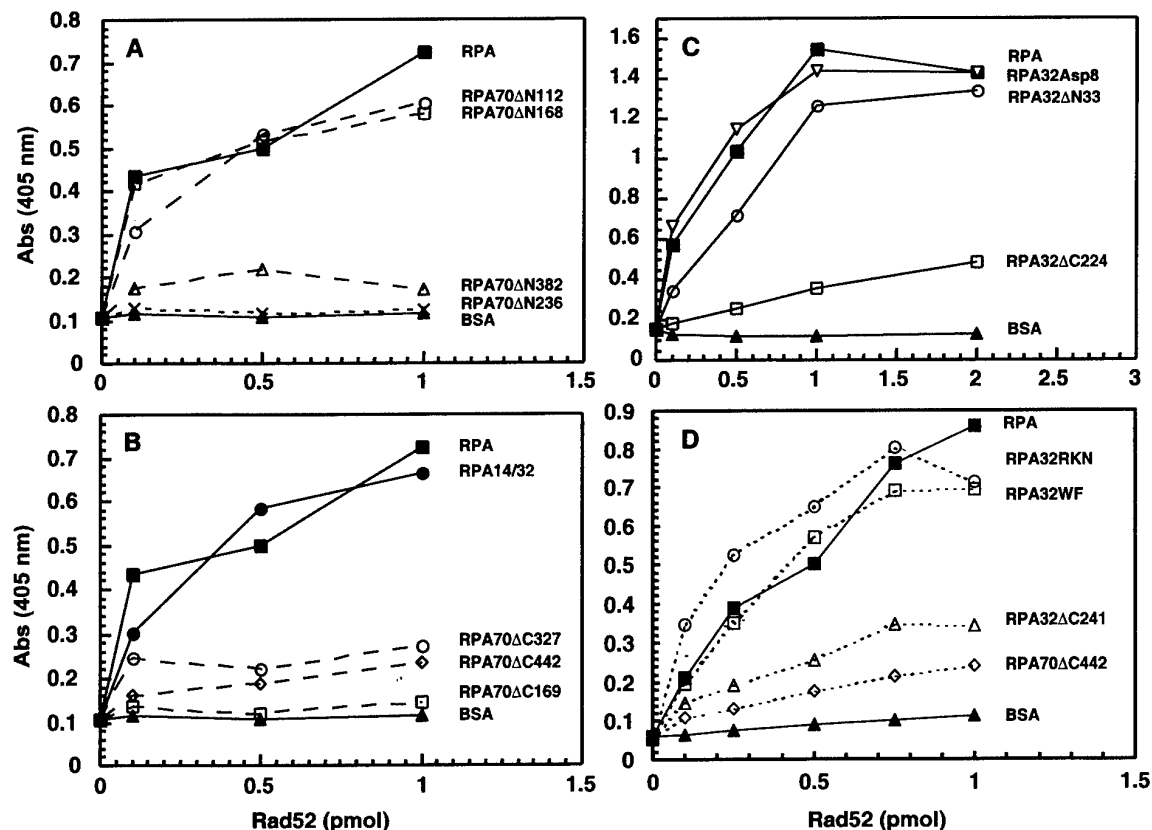
Figure 3. Deconvolution of the domains on RPA that bind Rad52. In the ELISA assay, wild-type or mutant RPA was immobilized on a microtiter plate. Increasing amounts of wild-type Rad52 were added to plates and washed. The bound Rad52 was detected with a specific monoclonal Rad52 antibody (mAb6, see Figure 1) followed by a peroxidase-coupled anti-mouse IgG antibody. Interactions were monitored by measuring ABTS absorbance at 405 nm after the addition of substrate and plotted against the amount of Rad52. (a) RPA and heterotrimeric mutants of RPA70, (b) RPA, RPA14/32 and RPA70 mutants, (c) RPA and heterotrimeric mutants of RPA32, and (d) RPA, heterotrimeric point mutants, RPA70 mutant and heterotrimeric mutant of RPA32. Multiple assays were performed and representative data are shown.

appears to be through increased affinity of RPA32 for ssDNA. Finally, by studying the size of the RPA:Rad52 complex in comparison to Rad52 and RPA alone, it was found that the interaction of RPA with Rad52 disrupts the higher-order aggregation of Rad52 rings and promotes single Rad52 rings in solution. Taken together with the similarity between Rad52 and Rad51-binding sites on RPA, these studies provide a molecular basis for Rad51 and Rad52 competition for binding to RPA. This competition between the protein–protein interaction surfaces of Rad52, Rad51 and RPA is likely to be critical for efficient DSB repair. The higher affinity of the RPA:Rad52 complex for ssDNA has implications for the mechanism of single-strand annealing.

Results

Identification of the regions of RPA important for binding Rad52

The association of Rad52 to RPA was studied using an ELISA method with purified Rad52,

wild-type and several mutant forms of RPA (Figure 2). For the ELISA, RPA was immobilized on a microtitre plate, excess sites were blocked with 5% milk and increasing concentrations of hRad52 were added, incubated and washed. Any Rad52 in complex with RPA or RPA mutants was then detected with a monoclonal antibody (mAb6, see Figure 1) that recognizes an epitope between residues 341 and 418 on the C terminus of Rad52. RPA heterotrimer deletion mutants in the N-terminal region of RPA70 are shown in Figure 3(a). In Figure 3(b), RPA heterotrimer was compared with the heterodimer and peptides of RPA70. In Figure 3(c) and (d), data on RPA heterotrimer mutants with deletions or mutations in RPA32 are shown in comparison to RPA heterotrimer and residues 1–441 of RPA70. The RPA mutants used here were used previously to map the regions of RPA binding to Rad51, XPA, DNA polymerase and T-antigen.[35,37,41,42]

Five primary conclusions were made on the basis of the ELISA data. First, Rad52 binding was reduced significantly when residues 224–271
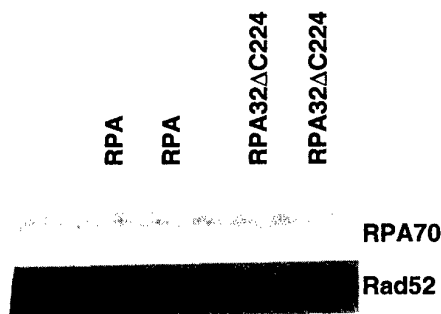
Figure 4. Immunoprecipitation of RPA:Rad52 and RPA32ΔC224:Rad52 complex. Reactions (in duplicate) in lanes 1 and 2 contained wild-type RPA, and lanes 3 and 4 contained RPA32ΔC224 as indicated. Only the data for antibody mAb3 are shown. All other antibodies gave similar results.

(Figure 3(c)) or residues 241–271 (Figure 3(d)) in the C-terminal domain (CTD) of RPA32 were deleted. This indicates a major role for the acidic C terminus of RPA32 in binding Rad52 and is consistent with previous results and predictions.[10,40] Second, when the N terminus of RPA32 is either deleted or mutated with changes from serine or threonine to aspartic acid (RPA32ΔN33, RPA32Asp8, Figure 2), there is no effect on Rad52 binding. Therefore, the N terminus of RPA32, in either its neutral or acidic/hyperphosphorylated form, is probably not involved in the RPA:Rad52 interaction (Figure 3(c)). Third, Rad52 binding was destroyed when residues 169–382 were deleted from RPA70 in the trimer (Figure 3(a)). It is interesting that deletion of this region of RPA70 disrupts Rad52 binding even though intact RPA32 is present. Fourth, all RPA70 peptides (which lack RPA14/32) bind Rad52 weakly, except RPA70ΔC169, which does not bind at all (Figure 3(b)). This result is consistent with those observed with the RPA heterotrimer mutants with N-terminal deletions in RPA70: no significant change in binding was observed when residues 1–112 or 1–168 were deleted (Figure 3(a)). Fifth, RPA14/32 binds Rad52 as tightly as the heterotrimer (Figure 3(b)), even though RPA70 is not present. In summary, these results show that the RPA:Rad52 complex is negatively affected when either residues 224–271 of RPA32 or residues 169–326 of RPA70 are missing from heterotrimeric RPA.

In immunoprecipitation reactions (Figure 4), a strong and significant interaction was seen between RPA and wild-type Rad52 and between RPA32ΔC224 and wild-type Rad52. All six anti-Rad52 antibodies pull down both the RPA:Rad52 complex and RPA32ΔC224 complex. The level of RPA32ΔC224 in a complex with Rad52 relative to wild-type RPA were similar. There appear to be some differences in the binding of Rad52 to RPA32ΔC224 in the two assays (Figures 3(c) and 4). However, it is difficult to compare the data obtained in the ELISA and immunoprecipitation reactions qualitatively, because RPA was in excess
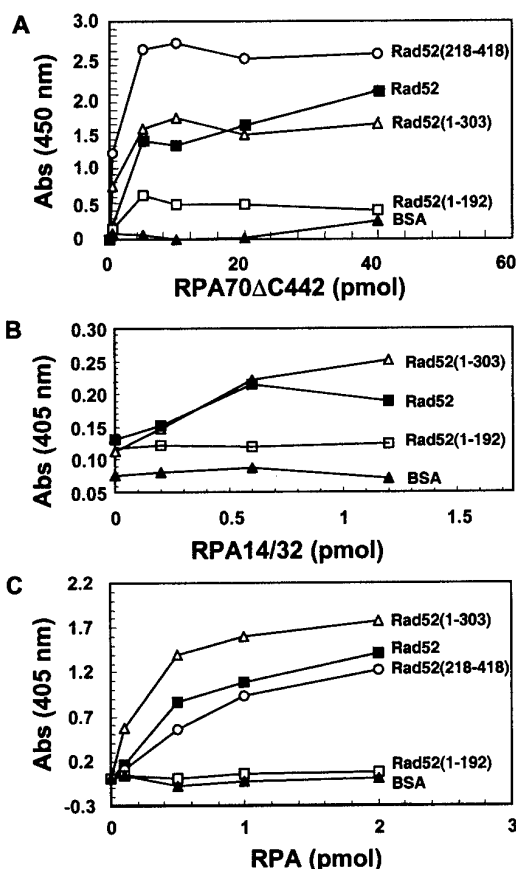
Figure 5. The binding of RPA70ΔC442, RPA14/32 and wild-type RPA to Rad52. In the ELISA assay, wild-type or mutant Rad52 was immobilized on a microtiter plate. Increasing amounts of RPA were added to plates and washed. The bound Rad52 was detected with monoclonal antibodies to RPA70 or RPA32 (Calbiochem) followed by a peroxidase-coupled anti-mouse IgG antibody. Interactions were monitored by measuring TMP substrate absorbance at 450 nm or ABTS substrate at 405 nm and plotted against the amount of RPA.

in the former while Rad52 was in excess in the latter. We conclude that these studies demonstrate a strong interaction between RPA and Rad52 in solution when the RPA32CTD has been deleted, confirming a role for RPA70 in binding Rad52.

The region of Rad52 important for binding RPA32 and RPA70

The interaction site on Rad52 for RPA70 and RPA32 was studied using a similar ELISA protocol. Wild-type or mutant Rad52 was immobilized to a microtitre plate, excess sites were blocked with 5% milk and increasing concentrations of RPA70ΔC442 was added, incubated and washed. Any RPA in complex with Rad52 or Rad52 mutants was then detected with a monoclonal antibody against RPA70 (Calbiochem). The data show that the primary interaction sites for both RPA70 and RPA32 are in the region including Rad52 residues

Table 1. DNA binding activity of forms of RPA, Rad52 and RPA:Rad52 complexes

GMSA data			K_A ($\times 10^9$ M^{-1})[a]	
	RPA forms (ratio)[b]	None	Rad52	Rad52(218–418)
1.	None		0.74 (0.24, V)	ND
2.	RPA (1:1)	1.4 (0.2, S)	0.75 (0.15, F)	1.3 (0.5, V)
3.	RPA (1:7)	1.4 (0.2, S)	7.5 (2.6, S)	25 (6.1, S)
4.	RPA14/32 (1:1)	ND	ND	ND
SPR data[c]			K_A ($\times 10^8$ M^{-1})[a]	
	RPA forms (ratio)[b]	None	Rad52	Rad52(218–418)
5.	None			ND
6.	RPA (1:7)	3.9 (0.5, S)		12 (1.7, S)
7.	RPA32RKN (1:7)	2.5 (1.3, S)		1.9 (0.5, S)
8.	RPA32WF (1:7)	2.2 (0.6, S)		2.4 (0.8, S)
9.	RPA32ΔC224 (1:7)	1.3 (0.1, V)		3.5 (0.2, S)
10.	RPA32ΔC241 (1:7)	3.1 (1.6, S)		2.4 (0.7, S)

[a] The error is indicated in parentheses and was estimated from the standard deviation of actual values (indicated by an S), from the variation if only two trials were done (V) or from the fitting error if the experiment was done only once (F); ND, no binding was detected.
[b] RPA:Rad52 complexes were mixed using the ratios indicated where the RPA component is on either the heterotrimer or heterodimer basis and the Rad52 component is on a monomer basis.
[c] Assay done in 1 M KCl.

193–303 (Figure 5). The Rad52(218–418), and Rad52(1–303) showed slightly higher binding activity than wild-type Rad52, perhaps due to increased exposure to the RPA-binding domain.

Effect of Rad52 binding on RPA ssDNA binding

The RPA70 binding site (residues 169–326) for Rad52 identified by protein–protein interaction studies includes all of ssDNA binding site DBD-A and a portion of DBD-B. Therefore, the ability of Rad52 to modulate the affinity of RPA for dT$_{30}$ ssDNA was studied (Table 1 and Figure 6). Using the gel mobility-shift assay (GMSA) under physiological salt concentrations, wild-type RPA had a K_A of 1.4×10^9 M^{-1}, wild-type Rad52 had a K_A of 0.74×10^9 M^{-1}, and no binding was detectable for the Rad52(218–418) mutant (Table 1, rows 1–3; see also Figure 6(a)). Surprisingly, the affinity of the RPA:Rad52 complexes for ssDNA was fivefold to 18-fold higher than RPA or Rad52 alone (Table 1, row 3). The stimulatory effect of the Rad52(218–418) mutant is particularly significant, since this mutant retains the full RPA binding surface but has no detectable affinity for DNA (Table 1, row 3; see also Figure 6(a)).

The effect of the molar ratio of Rad52 monomer to RPA heterotrimer on ssDNA binding affinity of the RPA:Rad52 complexes was studied using GMSA (Table 1 and Figure 6(b)). For wild-type proteins, the 1 to 7 ratio gave maximal binding and the 1 to 14 ratio gave similar binding (Figure 6(b)). Wild-type Rad52 was assumed to be in a heptameric ring. For the RPA:Rad52(218–418) complex, the stoichiometry of binding for the protein–protein complex was not known, so a series of ratios were tested for ssDNA affinity. DNA affinity increased as the ratio increased and was maximal at the 1 to 7 ratio (Figure 6(b)). With

both Rad52 and Rad52(218–418), no stimulation was observed at a 1:1 molar ratio (Table 1, line 2). This suggests that this ratio is too low for a stimulatory interaction or complex to form. Fivefold to 18-fold stimulation was observed at a 1:7 molar ratio (Table 1, row 3). This stimulation was probably not caused by non-specific protein effects, because all reactions contained 50 μg/ml of bovine serum albumin (BSA). These data indicate that the interaction of Rad52 with RPA increases the affinity of RPA for ssDNA significantly, in a Rad52 concentration-dependent manner.

In the GMSA, the affinities of the RPA:Rad52 and RPA:Rad52(218–418) complexes were all high enough to be near or at stoichiometric binding conditions (the apparent K_A determined was close to the concentration of DNA used, 13×10^{-9}M). Under stoichiometric binding conditions, the apparent affinity constant represents a minimum affinity of the complex. Therefore, the stimulatory effect of Rad52 was studied using surface plasmon resonance (SPR) under high-salt conditions in order to obtain equilibrium binding conditions (Table 1, rows 5–10). Raising the salt concentration to 1 M lowered the affinity of RPA for ssDNA by 3.6-fold ($K_A = 3.9 \times 10^8$ M^{-1}). Even under high-salt conditions, the binding of Rad52(218–418) was stimulatory and raised the affinity of RPA threefold to 12×10^8 M^{-1} (Table 1, row 6).

The effect of salt on the RPA:Rad52 complex was then explored through a modified ELISA assay (Figure 7). It was found that salt concentrations higher than 250 mM KCl reduced the wild-type RPA:Rad52 complex by more than 50% under the conditions of the ELISA. At 1 M salt, ~5% of the complex remained (Figure 7(a)). This is not surprising, since the interaction is thought to be mediated partly by electrostatics through an acidic patch on RPA32CTD and a basic patch on Rad52.[10] The
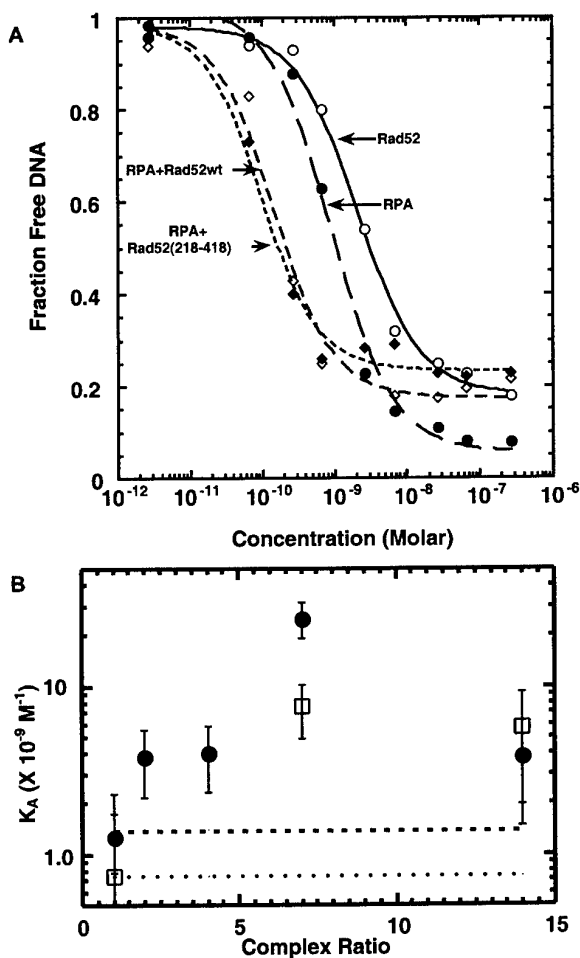
Figure 6. ssDNA binding data for RPA, Rad52 and RPA:Rad52 complexes. (a) Representative ssDNA binding isotherms obtained from GMSA as described in Materials and Methods for RPA (filled circles, long-dash broken line; fitted binding constant $K_a = 1.1 \times 10^9\,M^{-1}$), Rad52 (open circles, continuous line; $K_a = 0.75 \times 10^9\,M^{-1}$), RPA:Rad52 (1:7 ratio) complex (open diamonds, short-dash broken line; $K_a = 7.9 \times 10^9\,M^{-1}$) and RPA:Rad52(218–418) (1:7 ratio) complex (filled diamonds, dotted line; $K_a = 1.3 \times 10^{10}\,M^{-1}$) Lines are the best fit curves obtained by non-linear least-squares fitting. (b) Binding affinity for ssDNA for RPA, Rad52 and RPA:Rad52 complexes. The measured association constants were measured by GMSA and plotted against the molar ratio of Rad52 monomer to RPA heterotrimer. The broken line indicates the affinity of wild-type RPA heterotrimer and the dotted line indicates the affinity of wild-type Rad52. The affinity of RPA:Rad52 complexes at various ratios of Rad52 to RPA are plotted with open squares for wild-type Rad52, and filled circles for Rad52(218–418). The plotted K_A ($\times 10^9\,M^{-1}$) values were 0.74 (0.24, V), 0.75 (0.15, F), 7.5 (2.6, S), and 5.6 (3.7, F) for wild-type Rad52 at ratios of 0:1, 1:1, 1:7 and 1:14 to RPA, respectively. For Rad52(218–418) the values were 1.3 (0.5, V), 3.8 (1.6, F), 4.1 (1.7, F), 25 (6.1, S), and 3.9 (2.4, F) at ratios of 1:1, 1:2, 1:4, 1:7 and 1:14 to RPA, respectively.

RPA:Rad52(218–418) complex was studied by SPR and it was slightly more resistant to salt than wild-type, needing more than 400 mM salt to reduce the complex by 50% (Figure 7(c)). At 1 M salt, ~15% of the RPA:Rad52(218–418) complex remained. Results for RPA14/32:Rad52 were similar (Figure 7(b)). The RPA70ΔC442:Rad52(218–418) complex also showed sensitivity to salt and required more than 300 mM salt to reduce the complex by half, and retained 30% of the complex at 1 M salt (Figure 7(d)). This indicates that the majority of the RPA70 interaction is mediated by electrostatic interactions but to a slightly lesser extent than RPA14/32 or the wild-type heterotrimer. It was concluded that even though the salt conditions of the SPR assay appear to be diminishing the protein–protein interaction between RPA and Rad52, the stimulation of RPA's affinity for ssDNA was still seen (Table 1).

In order to help deconvolute the contributions of RPA70 and RPA32 to the stimulation of ssDNA binding by Rad52(218–418), five mutant forms of RPA were studied (RPA32RKN, RPA32WF, RPA32ΔC224, RPA32ΔC241, and RPA14/32; Figure 2). For the RPA32RKN mutant, conserved polar residues, homologous to those that interact with ssDNA in RPA70,[22] were replaced with alanine. The RPA32WF mutant has two conserved aromatic residues mutated to alanine. Disruption of the corresponding aromatic residues in scRPA has been found to disrupt interactions with DNA of the mutated domain.[23] When binding to a 30 residue oligonucleotide was examined, these mutants have the same affinity as wild-type for ssDNA (Figure 2). This is consistent with previous studies showing that the central domain of RPA70 is primarily responsible for binding to short oligonucleotides.[19] The RPA32RKN and RPA32WF forms of RPA also showed the same affinity for Rad52 as wild-type RPA (Figure 3(d)) but were not stimulated to bind ssDNA by Rad52(218–418) (Table 1, rows 7 and 8). Mutants with the CTD of RPA32 deleted, RPA32ΔC224 and RPA32ΔC241, have diminished binding for Rad52 (Figure 3(d)) and were not stimulated by Rad52(218–418) (Table 1, rows 9 and 10). No binding to ssDNA was detected for the RPA14/32 heterodimer alone or for the RPA14/32:Rad52 complex (Table 1, row 4), indicating that the presence of RPA70 in the RPA complex is required for stimulation. These results show that the increase in DNA affinity of the RPA:Rad52 complex is mediated through DNA binding by RPA32. They suggest that Rad52 binding to both RPA32 and RPA70 is required for stimulation.

RPA binding to Rad52 displaces higher-level self-association of Rad52

Human Rad52 forms large aggregates in solution. Two regions of Rad52 are responsible for aggregate formation (Figure 1). The self-association domain in the N-terminal half of Rad52 is
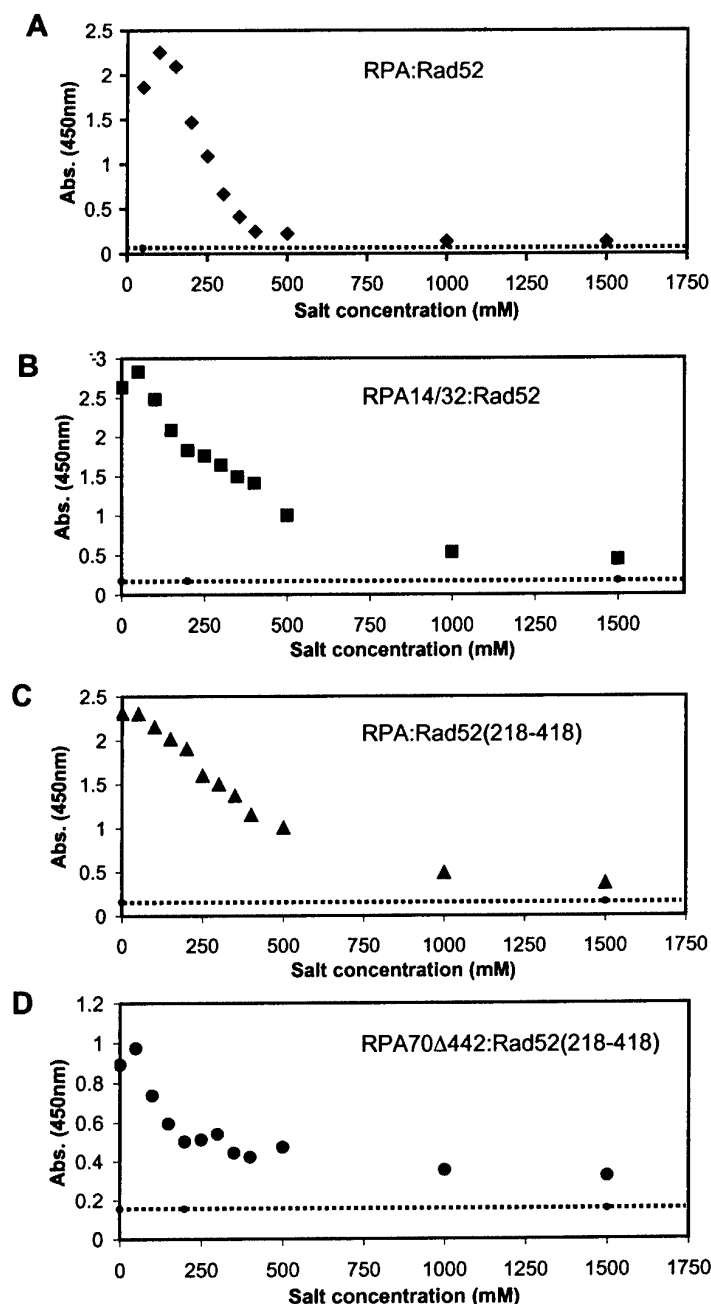
Figure 7. The effect of ionic strength on the RPA:Rad52 complex. A modified ELISA assay using the OPD substrate was used to study the effect of increasing ionic strength on the (a) wild-type RPA:Rad52 complex, (b) RPA14/32:Rad52 complex, (c) RPA:Rad52(218–418) complex, and (d) RPA70Δ442:Rad52(218–418). The dotted line indicates the baseline as determined with BSA. Antibody to RPA70 was used (Calbiochem) to detect wild-type RPA and RPA70ΔC442, and antibody to RPA32 was used to detect RPA14/32.

responsible for heptameric ring-formation and elements in the C-terminal half of the protein participate in the formation of higher-order complexes of rings.[14] The Rad52(218–418) mutant contains the C-terminal elements for the higher-order self-association and does not form rings. Rad52(218–418) contains the binding surface for RPA (Figure 1). The average molecular mass (M) of the proteins and complexes in solution were measured by static light-scattering (SLS) and the ability of Rad52(218–418) to self-associate into higher-ordered complexes in the presence of RPA14/32 and RPA heterotrimer was tested (Table 2 and Figure 8).

Individual proteins were characterized by SLS first. Due to the higher-order self-association of Rad52, the M value of the wild-type protein is very sensitive to concentration and is not suitable for SLS. The M value for Rad52(218–418) is also concentration-dependent, but less so than wild-type and a narrow concentration range could be studied. A consistent size at low concentrations between 0.2 and 1.2 mg/ml was $102(\pm 25)$ kDa and corresponded to a trimeric Rad52(218–418) complex (Table 2, row 1). Higher concentrations result in a shift in the M value to $153(\pm 40)$ kDa equivalent to a tetrameric complex of Rad52(218–418) as was shown previously.[14] The RPA14/32
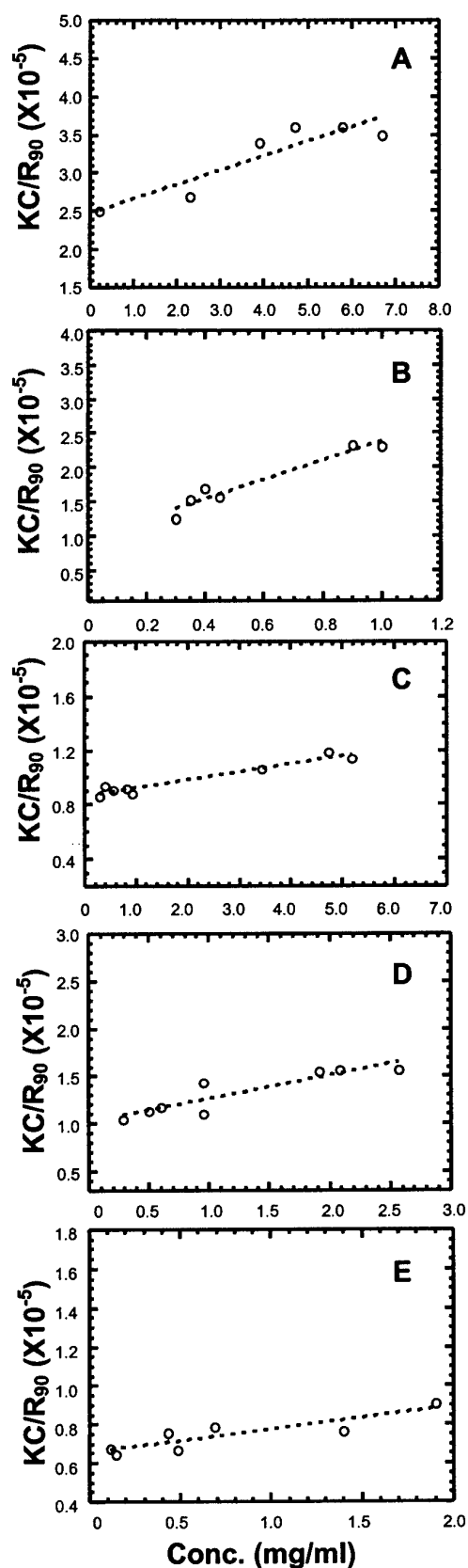
Figure 8. Static light-scattering data used for the molecular mass determinations summarized in Table 2. (a) RPA14/32, (b) Rad52(218–418), (c) RPA, (d) Rad52(218–418):RPA14/32, (e) Rad52(218–418):RPA. Linear least-squares fitting was performed in Kaleida-Graph and the correlation coefficients are 0.82, 0.92, 0.98, 0.96, and 0.89 for (a)–(e), respectively.

heterodimer alone had an M value of $42(\pm 11)$ kDa, which corresponds to a single heterodimer in solution (Table 2, row 3). Previous studies at three-fold higher protein concentrations indicated a dimer of dimers in solution.[14] SLS measurements of RPA heterotrimer alone show an M value of $117(\pm 11)$ kDa (Table 2, row 2), which is consistent with previous results with the RPA heterotrimer obtained by hydrodynamic analysis and analytical ultracentrifugation.[21,43] These data indicate that these preparations of RPA14/32 and RPA hetero-trimer have equal molar ratios of RPA14, RPA32 and RPA70 subunits.

Complex formation between RPA and Rad52 appears to disrupt the trimeric aggregates of Rad52(218–418). When Rad52(218–418) was added to RPA14/32 and RPA heterotrimer in an equal molar ratio of monomer to heterodimer or heterotrimer, the resulting complexes had M values of $99(\pm 22)$ kDa and $152(\pm 28)$ kDa, respectively (Table 2, rows 4 and 5). The RPA14/32:Rad52 (218–418) and RPA:Rad52(218–418) complexes show an increase in molecular mass of approximately one Rad52(218–418) subunit. There was no increase in the polydispersity, as indicated by the standard deviation of the R_H, upon complex formation. This indicates that aggregates of Rad52(218–418) or free RPA were not detected. These data indicate that the binding of RPA to Rad52(218–418) is very effective at disrupting the higher-order self-association of Rad52.

Discussion

Regions of RPA important for binding Rad52

Two interaction sites on RPA for Rad52 were defined by the ELISA studies on a large number of RPA mutants to include RPA70 residues 168–326 and RPA32 residues 224–270 (Figure 9). Previous work had identified a specific interaction between human Rad52 and RPA and implicated the acidic CTD of RPA32 as the primary binding region for Rad52.[10] The possibility of an interaction between RPA70 and Rad52 had been eliminated because two RPA70 mutants (called p70d293–373 and p70d374–458) studied retained the ability to bind Rad52. Apparently, these deletions did not disrupt the RPA70:Rad52 binding site, which has been found in this work to be located between residues 169 and 382. The relative affinities of the RPA32 and RPA70 sites for Rad52 remain to be determined.

The two interaction sites on RPA for Rad52 are shared by Rad51 and XPA (Figure 9). When the RPA:Rad51 complex was studied by

Table 2. Static light scattering data for forms of RPA, Rad52 and RPA:Rad52 complexes

Sample[a]	Conc. range (mg/ml)	R_H[b] (nm)	C_p/R_h[c]	SLS M (kDa)	Error[d] (kDa)	Predicted M (kDa)	Complex[e] size
1. Rad52(218–418)[f]	0.2–1.2	4.71 (1.54)	0.321	102	25	38	2.7
2. RPA	0.1–5.0	5.17 (1.10)	0.203	117	11	110	1.1
3. RPA14/32	0.2–4.0	3.78 (0.93)	0.246	42	11	44	0.96
4. RPA14/32:Rad52(218–418)	0.2–3.0	4.41 (1.34)	0.364	99	22	82	1.2
5. RPA:Rad52(218–418)	0.1–4.0	5.21 (0.98)	0.193	153	28	148	1.0

[a] Samples were mixed on a one RPA heterodimer or heterotrimer to one Rad52 monomer ratio.
[b] Average R_{11} with standard deviation in parentheses is reported from DynaLS.
[c] The average value of the polydispersity divided by the hydrodynamic radius.
[d] Derived from the reciprocal of the y intercept error (See Figure 8).
[e] Complex size is experimentally determined molecular mass divided by the predicted molecular mass.
[f] The size of Rad52(218–418) has been measured by several methods, including scanning transmission electron microscopy, gel-permeation chromatography and DLS, and ranged from three to four subunits depending on the protein concentration.[14] Due to the propensity of Rad52 to form higher-order complexes, wild-type was excluded from SLS experiments and Rad52(218–418) was kept at low concentrations.

immunoprecipitation a subset of the same RPA mutants were used.[37] The 168–326 region on RPA70 was shown to be important for complex formation with Rad51. A role for RPA32 in the complex was not studied completely, but RPA14/32 was shown to coimmunoprecipitate with Rad51. These results appear to imply a role for RPA32 in binding Rad51 that deserves further study. The regions identified for binding XPA are similar to Rad52 but do not overlap exactly.[41] Also, the XPA interaction with RPA14/32 was substantially lower than heterotrimeric RPA.

It is intriguing that the RPA heterodimer binds as tightly to Rad52 as the RPA heterotrimer. At present, a full explanation of this activity cannot be given but there are two likely explanations for this observation. The heterodimer may adopt a slightly different conformation when RPA70 is not present that promotes Rad52 binding. For example, the RPA32CTD could be more accessible in the absence of RPA70 and the binding of Rad52 promoted by ease of access to RPA32CTD. Alternatively, the CTDs of two RPA14/32, in a

A

```
                uu  u        *u          u
                bbb          bbbb
RPA32(252-267)  EGHIYS--TVDD-DHFKST
                EG|||S   VD| |||||T
RPA70(218-236)  EGKLFSLELVDESGEIRAT
                bbbbbbbbbbb  bbbbbb
                s s          sssss d d
```

B

```
H. sapiens        EGKLFSLELVDESGEIRAT
D. melanogaster   EGKLFSMDLMDESGEIRAT
S. cerevisiae     DGKLFNVNFLDTSGEIRAT
S. pombe          EGKLFSVNLLDESGEIRAT
X. laevis         EGKLFSIEMVDESGEIRAT
```

Figure 10. Sequence analysis of the putative binding site for Rad52 on RPA70. (a) In line 1, a u indicates RPA32 residues shown to bind UNG peptide[40] and a * indicates the position of the point mutation D228Y that disrupts Rad52-dependent double-strand break repair in *S. cerevisiae*.[45] In line 2, a b indicates RPA32 residues with β-strand secondary structure. Line 3, the sequence for residues 252–267 of RPA32. Line 4, identical homologous residues between RPA32 and RPA70 are indicated with the amino acid and similar residues are indicated with a vertical line. Lines 5 and 6, the sequence for residues 218–236 of RPA32 and the residues in β-strands are given.[22] Line 7, an s indicates surface-accessible residues and a d indicates residues interacting with ssDNA on RPA70. (b) Peptide sequences of RPA70 residues 218–236 from *Homo sapiens*, *S. cerevisiae*, *Schizosaccharomyces pombe*, *Drosophila melanogaster*, and *Xenopus laevis*. Amino acid residues that are identical with those of *H. sapiens* are in bold. Sequence alignments were performed using the Lipman–Pearson protein alignment available in Lasergene Navigator software (DNASTAR, Inc.) with the following settings: kTuple 2, gap penalty 4 and gap length penalty 6.

Figure 9. Comparison of binding of Rad52, Rad51, XPA and UNG to RPA. Real and putative DNA-binding domains (DBDs) are indicated in boxes as follows. On RPA70: DBD-A, includes residues 181–290; DBD-B, includes residues 300–422; DBD-C$_{ZN}$, includes residues 432–616 and contains a zinc finger; and DBD-NTD, includes residues 1–110. On RPA32: DBD-D, includes residues 43–171.[19,22,23,26,35,47,54] Another OB fold, indicated by a ?, exists on RPA14 that may or may not bind ssDNA.[24] The N terminus of RPA32, which becomes hyperphosphorylated during the cell-cycle and in response to DNA damage, is indicated by a p in a circle. The regions involved in binding Rad52 have been narrowed down to include RPA32 residues 224–271 and RPA70 residues 169–326; Rad51 to include RPA70 residues 169–326 and may possibly involve the C terminus of RPA32;[37] XPA to include RPA32 residues 224–271 and RPA70 residues 236–382;[41] and UNG binds to the RPA32CTD.[55] The regions on Rad52, XPA and UNG thought to bind RPA32CTD share limited homology.[40]

dimer-of-dimers, could closely approximate the surface of the RPA heterotrimer. There is evidence in the literature that RPA14/32 can assemble to form a dimer-of-dimers.[24,44] In this case, two RPA32 CTDs would be bound to Rad52, one in the normal RPA32 site of Rad52 and one in the Rad52 site normally occupied by RPA70. Evidence for the physiological relevance of the heterodimer in apoptosis makes the high affinity of it for Rad52 (and Rad51) even more intriguing.[29,32]

Putative Rad52 binding site on RPA70

We propose that the Rad52 interaction surface on RPA32 and RPA70 are similar in sequence composition. Two pieces of experimental evidence support this proposal. First, the ionic strength data (Figure 7) shows that both of the RPA14/32:Rad52 and RPA70Δ442:Rad52 complexes are disrupted by increasing concentration of salt, which indicates that both interaction surfaces involve electrostatic interactions, also supports this proposal. Secondly, the same region on Rad52 binds RPA14/32 and RPAΔ442 (Figure 5). To further explore this idea, a search for sequence homology was performed between RPA70(169–326) and RPA32(224–271). A homologous, acidic 19 residue peptide, including RPA70 residues 218–236 was found (Figure 10(a)). This putative Rad52 binding surface, RPA70(218–236), is 32% identical with and 79% similar in sequence to RPA32(252–267) and lies completely within DBD-A. This peptide contributes a small acidic patch to the surface of RPA70 and is neighbored by basic residues involved in binding ssDNA.

NMR and X-ray crystallographic structural information is available for the RPA32(252–267) and RPA70(218–236) peptides and is summarized on lines 1, 2, 6 and 7 of Figure 10(a).[22,25,40] The RPA32(252–267) peptide contains a binding surface for UNG2 and XPA, as well as Rad52.[40] In the NMR structure, the side-chains of residues 252, 253, 256, 261 and 267 are involved directly in binding the UNG peptide (line 1, Figure 9(a)) and are well conserved in the RPA70(218–236) peptide (Figure 10(b)). In the crystal structure of RPA70(181–422), the RPA70(218–236) peptide includes a tight turn between two antiparallel β-strands and is near residues involved in DNA binding (line 6, Figure 10(a)).[22,25] Notably, residues 218, 220, 228, 229, 230, and 232 are surface-accessible and are not involved in DNA binding (line 7, Figure 10(a)). DNA-binding residues are nearby and included in this sequence (residues 234 and 236) but their side-chains are mainly positioned on a different tight turn and on the opposite face of the β-sheet than the putative Rad52 binding surface. The 214–217 loop that moves upon DNA binding is just upstream from this sequence.[25] The sequence of the RPA70(218–236) peptide is well conserved (Figure 10(b)). Studies in yeast support the role of the RPA70(218–236) peptide in break repair. In *S. cerevisiae*, the mutation of Asp228 to

Tyr on scRPA70 altered Rad52-dependent DSB repair.[45] This mutation changes an acidic residue to a neutral residue, thereby lowering the electrostatic potential of the surface and possibly changing protein–protein interactions. In summary, the structural homology of the RPA32(252–267) and RPA70(218–236) peptides was not identical, but many secondary structure units are retained and the location on the surface of residues known to be important in protein–protein interactions are strictly conserved. Considering the available data, RPA70(218–236) is proposed to include the binding site for Rad52 on RPA70. Further experimentation will be needed to test this hypothesis.

The involvement of RPA32 in the enhanced ssDNA binding affinity of the RPA:Rad52 complex

The wild-type RPA:Rad52 complex has at least fivefold higher affinity for dT_{30} than RPA alone. In these studies, DNA-binding to a short oligonucleotide 30 residues in length was analyzed. This length corresponds to the occluded binding site size of RPA.[20] Under these conditions, cooperative binding should not occur and only 1:1 RPA:DNA complexes should form. This means that in the RPA:Rad52 complex, Rad52 is probably not interacting with the DNA. This interpretation is supported by the finding that Rad52(218–418), which does not interact with ssDNA but interacts with RPA strongly, enhanced the equilibrium association constant by at least 18-fold. We conclude the effect of Rad52 binding must change the structure of RPA to facilitate higher ssDNA binding. The reason enhancement of Rad52(218–418) is higher than wild-type Rad52 is not known and could be because the ring-forming region of this mutant is missing. Mutations of residues in the OB-fold of RPA32 obliterate this stimulation and thereby support a role for RPA32 in the enhanced binding of ssDNA. Deletion of the RPA32 C-terminal interaction domain for Rad52 also disrupts the increase in affinity. These data indicate that the interaction between RPA and Rad52 is needed to increase the affinity through RPA32. To our knowledge, this is the first example of complex formation increasing the affinity of RPA through the RPA32 subunit. Similar enhancement of RPA ssDNA binding affinity has been seen with the DNA-binding proteins SV40 T-antigen and Gal4/VP16 (K. A. Braun, Y. Lao & M.S.W., unpublished results).[46]

These experiments do not address the effects of Rad52 on cooperative binding of RPA or of binding to long ssDNA lattices. Additional studies will be necessary to determine whether Rad52 stimulates RPA binding under cooperative binding conditions.

Data from a mutational analysis of the relative contribution of the four DNA-binding domains of *S. cerevisiae* RPA to ssDNA-binding affinity

supports the role of RPA32 in binding ssDNA. It showed that DBD-A (in scRPA70) played a primary role in binding short oligonucleotides of 12 nt or less and DBD-D (in scRPA32) interacts with longer oligonucleotides of 27 nt or more.[23] A sequential model of binding was proposed in which DBD-A is responsible for the initial interaction with ssDNA, that domains A, B and C (scRPA70) contact 12–23 nt of ssDNA and that DBD-D (scRPA32) is needed for substrates greater than 23 nt in length. It has been reported that the binding affinity of the RPA14/32 heterodimer is stimulated when the N and C termini of RPA32 were truncated.[47]

Contrary to our initial hypothesis, these data indicate that the stimulation of RPA ssDNA affinity by Rad52 is through ssDNA binding to the RPA32 subunit and not the major ssDNA-binding site in RPA70. This stimulation is mediated by Rad52 binding, is enhanced at higher concentrations of Rad52, and requires that RPA70 be present in the heterotrimer. There are two likely mechanisms to explain these observations. First, the binding of Rad52 to RPA32 may directly open the ssDNA-binding domain within RPA32 (Figure 9, DBD-D). Second, the binding of Rad52 may be affecting the global structure of the heterotrimer and stimulate RPA32 binding in an indirect manner.

Implications for DSB repair mechanism

Three pathways are known to repair double-strand breaks.[1,48] Their relative importance and function between the species is still under investigation. Homologous recombination is thought to be the predominant pathway in *S. cerevisiae,* and non-homologous end-joining as the dominant pathway in humans. Together, RPA and Rad52 can also perform single-strand annealing to repair DSBs in DNA containing repetitive sequences. Homologous recombination has been reconstituted *in vitro* for human and *S. cerevisiae* proteins.[7,8,39] In yeast, the binding of scRad52 is thought to facilitate scRad51 filament formation by displacing scRPA during homologous recombination.[5] The enhanced affinity of the RPA:Rad52 complex for ssDNA indicates that the mechanism of homologous recombination in humans may be different from that in *S. cerevisiae* and it is unlikely that the binding of human Rad52 displaces RPA from ssDNA.On the other hand, the stimulation of RPA ssDNA binding by Rad52 may partly explain the enhanced single-strand annealing seen when RPA is combined with Rad52.[4,6,49] A full understanding of the interplay between ssDNA, RPA, Rad52 and Rad51 binding awaits further experimentation on both human and yeast proteins, including the understanding of the effect protein–protein interactions have on ssDNA binding constants.

Due to the similarities of UNG, XPA and Rad52 in binding RPA, a "hand-off" model has been put forward for the assembly and coordination of different components of the DNA repair machinery.[40] This model suggests that the dynamic assembly of the DNA repair machinery might be organized by multiple, competitive interactions with RPA. Our work contributes three pieces of data that support the hand-off model. First, the binding of Rad52 includes surfaces on both RPA32 and RPA70. Second, similar surfaces on RPA are employed for binding Rad52 and Rad51, that do not overlap completely in surface or activity with XPA (Figure 9). And third, the same surface on Rad52 that binds RPA is involved in the higher-order self-association of Rad52 rings. There is evidence that the higher-order complexes formed by Rad52 are important to its various functions in DSB repair. Rad52 interacts with itself to form heptameric ring complexes and higher-order interactions between ring complexes.[9,12,14] Human Rad52 was shown specifically to bind to DNA ends as an aggregated complex of rings.[12] Rad52 was also shown to facilitate the joining of DNA ends by bacteriophage T4 DNA ligase by Rad52-Rad52 intermolecular interactions.[12] The contribution of the higher-order self-association of Rad52 rings to single-strand annealing of complementary ssDNA ends has been confirmed by EM.[15] Here, we show that these Rad52 intermolecular interactions are disrupted in the presence of RPA, and thus RPA is competing for the same or nearby site on the C terminus of Rad52. The competition between RPA and Rad52 for the Rad52 C-terminal self-association surface may be of importance for the orchestration of the three DSB repair pathways. It was noted that high concentrations of human Rad52 were inhibitory to Rad51-mediated strand-exchange activity.[8,37] It is tempting to speculate that this inhibition was relieved by addition of RPA, perhaps through the displacement of higher-ordered Rad52 ring complexes by RPA binding. In conclusion, dynamic protein–protein and protein–DNA interactions involving complexes of RPA, Rad52 and Rad51 appear to be important component of DSB repair.

Materials and Methods

Generation of Rad52 monoclonal antibodies

Initial injections of 50 μg of wild-type Rad52 in complete Freund's adjuvant were given subcutaneously to eight to nine week old female Balb/C mice. Three additional boosts with 50 μg of antigen were given intraperatoneally without adjuvant at two week intervals. After the final injection, the mice were boosted two additional days and sacrificed by cervical dislocation on the fourth day. Splenocytes were isolated by passage through a wire mesh and red blood cells were removed by incubation with red blood cell lysis buffer (Sigma) on ice for ten minutes. Primary splenocytes were fused with the mouse myeloma cell line P3/NS1/1-Ag4-1 (American Type Culture Collection (ATCC), Rockville, MD.) in the presence of PEG (1300–1600 Da). The complete fusion was plated in 96-well plates and medium containing aminopterin was added the following day to eliminate unfused myeloma cells. Hybridoma

supernatants were screened by Western blot of bacterially expressed Rad52. Positive hybridomas were cloned by limiting dilution to isolate a clonal population of antibody-producing cells. Hybridomas were maintained in HY medium (Sigma) supplemented with 20% (v/v) fetal bovine serum (Hyclone Laboratories, Logan, UT). In total, 64 hybridomas cell lines were isolated. The epitopes of the secreted antibodies were mapped coarsely to the domains of Rad52 by Western blot with wild-type Rad52, Rad52(1–192), Rad52(1–303) and hRad52(1–340). Six antibodies that recognized different domains of Rad52 were identified and used in ELISA and immunoprecipitation.

Generation of Rad52 deletion mutant constructs

Wild-type human Rad52 (pRad52wt), Rad52(1–192), Rad52(1–303), and Rad52(1–340) pET28 expression plasmids, each with six histidine residues on the C terminus, were a gift from Dr M. Park (Los Alamos National Laboratories). Rad52(218–418) was prepared by amplifying the specific coding region of the wild-type gene in pRad52wt. The N-terminal PCR primer was: 5′-CAGCTGCAGCAGGTGACCTCCCCTTCC-3′ and the C-terminal PCR primer was 5′-GTGG-CCTGgaatTCAGT<u>tA</u>GATGGAT-3′, which contained an engineered unique downstream *Eco*RI restriction site after the stop codon (underlined). PCR was performed using Taq polymerase (Promega) in a DNA thermal cycler (Perkin Elmer) using standard conditions. The PCR product was cloned into a pBAD/Thio-TOPO fusion vector (INVITROGEN) by TA-TOPO cloning. This ligation creates a fused thioredoxin gene N-terminal to the Rad52(218–418) gene sequence. The fusion protein gene sequence was then amplified from the pBAD/Thio-TOPO fusion vector using oligonucleotides: upstream 5′-CCGACCGcAtATGGCCCTGGGACACC-3′ and the same downstream primer. The upstream primer contained the upstream thioredoxin start sequence and an engineered *Nde*I site. The sequence was ligated into the *Nde*I site and *Eco*RI site of a pET28 vector. The resulting fusion protein contained an N-terminal His$_6$ tag preceding a thioredoxin tag sequence and the Rad52(218–418) gene sequence.

Protein purification

Wild-type and mutant Rad52 were expressed and purified under reducing conditions as described.[14] The Rad52(218–418) purification was modified to include dialysis into 50 mM Caps (pH 10.2), 1 M KCl, 2% (v/v) glycerol, 0.5 mM *n*-hexyl-glucoside, 1 mM DTT, 1 mM EDTA and then loaded onto a Superdex 200 gel-filtration column. The eluted protein was stored in this buffer. Wild-type and mutant RPA were purified as described.[19,44,50,51] Protein concentrations were determined by the Bradford method using BSA as a standard. The concentrations of RPA, RPA 14/32, and Rad52(218–418) were corrected using extinction coefficients of 8.44×10^4, 2.34×10^4 and 3.41×10^4 at 280 nm from precipitated protein denatured with GuHCl. For Rad52(218–418) practically identical concentrations were given by both methods. For RPA, A_{280} gave 1.2-fold lower concentrations.

Protein complexes were formed for static and dynamic light-scattering by adding equal molar amounts of RPA or RPA14/32 with Rad52(218–418) in a 15 ml microconcentrator (Centricon-50). The protein solutions were diluted $\geq$ 20-fold in Rad52/RPA binding buffer (50 mM Hepes (pH 7.8), 150 mM KCl, 2% glycerol, 0.5 mM *n*-hexylglucoside, 1 mM DTT, 1 mM EDTA). Then the proteins were concentrated at 4 °C for 8–12 hours at 500 *g* and to allow complexes to form.

Enzyme-linked immunosorbant assay (ELISA)

The ELISA was performed as described.[14,35] The substrates used were (2′2′-azinobis[3-ethylbenzothiozoline-6-sulfonic acid] (ABTS), 3,3′,5,5′ tetramethyl benzidine(TMP) or *o*-phenylenediame (OPD) in phosphate buffer and 0.01% (v/v) hydrogen peroxide. For ABTS, the absorbance was monitored at 405 nm. For TMP and OPD, the absorbance at 450 nm was monitored.

In order to study the effect of salt on the RPA:Rad52 complexes, a slightly modified ELISA protocol was used where the second protein (RPA) was diluted with a range of different concentrations of salt before it was allowed to interact with Rad52. This interaction step was followed by a wash step before detection of bound RPA with antibody.

Immunoprecipitation

Purified RPA (10 pmol of either wild-type RPA or RPA32Δ224) was mixed with 20 pmol of Rad52 in a 6 μl reaction volume containing HM buffer (30 mM Hepes (pH 7.8), 0.5% (w/v) inositol, 0.01% (v/v) NP40, 1 mM DTT, 5 mM MgCl$_2$) at room temperature for one hour. Each reaction was immunoprecipitated with 300 μl of anti-Rad52 hybridoma conditioned supernatant and rocked at 4 °C for 30 minutes. Then 50 μg of anti-mouse affinity gel (ICN) was added to the antibody–antigen complex and the reaction rocked at 4 °C for 30 minutes. The beads were spun down and washed five times with TBST buffer (10 mM Tris–HCl (pH 8.0), 150 mM NaCl, 0.05% (v/v) Tween-20). Samples were separated by SDS-PAGE (8% polyacrylamide gel) and transferred to nitrocellulose. The nitrocellulose was cut horizontally at approximately 60 kDa. The top half was immunoblotted using a monoclonal antibody to RPA70 (Calbiochem). The bottom half was probed for histidine-tagged Rad52 with INDIA probe (Pierce) and visualized by chemiluminescence. Initial characterization by Western analysis using wild-type and mutant Rad52 allowed rough mapping of their epitopes: mAb1 and mAb2 mapped to residues 1–192, mAb3 to residues 193–303, mAb4 to residues 304–340, and mAb5 and mAb6 to residues 341–418 (Figure 1). To further characterize the Rad52 antibodies, the ability of any of the antibodies to disrupt the RPA:Rad52 interaction was explored by immunoprecipitation. In immunoprecipitation reactions, all six anti-Rad52 antibodies pull down the RPA:Rad52 complex and RPA32ΔC224 complex equivalently.

Gel mobility-shift assay (GMSA)

Gel mobility-shift assays were performed as described but with slight modifications.[18,21] Binding assays were carried out in 15 μl volume in FBB buffer (30 mM Hepes (diluted from 1 M stock at pH 7.8), 100 mM NaCl, 5 mM MgCl$_2$, 0.5% inositol, 1 mM DTT). The indicated amount of protein(s) was then incubated with 2 fmol of radiolabeled dT$_{30}$ and 50 μg/ml of BSA at 25 °C for 20 minutes. When protein mixtures were used, the proteins were premixed and incubated on ice for ten minutes prior to being added to the reaction mixtures Reactions

were then brought to a final concentration of 4% glycerol, 0.01% (w/v) bromophenol blue and electrophoresed on a 1% (w/v) agarose gel in 0.1 × TAE buffer. The gels were then dried on DE81 paper and radioactive bands were visualized by autoradiography. The radioactivity in each band was quantified using a Packard Instant Imager. Binding isotherms were obtained by plotting the fraction of oligonucleotide remaining unbound *versus* RPA concentration. Intrinsic binding constants were determined by non-linear least-squares fitting the data to the Langmuir binding equation (KaleidaGraph-Synergy Software) as described.[18,21]

Surface plasmon resonance (SPR)

Interaction of RPA, Rad52 or mutants with ssDNA was monitored using a surface plasmon resonance (SPR) biosensor instrument, Biacore 3000 (Biacore). The 5'-biotinylated dT30 DNA was diluted to 64 nM in a buffer containing 10 mM sodium acetate (pH 4.8), 1 M NaCl and injected manually onto an immobilized streptavadin surface of the BIAcore sensor chip SA to the desired density in different flow-cells. One flow-cell was left underivatized to allow for refractive index change correction. Proteins were diluted in the running buffer containing 10 mM Hepes (pH 7.4), 1 M NaCl, 2 mM MgCl$_2$, 0.005% (w/v) polysorbate-20, 1 mM DTT. Protein was injected into the ssDNA surface (30RU) using the kinject function of Biacore. Association phase was allowed for 600 seconds followed by 400 seconds of buffer injection period for dissociation. Following RPA and Rad52 binding, regeneration was performed with a quick injection of 100 mM NaOH. Data were analyzed using a simple Langmuir 1:1 model.

Static and dynamic light-scattering

Dynamic light-scattering (DLS) was carried out using a DynaPro-801 molecular sizing instrument equipped with a microsampler (Protein Solutions). The instrument has a laser wavelength of 828.7 nm and a fixed scattering angle of 90°. DLS is based on the collected autocorrelation function of the scattered intensity. The acquisition time for all experiments was ten seconds. A 50 µl sample was passed through the filtering assembly into a 12 µl chamber quartz cuvette. All proteins were filtered with 20 nm filters (Whatman). The data were analyzed first with the Dynamics 4.0 software and then the DynaLS software. These gave consistent values for the hydrodynamic radius (R_H) and polydispersity (C_p). All distributions were monomodal, meaning a single distribution of molecules, for this study as defined by the baseline values range from 0.997–1.002. The sum of squares (SOS) error represents the error in the decay of the autocorrelation function. Good SOS errors are 5% or less. The resolution slider values were optimized by the DynaLS software. The resolution slider value represents the maximum allowable information about the distribution without including effects of noise.

Each of the static light-scattering (SLS) data points, at various concentrations, represents a single DLS experiment. The average intensity for approximately 25–30 data points (30–45 minutes) at a 90° angle was measured. This average intensity for each protein concentration was used to calculate Rayleigh ratios with toluene as the reference solvent. The SLS by a protein depends on the concentration, the scattered light

intensity, and the molecular mass as follows:[52]

$$\frac{KC}{R_{90}} = \frac{1}{M} + 2B_{22}C$$

where C is the protein concentration, R_{90} is the Rayleigh ratio at 90°, B_{22} is the second virial coefficient, M is the average molecular mass of the protein in solution, and K is the optical constant. Since the particles under study are more than ten times smaller than the wavelength, the shape of the particles does not need to be considered.

$$K = \frac{1}{N_A}\left(\frac{2\pi n_o}{\lambda^2}\right)^2\left(\frac{dn}{dC}\right)^2$$

where N_A is Avogadro's number, λ is the wavelength, n_o is the refractive index of the solution and dn/dC is the refractive index increment of the protein solution with protein concentration. The value for dn/dC used here was 0.186 ml/g. The Raleigh ratio (KC/R_{90}) is plotted *versus* protein concentration and fit by linear regression. The molecular mass was obtained from the y intercept. The error was estimated from the linear least-squares fit to the data (KaleidaGraph). Sources of errors include intensity fluctuations and protein concentration measurements. All data points for SLS were monomodal distributions with SOS errors near 5% or below. For every SLS experiment, R_H was monitored and the differences due to higher concentration or aggregation were less than 5% of R_H. It was not possible to perform SLS experiments on wild-type Rad52 because of its significant dependence on R_H with concentration.[14]

References

1. Shinohara, A. & Ogawa, T. (1995). Homologous recombination and the roles of double-strand breaks. *Trends Biochem. Sci.* **20**, 387–391.
2. Sung, P. (1997). Function of yeast Rad52 protein as a mediator between replication protein A and the Rad51 recombinase. *J. Biol. Chem.* **272**, 28194–28197.
3. Benson, F. E., Baumann, P. & West, S. C. (1998). Synergistic actions of Rad51 and Rad52 in recombination and DNA repair. *Nature*, **391**, 401–404.
4. Shinohara, A., Shinohara, M., Ohta, T., Matsuda, S. & Ogawa, T. (1998). Rad52 forms ring structures and cooperates with RPA in single-strand DNA annealing. *Genes Cells*, **3**, 145–156.
5. New, J. H., Sugiyama, T., Zaitseva, E. & Kowalczykowski, S. C. (1998). Rad52 protein stimulates DNA strand exchange by Rad51 and replication protein A. *Nature*, **391**, 407–410.

6. Sugiyama, T., New, J. H. & Kowalczykowski, S. C. (1998). DNA annealing by RAD52 protein is stimulated by specific interaction with the complex of replication protein A and single-stranded DNA. *Proc. Natl Acad. Sci. USA*, **95**, 6049–6054.

7. McIlwraith, M. J., Dyck, E. V., Masson, J.-Y., Stasiak, A. Z., Stasiak, A. & West, S. C. (2000). Reconstitution of the strand invasion step of double-strand break repair using human Rad51 Rad52 and RPA proteins. *J. Mol. Biol.* **304**, 151–164.

8. Baumann, P. & West, S. C. (1999). Heteroduplex formation by human Rad52 protein effects of DNA end-structure, hRPA and hRad52. *J. Mol. Biol.* **291**, 363–374.

9. Van Dyck, E., Hajibagheri, N. M. A., Stasiak, A. & West, S. C. (1998). Visualisation of human Rad52 protein and its complexes with hRad51 and DNA. *J. Mol. Biol.* **284**, 1027–1038.

10. Park, M. S., Ludwig, D. L., Stigger, E. & Lee, S. H. (1996). Physical interaction between human RAD52 and RPA is required for homologous recombination in mammalian cells. *J. Biol. Chem.* **271**, 18996–19000.

11. Kagawa, W., Kurumizaka, H., Ikawa, S., Yokoyama, S. & Shibata, T. (2001). Homologous pairing promoted by the human Rad52 protein. *J. Biol. Chem.* **276**, 35201–35208.

12. Van Dyck, E., Stasiak, A. Z., Stasiak, A. & West, S. C. (1999). Binding of double-strand breaks in DNA by human Rad52 protein. *Nature*, **398**, 728–731.

13. Stasiak, A. Z., Larquet, E., Stasiak, A., Muller, S., Engel, A., Dyck, E. V. *et al.* (2000). The human Rad52 protein exists as a heptameric ring. *Curr. Biol.* **10**, 337–340.

14. Ranatunga, W., Jackson, D., Lloyd, J. A., Forget, A. L., Knight, K. L. & Borgstahl, G. E. O. (2001). Human Rad52 exhibits two modes of self-association. *J. Biol. Chem.* **276**, 15876–15880.

15. Dyck, E. V., Stasiak, A. Z., Stasiak, A. & West, S. C. (2001). Visualization of recombination intermediates produced by RAD52-mediated single-strand annealing. *EMBO Rep.* **2**, 905–909.

16. Wold, M. S. (1997). RPA: a heterotrimeric single-stranded DNA-binding protein required for eukaryotic DNA metabolism. *Annu. Rev. Biochem.* **66**, 61–91.

17. Iftode, C., Daniely, Y. & Borowiec, J. A. (1999). Replication protein A (RPA): the eukaryotic SSB. *Crit. Rev. Biochem. Mol. Biol.* **34**, 141–180.

18. Kim, C., Snyder, R. O. & Wold, M. S. (1992). Binding properties of replication protein A from human and yeast cells. *Mol. Cell. Biol.* **12**, 3050–3059.

19. Gomes, X. V., Henricksen, L. A. & Wold, M. S. (1996). Proteolytic mapping of human replication protein A: evidence for multiple structural domains and a conformational change upon interaction with single-stranded DNA. *Biochemistry*, **35**, 5587–5594.

20. Gomes, X. V. & Wold, M. S. (1996). Functional domains of the 70-kilodalton subunit of human replication protein A. *Biochemistry*, **35**, 10558–10568.

21. Kim, C., Paulus, B. F. & Wold, M. S. (1994). Interactions of human replication protein A with oligonucleotides. *Biochemistry*, **33**, 14197–14206.

22. Bochkarev, A., Pfuetzner, R. A., Edwards, A. M. & Frappier, L. (1997). Crystal structure of the DNA binding domain of replication protein A bound to DNA. *Nature*, **385**, 176–181.

23. Bastin-Shanower, S. A. & Brill, S. J. (2001). Functional analysis of the four DNA binding domains of replication protein A: the role of RPA2 in ssDNA binding. *J. Biol. Chem.* **276**, 36446–36453.

24. Bochkarev, A., Bochkareva, E., Frappier, L. & Edwards, A. M. (1999). The crystal structure of the complex of replication protein A subunits RPA32 and RPA14 reveals a mechanism for single-stranded DNA binding. *EMBO J.* **18**, 4498–4504.

25. Bochkareva, E., Belegu, V., Korolev, S. & Bochkarev, A. (2001). Structure of the major single-stranded DNA-binding domain of replication protein A suggests a dynamic mechanism for DNA binding. *EMBO J.* **20**, 612–618.

26. Jacobs, D. M., Lipton, A. S., Isern, N. G., Daughdrill, G. W., Lowry, D. F., Gomes, X. & Wold, M. S. (1999). Human replication protein A: global fold of the N-terminal RPA-70 domain reveals a basic cleft and felxible C-terminal linker. *J. Biomol. NMR*, **14**, 321–331.

27. Blackwell, L., Borowiec, J. & Mastrangelo, I. (1996). Single-stranded DNA binding alters human replication protein A structure and facilitates interaction with DNA-dependent protein kinase. *Mol. Cell. Biol.* **16**, 4798–4807.

28. Din, S.-U., Brill, S. J., Fairman, M. P. & Stillman, B. (1990). Cell cycle regulated phosphorylation of DNA replication factor A from human and yeast cells. *Genes Dev.* **4**, 968–977.

29. Treuner, K., Okuyama, A., Knippers, R. & Fackelmayer, F. O. (1999). Hyperphosphorylation of replication protein A middle subunit (RPA32) in apoptosis. *Nucl. Acids Res.* **27**, 1499–1504.

30. Rodrigo, G., Roumagnac, S., Wold, M. S., Salles, B. & Calsou, P. (2000). DNA replication but not nucleotide excision repair is required for UVC-induced replication protein A phosphorylation in mammalian cells. *Mol. Cell. Biol.* **20**, 2696–2705.

31. Henricksen, L. A., Carter, T., Dutta, A. & Wold, M. S. (1996). Phosphorylation of human replication protein A by the DNA-dependent protein kinase is involved in the modulation of DNA replication. *Nucl. Acids Res.* **24**, 3107–3112.

32. Treuner, K., Findeisen, M., Strausfeld, U. & Knippers, R. (1999). Phosphorylation of replication protein A middle subunit (RPA32) leads to a disassembly of the RPA heterotrimer. *J. Biol. Chem.* **274**, 15556–15561.

33. Loo, Y.-M. & Melendy, T. (2000). The majority of human replication protein A remains complexed throughout the cell cycle. *Nucl. Acids Res.* **28**, 3354–3360.

34. Dimitrova, D. S. & Gilbert, D. M. (2000). Stability and nuclear distribution of mammalian replication protein A heterotrimeric complex. *Expt. Cell Res.* **254**, 321–327.

35. Braun, K. A., Lao, Y., He, Z., Ingles, C. J. & Wold, M. S. (1997). Role of protein–protein interactions in the function of replication protein A (RPA): RPA modulates the activity of DNA polymerase α by multiple mechanisms. *Biochemistry*, **36**, 8443–8454.

36. Stigger, E., Drissi, R. & Lee, S. H. (1998). Functional analysis of human replication protein A in nucleotide excision repair. *J. Biol. Chem.* **273**, 9337–9343.

37. Golub, E. I., Gupta, R. C., Haaf, T., Wold, M. S. & Radding, C. M. (1998). Interaction of human RAD51 recombination protein with single-stranded DNA binding protein, RPA. *Nucl. Acids Res.* **26**, 5388–5393.

38. Hays, S. L., Firmenich, A. A., Massey, P., Banerjee, R. & Berg, P. (1998). Studies of the interaction between Rad52 protein and the yeast single-stranded DNA binding protein RPA. *Mol. Cell. Biol.* **18**, 4400–4406.

39. Song, B. W. & Sung, P. (2000). Functional interactions among yeast Rad51 recombinase, Rad52 mediator,

and replication protein A in DNA strand exchange. *J. Biol. Chem.* **275**, 15895–15904.

40. Mer, G., Bochkarev, A., Gupta, R., Bochkareva, E., Frappier, L., Ingles, C. J. *et al.* (2000). Structural basis for the recognition of DNA repair proteins UNG2, XPA and Rad52 by replication factor RPA. *Cell*, **103**, 449–456.

41. Walther, A. P., Gomes, X. V., Lao, Y., Lee, C. G. & Wold, M. S. (1999). Replication protein A interactions with DNA. 1. Functions of the DNA-binding and zinc-finger domains of the 70-kDa subunit. *Biochemistry*, **38**, 3963–3973.

42. Lao, Y. (2001). Multiple interactions between DNA and human replication protein A (RPA). PhD Dissertation, University of Iowa, Department of Biochemistry, Iowa City, IA.

43. Sibenaller, Z. A., Sorensen, B. R. & Wold, M. S. (1998). The 32- and 14-kilodalton subunits of replication protein A are responsible for species-specific interactions with single-stranded DNA. *Biochemistry*, **37**, 12496–12506.

44. Habel, J. E., Ohren, J. F. & Borgstahl, G. E. O. (2001). Dynamic light scattering analysis of full-length, human RPA14/32 dimer: purification, crystallization and self-association. *Acta Crystallog. sect. D*, **D57**, 254–259.

45. Smith, J. & Rothstein, R. (1999). An allele of *RFA1* suppresses RAD52-dependent double-strand break repair in *Saccharomyces cerevisiae*. *Genetics*, **151**, 447–458.

46. Lao, Y., Gomes, X. V., Ren, Y., Taylor, J. S. & Wold, M. S. (2000). Replication protein A interactions with DNA. III. Molecular basis of recognition of damaged DNA. *Biochemistry*, **39**, 850–859.

47. Bochkareva, E., Frappier, L., Edwards, A. M. & Bochkarev, A. (1998). The RPA32 subunit of human replication protein A contains a single-stranded DNA-binding domain. *J. Biol. Chem.* **273**, 3932–3936.

48. Haber, J. E. (1999). Gatekeepers of recombination. *Nature*, **398**, 665–667.

49. Mortensen, U. H., Bendixen, C., Sunjevaric, I. & Rothstein, R. (1996). DNA strand annealing is promoted by the yeast Rad52 protein. *Proc. Natl Acad. Sci. USA*, **93**, 10729–10734.

50. Henricksen, L. A., Umbricht, C. B. & Wold, M. S. (1994). Recombinant replication protein A: expression, complex formation and function characterization. *J. Biol. Chem.* **269**, 11121–11132.

51. Gomes, X. V. & Wold, M. S. (1995). Structural analysis of human replication protein A; mapping functional domains of the 70-kDa subunit. *J. Biol. Chem.* **270**, 4534–4543.

52. Kratochvil, P. (1987). *Classical Light Scattering from Polymer Solutions*, Elsevier, Amsterdam.

53. Shen, Z., Peterson, S. R., Comeaux, J. C., Zastrow, D., Moyzis, R. K., Bradbury, E. M. & Chen, D. J. (1996). Self-association of human RAD52 protein. *Mutat. Res.* **364**, 81–89.

54. Pfuetzner, R. A., Bochkarev, A., Edwards, A. M. & Frappier, L. (1997). Replication protein A: characterization and crystallization of the DNA binding domain. *J. Biol. Chem.* **272**, 430–434.

55. Nagelhus, T. A., Haug, T., Singh, K., Keshav, K. F., Skorpen, F., Otterlei, M. *et al.* (1997). A Sequence in the N-terminal region of human uracil-DNA glycosylase with homology to XPA interacts with the C-terminal part of the 34-kDa subunit of replication protein A. *J. Biol. Chem.* **272**, 6561–6566.

How to Use Dynamic Light Scattering to Improve Your Chances of Growing Crystals of a Macromolecule

Gloria E. O. Borgstahl

The Eppley Institute for Cancer Research, 987696 Nebraska Medical Center, Omaha, NE,

68198-7696, USA

Abstract

Dynamic light scattering (DLS) has become one of the most useful diagnostic tools for crystallization. The main purpose of using DLS in crystal screening is to help the investigator understand the size distribution, stability and aggregation state of macromolecules in solution. It can also be used to understand how experimental variables influence aggregation. With commercially available instruments, DLS is easy to perform, and most of the sample is recoverable. Most usefully, the homogeneity or monodispersity of a sample, as measured by DLS, can be predictive of crystallizability.

Keywords: solubility, aggregation, hydrodynamic radius, monodispersity, polydispersity, dynamic light scattering

1. Introduction

Along the road to atomic structure determination by X-ray crystallography, a major challenge is the growth of high quality crystals of the macromolecule of interest. The level of interest in the macromolecule seems to correlate well with the level of difficulty in its crystallization. It is helpful to optimize the composition of the protein sample and the experimental conditions, such as buffer components and temperature, to increase the likelihood of crystallization. To optimize these parameters it is necessary to analyze the aggregation state and stability of a macromolecular sample. There are many methods that can be used to measure size or aggregation state, including sedimentation equilibrium, size exclusion chromatography, native gel electrophoresis and light scattering. Of these methods, dynamic light scattering (DLS), a.k.a. quasielastic light scattering, is the easiest to implement, the quickest to perform, and the least destructive to the sample (Figure 1). For complex cases a combination of these methods may be needed to interpret the data. Samples that are monodisperse in solution, as measured by DLS, are much more likely to crystallize (1, 2). Along with this chapter, there are several other useful chapters written on the use of DLS analysis in crystallization (3-5)

The DLS instrument is easy to use and detailed knowledge of the underlying physics of molecular sizing is usually not needed. Therefore, only a brief explanation is included here. A microcuvette of protein solution is illuminated by laser light (Figure 2). The molecules in solution are undergoing Brownian motion and cause fluctuations in the scattered light intensity. This change in light intensity is measured by a detector placed at a 90 degree angle to the incident laser light. The translational diffusion coefficient D_T is derived from these data using an autocorrelation function. In general, small particles diffuse "faster" than large particles. A

hydrodynamic radius (R_H) of the molecules in solution can be calculated from D_T. In general, particles must differ in R_H by 50% or more to be well separated by DLS (Figure 3). Molecular weight (MW) can also be estimated, if the shape of the molecule is assumed, e.g. spherical or elongated. DLS as an estimator of MW is not recommended and must be used with caution. The shape definitions used to estimate MW may not accurately represent the particles in solution and for polydisperse samples the R_H and MW will be based on a weighted average of more than one species. Multiple angle static light scattering downstream from size exclusion chromatography is the recommended light scattering method to measure absolute molecular weight of molecules in solution. In this article, DLS is primarily used to assess the aggregation state of a sample and to measure polydispersity which is predictive of crystallizability.

2. Materials

1. Protein Solutions DynaPro MS/X instrument with temperature control (0 to 60° C) installed and correctly configured.
2. Dynamics software version 6 installed on a compatible PC.
3. Protein Solutions 12 µl quartz cuvettes.
4. Protein Solutions microfiltration system.
5. Syringe tip 0.2 µm filters.
6. 20-30 µl protein sample.
7. Water, 1% Triton X100, and a range of appropriate buffer and salt solutions, all 0.2 µm filtered.
8. Compressed air, either house air or in a can.
9. Lens paper.
10. Small ultrasonic cleaner for cleaning cuvettes.
11. Sterile plastic transfer pipettes.
12. 100 µl pipetteman with capillary pipette tips.
13. Tabletop microcentrifuge and appropriate tubes.
14. Microconcentrators.
15. Good buffers (sodium salts) for use in Mueser's solubility screen, each at 100mM: MES-NaOH pH 5.8; PIPES-HCl pH 6.5; HEPES-HCl pH7.5; TAPS-HCl pH 8.5.
16. Chloride salts for use in Mueser's solubility screen, each at 100 mM: NH_4Cl; NaCl; KCl; LiCl; $MgCl_2$; $CaCl_2$.
17. Ammonium salts for use in Mueser's solubility screen, each at 100 mM: NH_4 formate; NH_4 acetate; NH_4 cacodylate; NH_4SO_4; NH_4PO_4; NH_4citrate

3. Methods

The methods described below outline (1) how to prepare the sample, (2) how to take DLS measurements and (3) how to interpret your results. The DynaPro instrument is run by the Dynamics software package (see Note 1). The methods and strategies described in this article can be applied to any dynamic light scattering instrument, although the specific details of the instrument and software may be different.

3.1 Preparation of instrument

3.1.1   *Measuring DLS data*

While preparing for the experiment, many DLS measurements should be taken to check the state of the instrument. First turn on the DynaPro MS/X instrument, the temperature control unit, and start the Dynamics software. Place the quartz cuvette containing your sample or water in the sample holder on the optics block. The frosted side of the cuvette must point to the left side of the holder, as marked on the instrument. In the software, open a "New" experiment. On the left side of the Experiment Window is the "Tree View". The Tree View is used to select groups or categories of information for viewing in the display side of the Experiment Window. There are three main nodes in the Tree View - Hardware, Parameters, and Measurements. Connect the instrument using the Hardware node. Set the temperature using the Parameters → Instrument node. Then proceed to take DLS measurements by clicking on the Green Start Button on the Experiment Window tool bar. Sub-categories in the Measurements node are the individual measurements (Meas #), each of which is further broken down into Acquisitions (Acq #) and Readings (Read #). The display format for the information in the Measurement Node is dependent upon which view button is selected in the Experiment Window tool bar (e.g. Datalog Grid or Regularization Graph). By default, each data acquisition is accumulated over a 10 second window of time. During the course of an experiment, each acquisition collected is displayed in the Measurements node along with the corresponding calculated data. Ten or more acquisitions are recommended per measurement. Each acquisition is the average of 10 readings. The Cumulants, displayed in the Data Log Grid, and Regularization Analysis data is calculated by the software and can be displayed at any level of detail, including the average over all the data, the average over each acquisition, or over each reading. To stop data collection, click on the Red Stop Button in the Experiment Window tool bar.

3.1.2   *Cuvette cleaning and clean water count*

The DLS cuvette and apparatus must be very clean to ensure good data quality. Therefore, it is highly recommended that the first step of the DLS experiment is to measure a good clean water count. The clean water count also checks the condition of the instrument components.

1. Fill the cuvette with 0.2 μm filtered deionized water. Avoid air bubbles.

2. Take DLS measurements to get a clean water count rate.

3. If the clean water count is reasonable and steady, you can start taking DLS measurements on your sample. For the DynaPro MS/X instrument counts <25,000 are good. Less sensitive instruments, such as the DynaPro 801, may have counts <10,000 for clean water. See Example 1 for an example of acceptable clean water data. Reasonable clean water count rates are similar to those made when the cuvettes and instrument were new. The clean water count rates should be noted in the instrument log book. If it is too high the cuvettes and/or the microfilter kit need to be thoroughly cleaned or, in the worst case, should be replaced.

Remember, any large particles, such as dust, will scatter light intensely and will interfere with the DLS signal from the molecules of interest. Therefore it is necessary to thoroughly clean the cuvette before and after use. Be careful not to scratch the cuvettes! Clean all dust off the outer surface. The following cuvette cleaning procedure is recommended (see Note 2):

1. Using a sterile plastic transfer pipette, flush the cuvette multiple times with a 1% Triton X100 solution.

3

2. Rinse the cuvette 3 to 5 times with sterile-filtered, deionized water.

3. The interior of the cuvette can be dried using compressed air. Alternatively, if you have more time, invert the cuvette and allow it to dry.

4. Polish the exterior surface with lens paper and remove dust with compressed air. Note, tissues and other wipes should not be used as they can scratch the surface of the cuvette. The cuvette cap must also be dust free.

5. Repeat the clean water count and cleaning procedure until a reasonably low clean water count is obtained. The clean water count must be stable for 2 to 3 minutes.

3.2 Preparation of sample

3.2.1 Estimation of minimal concentration

In order to make efficient use of your samples, it is helpful to know the minimum protein concentration needed for DLS measurements. Usually, it is safe to assume that DLS measurements made at low protein concentration represent fairly well the sample at the much higher concentrations typically used by crystal farmers. Also, if needed, DLS measurements can be repeated at higher concentrations. The minimal protein concentration needed is dependent on the molecular weight of the macromolecule and the particular instrument. Smaller proteins will need to be at a higher concentration. For example, for the DynaPro MS/X the minimal concentration for a 10 kDa protein is ~0.6 mg/mL and for a 100 kDa protein is 0.06 mg/mL. To estimate the minimum protein concentration that is needed for any DynaPro model use Tools→Calculations→Optimization in Dynamics V6. To obtain higher quality DLS data use a protein concentration 2-3 fold higher than that recommended by the Calculator.

3.2.2 Sample Preparation

Before DLS measurements can be taken the sample must also be cleaned of any dust or other particles. All buffers must be also cleaned by filtration. This can be done by using the microfilter kit provided by Protein Solutions or by centrifugation. Centrifugation is the easiest. The microfilter kit is more difficult to use but has the advantage of removing particles by pore size (see Note 3). The procedure used to clean the sample for DLS must also be used to prepare the sample before crystallization.

Centrifugation procedure:

1. Prepare the sample (e.g. thaw frozen stock, dilution of stock, or mixed components of a complex) in a suitable clean, dust free microcentrifuge tube. The microcentrifuge tubes can be purged of dust with compressed air.

2. Centrifuge 5 to 10 minutes at 13,000 rpm in a table top microcentrifuge.

3. Transfer supernatant with a 100 µl pipetman with clean capillary tips to a dust free, clean microcentrifuge tube or pipette the supernatant directly into the clean DLS cuvette. Do not disturb the pellet. Remember, only the top portion of the sample is dust free after centrifugation.

Microfilter kit procedure:

1. Disassemble the Microfilter system and syringe completely. Thoroughly clean all parts by rinsing/soaking in deionized water and then air dry the parts. If needed,

4

ultrasonication or 1% Triton X100 can be used to clean the parts followed by thorough rinsing with deionized water.

2. Partially reassemble Microfilter system by fitting the Teflon housing into the metal housing and seat the O-rings properly in each half.

3. Using the tweezers, place a filter disk into the 'needle' half of the metal housing on top of the O-ring (see Note 4).

4. Tightly screw the two metal housing pieces together. The filter disk will be held in place by the two O-rings.

5. Reassemble the syringe and load with filtered water. Insert the syringe needle into the Teflon needle guide in the filter housing. Filter water through the microfilter system by pressing gently on the syringe plunger. Dispense into the cuvette and take clean water count data again to ensure that the Microfilter System is clean. Keep passing water through the Microfilter System until the clean water count test is passed.

6. Load the syringe with filtered buffer. Thoroughly and gently rinse the filter with buffer before filtering your protein sample.

7. Remove the syringe from the housing and dispense any remaining buffer to waste.

8. If you are using the 12 µl cuvette, then load the syringe with 20 µl or more of protein sample and reinsert the syringe needle into the filter housing. Approximately, 5-8 µl of sample will be lost to the filter system.

9. Gently depress the syringe plunger to dispense 1-2 drops onto a paper. These two drops are sufficient to displace any remaining buffer in the needle that was used to wet the filter disk.

10. The sample can now be directly loaded directly into the cuvette from the microfilter needle. Remove any air bubbles that are created, for example by sucking them back into the needle. Place the cap on the cuvette.

11. Disassemble the microfiltration system and thoroughly clean and dry all components before placing them back into the case.

3.3 Measurement of DLS data on the sample

3.3.1 Measuring DLS data on the sample

Place the quartz cuvette containing your sample in the sample holder on the optics block. Set the temperature (See Note 5) and proceed to take DLS measurements. At least 10 to 20 acquisitions should be taken for each solution condition. To check reproducibility, the measurements should be done in duplicate, or triplicate if there is enough sample. After measurement, the sample can be recovered using a pipetman and capillary tips for use in crystallization screens or other experiments.

3.3.2 Interpretation of DLS data

Before you start to analyze your DLS results make sure the solvent and sample conditions are properly entered into the Dynamics software. The viscosity and refractive index of the buffer you are studying can adversely affect the estimate of R_H and D_T, respectively. The Dynamics

5

software has a pull down menu of frequently used buffers under the Parameters → Solvent node. These are fairly accurate if your protein concentrations are low (see Note 6).

When interpreting the DLS data there are several things to keep in mind. First, know the limitations of the instrument. For example, the Protein Solutions MS/X has a lower limit of 0.5 nm and an upper limit of 1 μm particle size. Be aware that you will not be able to deconvolute the intensity measurements coming from your sample of interest, the buffer system the protein is in, or impurities in the solution. If you are using a complicated buffer system, DLS data on the buffer alone can be helpful in interpreting the results (See Example 2). Data from other experiments such as native PAGE, electron microscopy, size exclusion chromatography can be helpful in interpreting results (6).

In studying the results from Dynamics, first study the measurements statistics table to evaluate the quality of your data and the modality of your sample (Figure 3). Outliers can be filtered out using the "Data Filter" or individually marked manually. Both methods are accessed by a right click on the Measurements DataLog Grid. Guidelines for marking outliers are given in the Help software. Guidelines for the interpretation of the statistics in the Measurements DataLog Grid are outlined in Table 1 and described below.

1. Use the Baseline parameter to judge if your sample is monomodal, bimodal or multimodal. The quality of the fit of the data to a given autocorrelation function is indicated by the baseline value. Monomodal distributions are defined by a Baseline ranging from 0.997 to 1.002. Bimodal distributions have a Baseline range of 1.003 to 1.005. Baselines greater than 1.005 are from multimodal samples, dust or noise.

2. The Dynamics software determines the uniformity of sizes through a monomodal (single particle size with a Gaussian distribution) curve fit analysis called Cumulants. The quality of the data is represented in the SOS error statistic reported for each sample acquisition (a single correlation curve) in the Data Log Grid View of Dynamics V6. The SOS error is the sum of squares difference between the measured data and the Cumulants calculated intensity correlation curves. The SOS errors less than 20.0 are good and errors less than 5.0 are considered negligible (see Note 7) and probably represent the best samples. We have noted that, with the higher sensitivity provided by the DynaPro MS/X, the SOS errors on polydisperse samples tend to be higher than on less sensitive instruments such as the DynaPro 801, nevertheless the rules in Table 1 still hold true.

3. The polydispersity statistic will tell you the likelihood of crystallizing your sample. The polydispersity (Pd or standard deviation) is indicative of the distribution in the peak or subpeak. By default, %Pd, or normalized polydispersity, is listed in the Datalog Grid and the Regularization Results Summary in Dynamics version 6.0. Here, %Pd is calculated by dividing Pd by R_H and reported as a percent. In older versions of the Dynamics software, this statistic was called C_p/R_H. If your sample is monomodal, the mean %Pd of the sample can be read straight off the Datalog Grid. If your sample is multimodal then Mean R_H and %Pd for each peak can be obtained from the Regularization Graph. If the sample is monomodal and the %Pd is less than 15% your sample is monodisperse and very likely to crystallize during screening (see Note 8). Go onto screen the sample for crystallization (Figure 1), perhaps gauging your level of effort on the quality of the DLS analysis of that sample.

3.4 How to use DLS data to find conditions that will improve crystallization results

6

If your sample is multimodal, or monomodal but polydisperse (%Pd>30%), or simply will not crystallize, the following experimental considerations can help improve your DLS and crystallization results.

1. Increasing the solubility of the sample will typically decrease the aggregation and polydispersity of the sample. Therefore, it is helpful to perform the Mueser solubility screen on your sample to optimize buffer conditions. The following protocol that has been adopted successfully several times (7, 8). It is especially powerful when coupled to the DLS polydispersity analysis.

   a. Dialyze 2 - 5 mg protein against deionized water (no buffer, no salt). Most proteins will precipitate under these conditions. If not, you're lucky.
   b. Resuspend the precipitated protein and aliquot the precipitate into 20, 1.5 ml microcentrifuge tubes. Centrifuge at maximum speed in a table top centrifuge for 2 to 5 min to repellet the protein. Remove the supernatant.
   c. Each tube will be a separate experiment. Add either buffer, chloride salt or ammonium salt (20 µl of 100 mM solutions described in Materials sections 15, 16 and 17) and resuspend the pellet. Let stand at room temperature for 10 min, centrifuge to pellet the undissolved protein, and measure the protein concentration of the supernatant amount redissolved. If the pellets completely dissolve then use less volume or more protein.
   d. When you have information about which buffer and/or salt are best, it is suggested that you try a cross-coupled experiment. For example, if LiCl and $(NH_4)_2SO_4$ give good solubility, then perhaps $(Li)_2SO_4$ is worth trying.
   e. Test the final buffer condition for maximum solubility using mini concentrators. The best starting protein concentration for crystallization is one-half of the maximum solubility.

2. Perform a series of DLS experiments to test the effect of ionic strength, pH, protein concentration, organic solvents, detergents and other additives on the polydispersity of your sample (See Example 3). Perform crystallization experiments at the solution condition where your sample is the most monodisperse and stable over time.

3. Test the effect of temperature on your sample. Find the temperature that your protein is the most monodisperse and then set the crystallization incubator to this temperature for crystal growth. The Event Scheduler can automate these experiments (right click on Parameters node to access the Event Scheduler).

4. Test the effect of binding partners (protein, peptides or oligonucleotides) or substrates on R_H and monodispersity. The effect of stoichiometry of mixing can also be tested. (See Example 4). Anything that makes the molecule smaller and more compact may render it more crystallizable (9).

5. Use DLS analysis to help optimize protein purification protocol, e.g. to avoid inappropriate disulfide bond formation (10).

6. The protein itself should be considered a crystallization variable (11). Use DLS analysis to help select the best construct. For example, perhaps 3 deletions of different length are made from the N-terminus of the protein. Then put your biggest crystallization effort into the sample with the best monodispersity.

7. DLS is also helpful to test the effects of storage procedures, e.g. freezing versus refrigeration and to assess shelf life.

7

4. Notes

1. Dynamics has a "Help" pull down menu that contains "Help Topics" and "PSI books". Help Topics explain how to perform the DLS experiment and how to use the software. PSI books are an excellent resource for a detailed understanding of light scattering theory and mathematics. Protein Solutions has also written "Dynapro Data Interpretation Guide"; be sure to get a copy. In addition, several texts and articles have been written on the collection and analysis of DLS data (12-16).

2. If the protocol described does not clean the cuvette try placing it in a sonicating bath for 15 to 20 minutes and then clean it again. Do not use *concentrated* acids and bases to clean the cuvette as they can etch the surface. Do not use organic solvents (e.g., ethanol) to rapidly dry the cuvette as they can leave a thin residue on the surface. Always clean the cuvette thoroughly after use and before storage. If it is not stored in a clean state, you will cause the next user many headaches and bad lab karma. If the cuvette window becomes scratched it will need to be replaced, (costa mucho dinero!).

3. The sample may be unexpectedly lost during the filtration process. This could be due to aggregation, unexpected quaternary structure or unusual binding to the filter. Also it is important to take a protein reading or run a SDS-PAGE PHAST gel (Amersham Biosciences) on 1 µl of sample before and after filtration to access how much, if any, is lost due to filtration. Consider pore size and the molecular weight of your protein. The Dynamics software includes a molecular weight calculator that will estimate R_H for you. Use it to see which pore size to use. For example, don't use 0.020 µm size pores if your protein is larger than 150 kDa. If needed, a filter with larger pore size can be used.

4. The Whatman Anotop filters used with the microfilter kit are very brittle. Care must be taken in handling them so that they do not crack. They must also be seated properly on the O ring so that solution cannot pass around the filter.

5. Useful information on the effect of temperature on aggregation can be gained from starting the DLS measurements at 4 °C and then stepping up the temperature in 5 degree increments and taking DLS measurements at each temperature from the same sample. The Event Scheduler node in Dynamics software can be used to automate these measurements. To access the Even Scheduler right click on the Parameters node. The sample should be incubated 30 minutes at each temperature before DLS data (10-20 measurements) are taken. The maximum temperature for the DynaPro MS/X is to 60 °C. Temperature can be used to control the aggregation of a protein (17). Ramping down from high temperature has been used in the crystallization of macromolecules, e.g. insulin (18).

6. The viscosity is influenced by protein concentration and buffer components such as alcohols and glycerol. For precise measurements of R_H, viscosity and refractive index can be measured with a viscometer and refractive index detector, respectively, and then entered by hand into the software.

7. Regularization analysis will be able to give you some size information about your sample even if the SOS error is high and your Baseline is high. Both of these statistics absorb error so the amount of trust you should place in the data in these cases should be proportionately low.

8. The %Pd is the statistic most useful for predicting crystallizability, if your sample is monomodal. A special exception is made for bi or multimodal samples where one or more of the peaks are due to something in the solvent (e.g. detergent micelles) that produces light scattering.

If the protein peak can be identified from the noise through appropriate control experiments, the

Cp/R_H for this peak off the regularization graph can be used to predict crystallizability. Also, the

concentration of detergent can be optimized by DLS to eliminate the presence of micelles in the

protein solution.

Acknowledgments

References

1. Zulauf, M., and D'Arcy, A. (1992) Light Scattering of Proteins as a Criterion for Crystallization. *J. Cryst. Growth* **122,** 102-06.
2. D'Arcy, A. (1994) Crystallizing proteins - A rational approach. *Acta Cryst.* **D50,** 469-71.
3. Wilson, W. W. (2003) Light scattering as a diagnostic for protein crystal growth - A practical approach. *J. Structural Biol.* **142,** 56-65.
4. Bergfors, T. M. (1999) Protein Crystallization Techniques, Strategies and, Tips, International University Line, La Jolla, CA.
5. Ferre-D'Amare, A. R., and Burley, S. K. (1997) Dynamic Light Scattering in Evaluating Crystallizability of Macromolecules. *Methods in Enzymology* **276,** 157-66.
6. Ranatunga, W., Jackson, D., Lloyd, J. A., Forget, A. L., Knight, K. L., and Borgstahl, G. E. O. (2001) Human Rad52 Exhibits Two Modes of Self-association. *J. Biol. Chem.* **276,** 15876-80.
7. Mueser, T. C., Rogers, P. H., and Arnone, A. (2000) Interface sliding as illustrated by the multiple quaternary structures of liganded hemoglobin. *Biochemistry* **39,** 15353-64.
8. Collins, B. K., Tomanicek, S. J., Lyamicheva, N., Kaiser, M. W., and Mueser, T. C. (2003) A Preliminary Solubility Screen Used to Improve Crystallization Trials. Crystallization and preliminary X-ray structure determination of Aeropyrum pernix Flap Endonuclease-1. *Acta Cryst. D in press.*
9. Jackson, D., Dhar, K., Wahl, J. K., Wold, M. S., and Borgstahl, G. E. (2002) Analysis of the human replication protein A:Rad52 complex: evidence for crosstalk between RPA32, RPA70, Rad52 and DNA. *J Mol Biol* **321,** 133-48.
10. Habel, J. E., Ohren, J. F., and Borgstahl, G. E. O. (2001) Dynamic light scattering analysis of full-length, human RPA14/32 dimer: purification, crystallization and self-association. *Acta Cryst. D* **D57,** 254-59.
11. Dale, G. E., Oefner, C., and D'Arcy, A. (2003) The protein as a variable in protein crystallization. *J Struct Biol* **142,** 88-97.
12. Pusey, P. N., Koppel, D. E., Schaefer, D. W., Camerini-Otero, R. D., and Koenig, S. H. (1974) Intensity Fluctuation Spectroscopy of Laser Light Scattered by Solutions of

Figure 3

Spherical Viruses: R17, Obeta, BSV, PM2 and T7. I. Light-Scattering Technique. *Biochemistry* **13,** 952-59.

13. Camerini-Otero, R. D., Pusey, P. N., Koppel, D. E., Schaefer, D. W., and Franklin, R. M. (1974) Intensity Fluctuation Spectroscopy of Laser Light Scattered by Solutions of Spherical Viruses: R17, Obeta, BSV, PM2 and T7. II. Diffusion Coefficients, Molecular Weights, Solvation , and Particle Dimensions. *Biochemistry* **13,** 960-70.

14. Pecora, R. (1985) Dynamic Light Scattering: Applications of Photon Correlation Spectroscopy, Plenum Press.

15. Brown, R. G. W. (1990) Miniature Laser Light Scattering Instrumentation for Particle Size Analysis. *Applied Optics* **29,** 1.

16. Phillies, G. D. J. (1990) Quasieleastic Light Scattering. *Analytical Chemistry* **62,** 1049A-57A.

17. Ranatunga, W., Jackson, D., II, R. A. F., and Borgstahl, G. E. O. (2001) Human Rad52 Protein Has Extreme Thermal Stability. *Biochemistry* **40,** 8557-62.

18. Long, M. M., Bishop, J. B., Nagabhushan, T. L., Reichert, P., Smith, G. D., and DeLucas, L. J. (1996) Protein crystal growth in microgravity: bovine insulin, human insulin and human alpha interferon. *J. Crystal Growth* **168,** 233-43.

Figure 3

Table 1. Interpretation and use of the statistical parameters calculated by Dynamics V6.[a]

Parameter	Interpretation
Baseline	
0.997-1.002	Monomodal distribution
1.003-1.005	Bimodal distribution
>1.005	Multimodal distribution
Sum of Squares (SOS)	
1.000-5.000	Low noise, negligible error
5.000-20.000	Background error due to noise, low protein concentration, or a small amount of polydispersity
>20.000	High noise/error due to high polydispersity in size distribution (aggregation), irregular solvent
Normalized Polydispersity	Note, this parameter should be used for monomodal distributions only.
%Pd < 15	Monodisperse solution, very likely to crystallize
%Pd < 30	A moderate amount of polydispersity, more likely to crystallize
%Pd > 30	A significant amount of polydispersity, less likely to crystallize

[a]Adapted from the DynaPro Operator Manual, Protein Solution, Inc. Note %Pd in Dynamics V6 was called C_p/R_H in older versions of the software.

Figure 3

Figure Legends

Figure 1. Flow diagram of methods involved in growing protein crystals. By placing, DLS and solubility analysis in the center of the process the chances of growing crystals are optimized

Figure 2. Simplified schematic of the DLS experiment.

Figure 3. Examples of solutions that differ in composition (left) and fake DLS regularization histograms (right). The relative amount of light scattered by each bin, %Intensity, is plotted against the discrete particle sizes, R_H, in nanometers on a log scale. (A) A monodisperse, monomodal solution of monomers (with mean R_H of 3.4 nm, %Pd of 10%). Very likely to crystallize. (B) A monodisperse, monomodal solution of dimers (with mean R_H of 6.8 nm, %Pd of 14%). The polydispersity is greater than the monomeric solution but it is still very likely to crystallize. (C) A bimodal solution of monomers contaminated by trimers (with mean R_H of 3.4 and 10.2 nm). Less likely to crystallize so put in less screening effort. (D) A multimodal solution of monomer, trimer and dodecameric aggregates (with mean R_H of 3.4, 10.2, and 19.3 nm). Unlikely to crystallize but you might as well give it a little try.

Note, the mean R_H is defined by the weighted average of the number of bins comprising the peak. The polydispersity of each peak is indicated by the width. Species that differ in R_H by more than 50% are separable if their polydispersity is small. For example the dimers and trimers differ in size by only 33%. Thus, if solution B was mixed with solution C there would be a single peak (monomodal) and it would be very broad ranging from 2.6 to 13.8 nm. This mixture would be monomodal with mean R_H of 5.9 nm, very polydisperse with %Pd of around 50%, and highly unlikely to crystallize.

Example 1. Acceptable Clean Water Count Data.

Data Log Grid

Item	Time (s)	Temp (C)	Intensity (Cnt/s)	R (nm)	%Pd	MW-R (kDa)	Amp	Baseline	SOS
Acq 1	9.5	25	16340	0.3	0.1	0	0.026	1.002	165.138
Acq 2	19.5	25	18240	0.1	0.1	0	0.174	1.002	117.940
Acq 3	29.5	25	18195	0.1	0.1	0	0.159	1.001	100.560
Acq 4	39.5	25	18559	0.2	0.1	0	0.100	1.001	71.775
Acq 5	49.5	25	19285	0.6	0.1	1	0.013	1.001	118.706
Acq 6	59.5	25	17181	0.5	0.2	1	0.025	1.001	150.398
Acq 7	69.5	25	17748	0.1	0.1	0	0.297	1.002	149.658
Acq 8	79.6	25	19150	0.1	0.1	0	0.232	1.000	99.076
Acq 9	89.6	25	16615	0.5	0.1	1	0.057	1.000	124.772
Acq 10	99.7	25	15131	0.1	0.1	0	0.762	1.000	138.819

Mean

Item	Time (s)	Temp (C)	Intensity (Cnt/s)	R (nm)	%Pd	MW-R (kDa)	Amp	Baseline	SOS
Meas 1	99.7	25	17644.4	0.26	0.1	0	0.185	1.001	123.684

Regularization Graph
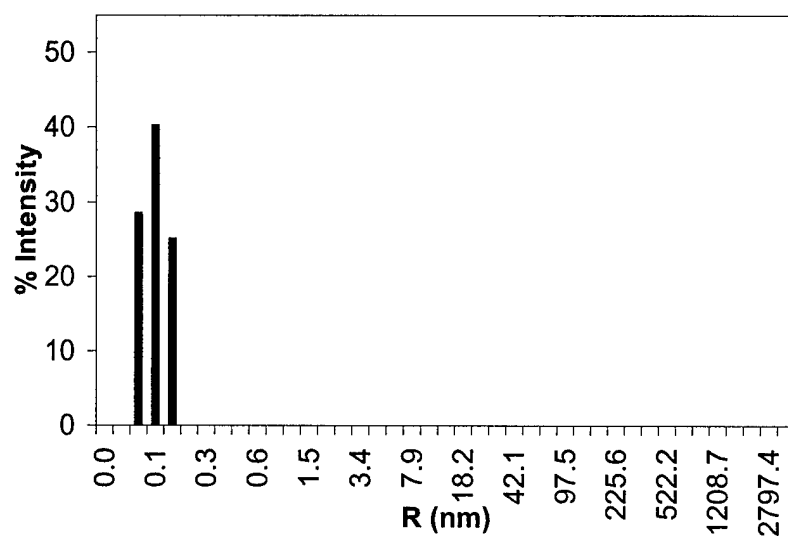
Regularization Results Summary

Item	R (nm)	%Pd	MW-R (kDa)	%Int	%Mass
☑ Peak 1	0.1	21.2	0	100.0	100.0

Interpretation: This is excellent water count data for the DynaPro MS/X. The regularization data at $R_H < 0.5$ nm is due to noise in the detector. Some people call it the solvent peak, but it is really due to after pulse noise in the photodiode. This noise surfaces from time to time in the data if the protein concentrations are too low. In this case, it can be ignored or filtered out of the

14

regularization fit by clicking on the check mark for that peak in the Regularization Results Summary. Note, that the SOS errors are high with water count data since there are no macromolecules present.

Example 2. Part A. DLS data on Replication Protein A (RPA) buffer

Data Log Grid

Item	Time (s)	Temp (C)	Intensity (Cnt/s)	R (nm)	%Pd	MW-R (kDa)	Amp	Baseline	SOS
Acq 1	10	25	80513	52.2	120.5	35238	0.24	1.003	302.977
Acq 2	20	25	73262	51.6	120.1	34243	0.26	1.01	508.992
Acq 3	30	25	59220	32.1	146	11281	0.19	1.003	518.801
Acq 4	40.1	25	71035	47.1	118.3	27704	0.25	1.006	478.842
Acq 5	50.1	25	59948	36.6	159.8	15337	0.19	1.003	461.535
Acq 6	60.1	25	66565	41.9	154.4	20973	0.19	1.009	399.663
Acq 7	70.1	25	91962	83.1	144.2	104370	0.3	1.067	492.541
Acq 8	80.1	25	94199	113.1	208.5	214887	0.32	1.131	609.86
~~Acq 9~~	~~90.1~~	~~25~~	~~133398~~	~~326.3~~	~~244.7~~	~~2562320~~	~~0.534~~	~~1.344~~	~~1531.05~~
~~Acq 10~~	~~100.1~~	~~25~~	~~371576~~	~~1072.3~~	~~50.9~~	~~41449400~~	~~1.046~~	~~2.359~~	~~458.088~~
Mean									
Meas 1	220.3	25	299261	103.7	188.9	175181	0.29	1.15	531.697

For this sample, 20 data points were taken but only the first 10 are shown. The following data filter was applied before regularization of the data: minimum amplitude 0, maximum amplitude 1, baseline limit 1 ± 1, maximum SOS 1000. Thus, data for Acq 9 & 10 did not pass the filter and were not used as indicated by the strikethrough. For this data 13% did not pass the filter.

Regularization Graph
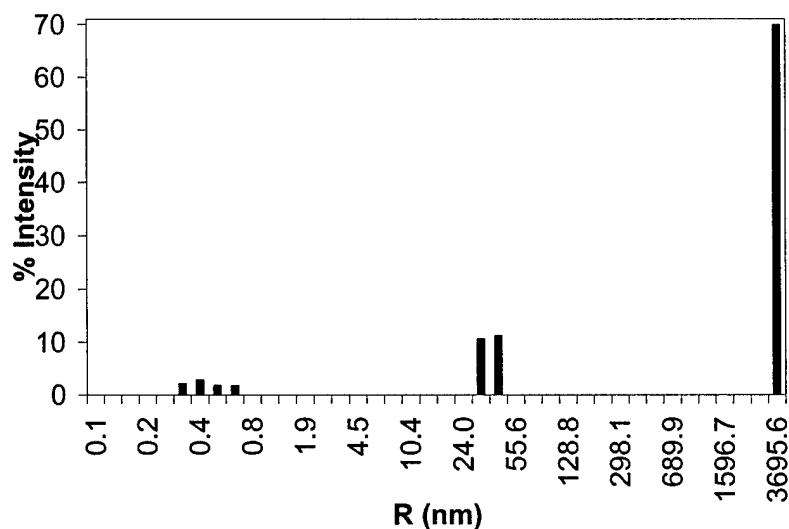
Regularization Results Summary

Item	R (nm)	%Pd	MW-R (kDa)	%Int	%Mass
☑ Peak 1	0.4	30.6	0	8.4	100.0
☑ Peak 2	37.1	13.8	15783	21.7	0.0
☑ Peak 3	3695.6	0.0	749619000	69.9	0.0

16

Interpretation: The SOS and baseline are very high because there is no macromolecule present and the buffer is polydisperse. Compared to Example 1, Peak 1 can be attributed to noise in the detector. Peaks 2 and 3 are from components in the buffer and are probably due to cHEGA10 detergent micelles.

Example 2. Part B. DLS data on RPA heterotrimer at 0.9 mg/ml

Data Log Grid

Item	Time (s)	Temp (C)	Intensity (Cnt/s)	R (nm)	%Pd	MW-R (kDa)	Amp	Baseline	SOS
Acq 1	9	25	464697	11.9	104.1	1101	0.588	0.999	938.809
Acq 2	19	25	366039	7.6	61.6	385	0.587	1.003	150.868
Acq 3	29.1	25	383781	8	74.2	439	0.574	1.006	194.406
~~Acq 4~~	~~39.1~~	~~25~~	~~1295610~~	~~148.0~~	~~241.4~~	~~402739~~	~~0.233~~	~~1.319~~	~~1136.620~~
~~Acq 5~~	~~49.1~~	~~25~~	~~1255210~~	~~147.0~~	~~191.2~~	~~396358~~	~~0.304~~	~~1.327~~	~~1558.530~~
~~Acq 6~~	~~59.1~~	~~25~~	~~610538~~	~~19.3~~	~~115.9~~	~~3426~~	~~0.529~~	~~1.017~~	~~1780.420~~
Acq 7	69.1	25	485968	12.4	101.9	1228	0.594	1.004	803.41
Acq 8	79.1	25	648094	15.9	103.8	2180	0.53	1.018	838.817
Acq 9	89.2	25	393460	8.9	91.2	553	0.623	1.002	288.664
Acq 10	99.2	25	374938	8.3	75.5	470	0.627	1	235.677
Mean									
Meas 1	249.4	25	517431	10.1	95.3	761	0.574	1.013	529.7265

Greater than 20 data points were taken, only the first 10 are shown. The following data filter was applied before regularization of the data: minimum amplitude 0, maximum amplitude 1, baseline limit 1 ± 1, maximum SOS 1000. Thus, data for Acq 4, 5 & 6 did not pass the filter and were not used as indicated by the strikethrough. For this data 20% did not pass the filter.

Regularization Graph
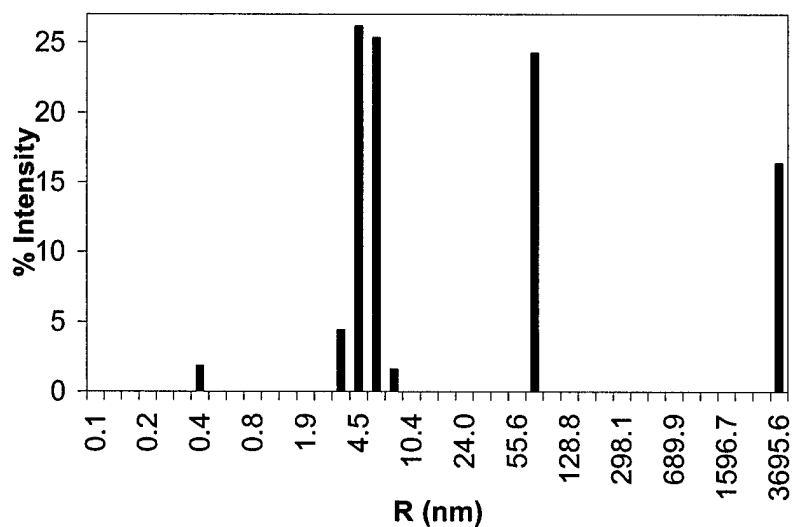
Regularization Results Summary

Item	R (nm)	%Pd	MW-R (kDa)	%Int	%Mass
☑ Peak 1	0.4	0.0	0	1.7	98.6
☑ Peak 2	5.1	18.5	154	55.3	1.4
☑ Peak 3	73.6	0.0	78597	23.4	0.0
☑ Peak 4	3695.6	0.0	749619000	19.6	0.0

Interpretation: The data are very polydisperse as indicated by high baseline and high SOS error. Due to the polydispersity of the buffer, comparison to the buffer alone DLS data is needed for interpretation of the protein sample DLS data. Peak 1, observed in the buffer only data too, is due to the low protein concentration used. Peak 4, and Peak 3 in buffer only data, is due to the polydispersity of the buffer and probably represent cHEGA10 micelles. Identification of Peak 3 components is ambiguous and may be due to the buffer components, protein or both. Peak 2 is due to the protein, in this case RPA heterotrimer (~110 kDa). DLS could be used in this case to find the minimal concentration of CHEGA10 to solubilize the protein without micelles. Note that the peak attributed to detector noise is dominating the % Mass calculation.

Example 3. Part A. Monodisperse DLS data on crystallizable RPA14/32 heterodimer, at a

concentration of 10 mg/mL

Data Log Grid

Item	Time (s)	Temp (C)	Intensity (Cnt/s)	R (nm)	%Pd	MW-R (kDa)	Amp	Baseline	SOS
Acq 1	10	25	1872940	3.9	22.5	80	0.496	1.000	0.812
Acq 2	20	25	1872590	3.9	14.7	83	0.552	1.000	1.145
Acq 3	30	25	1888920	3.9	17.2	81	0.544	1.000	0.761
Acq 4	40.1	25	1894110	3.9	24	82	0.521	1.000	1.124
Acq 5	50.1	25	1908650	3.9	29.1	84	0.51	1.000	1.83
Acq 6	60.1	25	1892830	3.9	23.5	82	0.504	1.000	1.239
Acq 7	70.1	25	1891400	3.9	21.5	82	0.495	1.000	0.862
Acq 8	80.1	25	1888290	3.9	23.6	83	0.489	1.000	1.355
Acq 9	90.1	25	1882720	3.9	10.9	83	0.49	1.000	1.385
Acq 10	100.1	25	1876270	3.9	29.7	82	0.49	1.000	1.071

Mean

Item	Time (s)	Temp (C)	Intensity (Cnt/s)	R (nm)	%Pd	MW-R (kDa)	Amp	Baseline	SOS
Meas 1	300.4	25	1867130	3.9	12.2	83	0.509	1.000	1.1375

Greater than 20 data points were taken, only the first 10 are shown. The application of a data

filter was not needed.

Regularization Graph
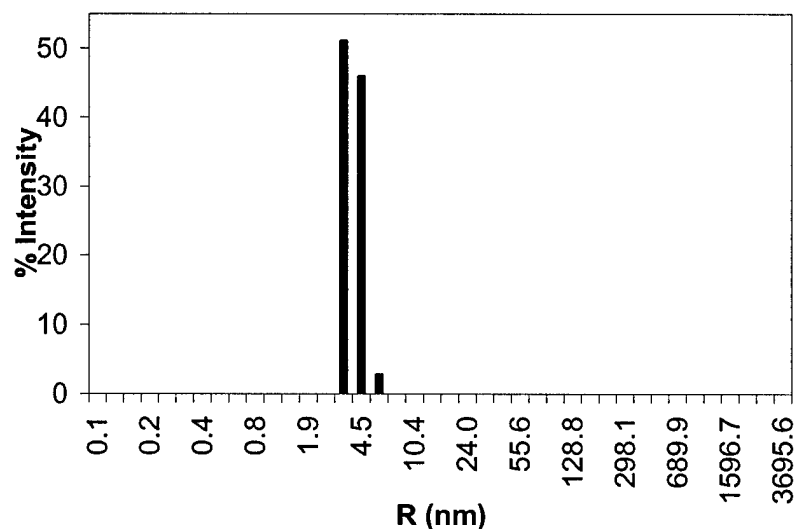
Regularization Results Summary

Item	R (nm)	%Pd	MW-R (kDa)	%Int	%Mass
☑ Peak 1	4.0	15.8	84	100.0	100.0

Interpretation: The sample gave a monomodal fit with a baseline of 1.000 and SOS of 1. RPA14/32 is a 46 kDa heterodimer with a predicted R_H of 3.1 nm. A dimer of heterodimers has a predicted R_H of 4.1 nm. Therefore, these data indicate primarily a dimer of heterodimers in solution. With a %Pd of 16%, this sample crystallized readily out of several crystallization conditions and several space groups (10).

Example 3. Part B. Multimodal DLS data on RPA14/32 heterodimer, at a concentration of

5 mg/mL, diluted with 30 mM Hepes pH 7.8

Data Log Grid

Item	Time (s)	Temp (C)	Intensity (Cnt/s)	R (nm)	%Pd	MW-R (kDa)	Amp	Baseline	SOS
Acq 1	10	25	3976320	69.5	120.1	68813	0.336	1.010	401.397
Acq 2	20	25	2970080	42.4	137	21568	0.377	1.003	837.184
Acq 3	30	25	2968450	43.6	118.7	23036	0.384	1.003	832.709
Acq 4	40.1	25	2327790	21.9	115.9	4613	0.386	1.003	958.650
Acq 5	50.1	25	2388140	22.8	118	5087	0.371	1.003	833.651
Acq 6	60.1	25	2560250	29.7	116.5	9434	0.388	1.003	984.212
Acq 7	70.1	25	2680860	32.8	116.8	11840	0.39	1.002	902.132
Acq 8	80.1	25	2796570	35.8	118	14553	0.368	1.000	849.627
Acq 9	90.1	25	2777060	36	114.7	14790	0.365	1.001	876.540
Acq 10	100.2	25	2600990	27.6	116.2	7896	0.374	1.001	914.389
Mean									
Meas 1	310.5	25	2925130	38.3	118.1	17040	0.362	1.002	819.282

Greater than 20 data points were taken, only the first 10 are shown. The application of a data

filter was not needed.

Regularization Graph
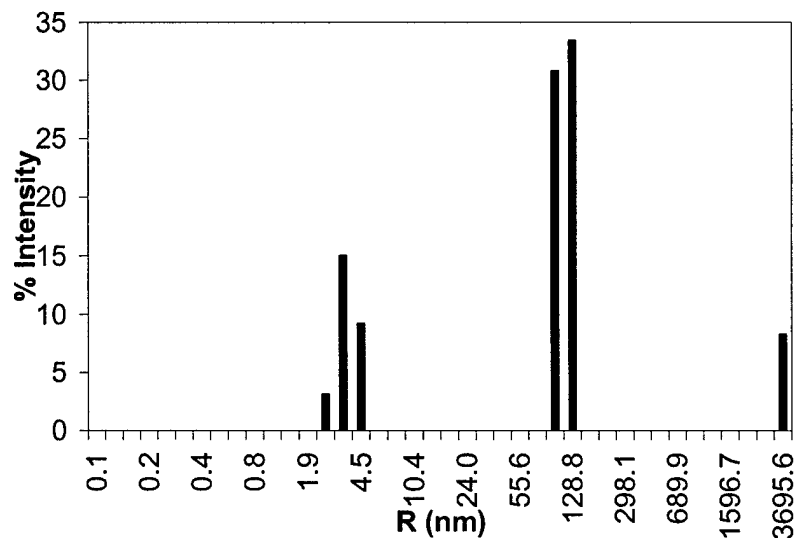
Regularization Results Summary

Item	R (nm)	%Pd	MW-R (kDa)	%Int	%Mass
☑ Peak 1	3.7	17.4	70	27.4	99.9
☑ Peak 2	113.7	13.8	217490	64.3	0.0
☑ Peak 3	3695.6	0.0	749619000	8.3	0.0

22

Interpretation: The increased baseline and very high SOS error indicate that dilution with this buffer introduces polydispersity into the sample. The regularization fit indicates 3 peaks. Peaks 2 and 3 are from aggregated protein. When many data acquisitions are taken this aggregation becomes worse over time (data not shown). Therefore, this is not a suitable buffer condition for this protein.

Example 3. Part C. Monodisperse DLS data on RPA14/32 heterodimer at a concentration of 5

mg/mL, diluted with 30 mM Hepes pH 7.8, 200 mM KCl, and 10 mM DTT; crystallizable in this

solution condition.

Data Log Grid

Item	Time (s)	Temp (C)	Intensity (Cnt/s)	R (nm)	%Pd	MW-R (kDa)	Amp	Baseline	SOS
Acq 1	9	25	1047070	3.6	14.6	68	0.531	1.000	1.244
Acq 2	19	25	1053610	3.8	30.6	77	0.540	1.000	2.441
Acq 3	29	25	1053860	3.7	35.1	73	0.528	1.000	1.797
Acq 4	39.1	25	1061240	3.8	26.2	76	0.509	1.000	2.154
Acq 5	49.1	25	1067120	3.7	21.3	73	0.515	1.000	0.983
Acq 6	59.1	25	1029520	3.8	21.4	77	0.593	1.000	2.747
Acq 7	69.1	25	1026860	3.9	28.5	80	0.599	1.000	2.787
Acq 8	79.1	25	1034900	3.8	19.3	77	0.592	1.000	1.178
Acq 9	89.1	25	1054730	3.8	30.4	77	0.566	1.000	2.361
Acq 10	99.1	25	1074230	3.8	32.9	79	0.545	1.000	2.580
Mean									
Meas 1	329.5	25	1056810	3.8	24.2	75	0.532	1.000	1.581

Greater than 20 data points were taken, only the first 10 are shown. The application of a data

filter was not needed.

Regularization Graph
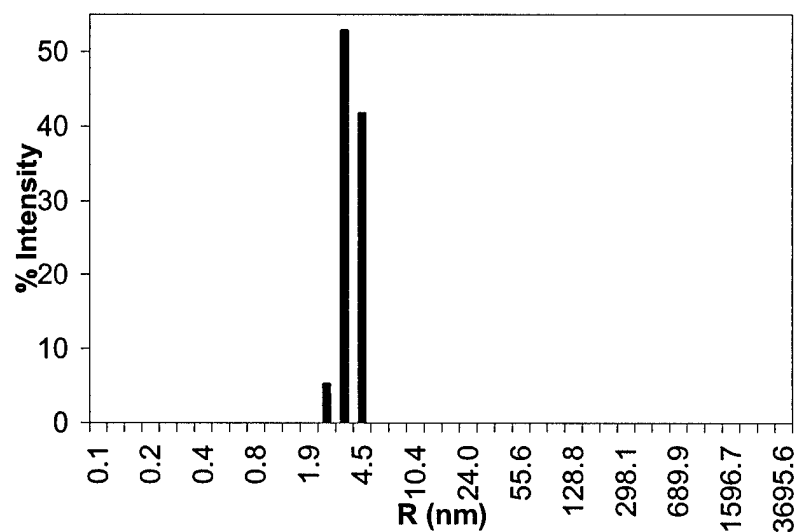
Regularization Results Summary

Item	R (nm)	%Pd	MW-R (kDa)	%Int	%Mass
☑ Peak 1	3.8	15.9	77	100.0	100.0

Interpretation: When compared with parts A and B of Example 3, dilution of the protein into

this buffer is good. The baseline of 1.000 and SOS of 1.6 shows that the sample is monomodal.

24

The %Pd of 16 indicates that the protein is still monodisperse after dilution. Therefore, the protein is stable in this buffer and this is a good starting point for crystallization trials.

**Example 4.** DLS data on a RPA:Rad52 complex at a concentration of 8 mg/mL

Data Log Grid

Item	Time (s)	Temp (C)	Intensity (Cnt/s)	R (nm)	%Pd	MW-R (kDa)	Amp	Baseline	SOS
Acq 1	9	25	4495800	10.8	64.5	872	0.311	1.001	14.876
Acq 2	39.1	25	5018720	10.8	54.1	875	0.332	1.000	20.763
Acq 3	49.1	25	4969060	10.7	61.9	870	0.328	1.000	19.873
Acq 4	69.1	25	4941200	11	61.2	921	0.325	0.999	21.940
Acq 5	89.2	25	4953440	11.2	64.7	969	0.334	1.000	20.287
Acq 6	99.2	25	4894110	10.9	69.8	903	0.327	0.999	18.665
Acq 7	109.2	25	4878090	10.9	72.9	894	0.327	0.999	19.605
Acq 8	119.3	25	4881350	11	72	925	0.330	1.000	21.353
Acq 9	129.3	25	4869450	10.9	61.5	901	0.330	1.001	20.228
Acq 10	139.3	25	4835920	10.8	65.7	879	0.334	1.000	18.834
Mean									
Meas 1	289.5	25	4939260	10.9	61	904	0.32	1.000	18.077

Greater than 20 data points were taken, only the first 10 are shown. The application of a data

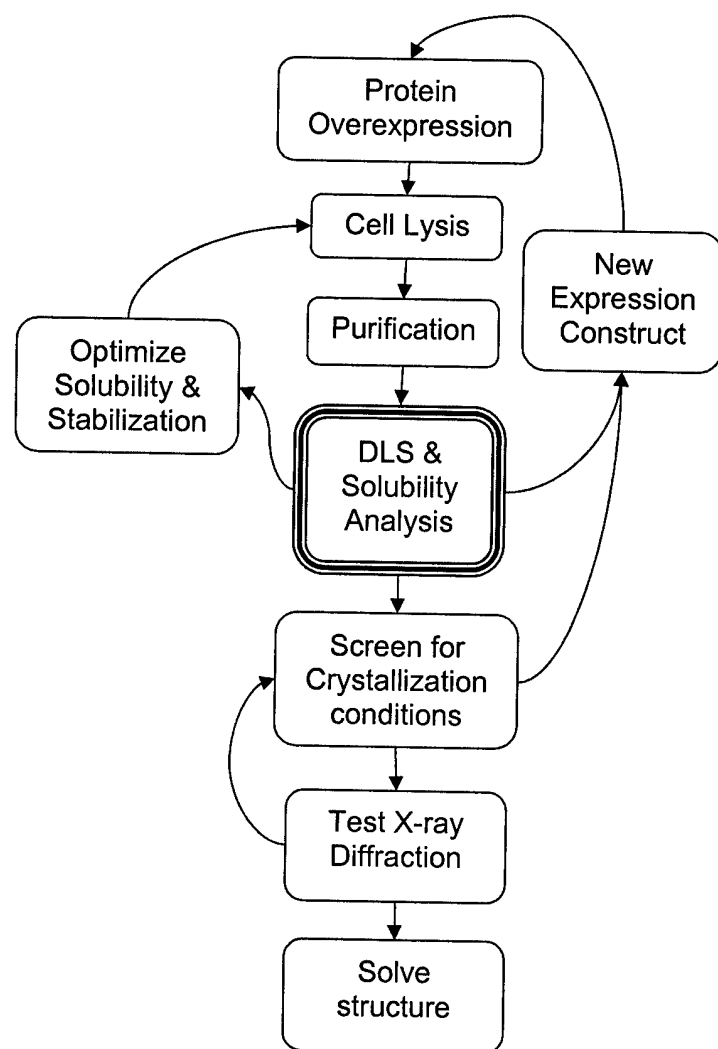filter was not needed.

Regularization Graph
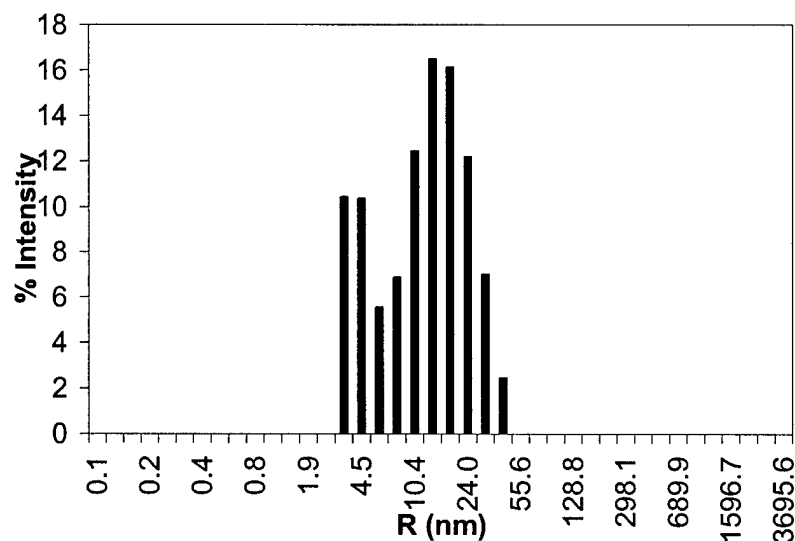
Regularization Results Summary

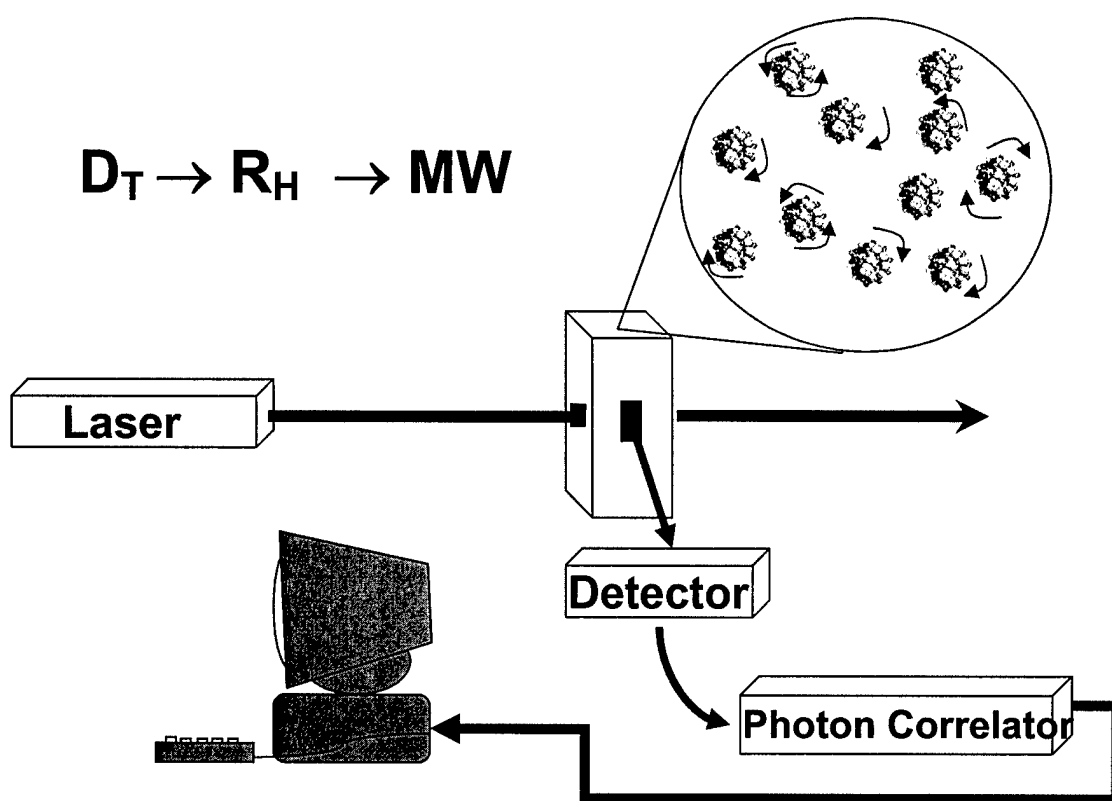| Item	R (nm)	%Pd	MW-R (kDa)	%Int	%Mass
☑ Peak 1	4.4	21.8	106	26.4	92.0
☑ Peak 2	18.0	45.5	2901	73.6	8.0

Interpretation: The sample in this case is a complex of two proteins, RPA heterotrimer (110

kDa) and Rad52 heptameric ring (~350 kDa), mixed with an approximate one to one molar ratio.

The data are polydisperse as indicated by the high SOS error. The regularization analysis shows

that the sample is bimodal and polydisperse. This sample did not crystallize. Possible reasons

are that the molar ratio was not exact or that a portion of the molecules is inactive. The next step is to vary the stoichiometry of RPA to Rad52 to try to obtain 100% monodisperse complex in solution. If this is not successful the complex will need to be separated from free RPA by size exclusion chromatography before crystallization trials.

Borgstahl Figure 1

$$D_T \rightarrow R_H \rightarrow MW$$

Laser

Detector

Photon Correlator